THEORETICAL INVESTIGATION OF THE GROWTH MECHANISM OF GOLD THIOLATE NANOPARTICLES

by

BRIAN MICHAEL BARNGROVER

B.S., Kansas Wesleyan University, 2010

AN ABSTRACT OF A DISSERTATION

submitted in partial fulfillment of the requirements for the degree

DOCTOR OF PHILOSOPHY

Department of Chemistry
College of Arts and Sciences

KANSAS STATE UNIVERSITY
Manhattan, Kansas

2015

Abstract

This body of work describes a theoretical study of the growth mechanism of gold thiolate nanoparticles from Au(III) as synthesized in the Brust-Schiffrin method. The Au(III) salt can be reduced to form Au(I) by two thiols or a hydride. Depending on the polarity of the solvent, the Au(I) species will either yield rings and anionic chains, remain in isolation, or create an ionic complex with the phase transfer agent. No matter what form the Au(I) species takes, a second reduction must occur to yield Au(0). If the solvent is polar, such as methanol or water, and the Au(I) species is a ring or anionic chain, then a hydride can reduce the structure and create a gold-gold bond and dissociate a thiol from the structure. The gold atoms involved in the gold-gold bond would have a formal Au(0) oxidation state. However if the Au(I) species can be kept from forming rings or chains in the polar solvent or if the system is in a nonpolar solvent, then two Au(I) species in close proximity in the presence of hydride can react to yield a non-radical Au(0) species.

The oxidation of bare gold nanoclusters by thiol will also be examined, such as in the case of SMAD-produced gold nanoparticles. In this process, the gold nanoclusters are initially in the Au(0) oxidation state. However the SR-Au-SR "staple" motifs that are known to passivate gold nanoparticles contain Au(I) species. The adsorption of thiol on various sizes of gold clusters in several charge states will be calculated and the mechanism for the oxidation of Au_3 and three-dimensional Au_{12} will be modeled. The rate-limiting step is found to be the thiol hydrogen dissociation onto the gold cluster. Once this dissociation occurs, the hydrogen can move freely around the surface.

Finally, $Au_{25}(SH)_{18}^-$ will be investigated as a catalyst for selective hydrogenation of α,β-unsaturated aldehyde. The dependence of the energetics of hydrogen gas dissociation on

$Au_{25}(SH)_{18}^-$ on the functional and Grimme dispersion correction employed will also be examined.

THEORETICAL INVESTIGATION OF THE GROWTH MECHANISM OF GOLD THIOLATE NANOPARTICLES

by

BRIAN MICHAEL BARNGROVER

B.S., Kansas Wesleyan University, 2010

A DISSERTATION

submitted in partial fulfillment of the requirements for the degree

DOCTOR OF PHILOSOPHY

Department of Chemistry
College of Arts and Sciences

KANSAS STATE UNIVERSITY
Manhattan, Kansas

2015

Approved by:

Major Professor
Christine M. Aikens

Copyright

Abstract

This body of work describes a theoretical study of the growth mechanism of gold thiolate nanoparticles from Au(III) as synthesized in the Brust-Schiffrin method. The Au(III) salt can be reduced to form Au(I) by two thiols or a hydride. Depending on the polarity of the solvent, the Au(I) species will either yield rings and anionic chains, remain in isolation, or create an ionic complex with the phase transfer agent. No matter what form the Au(I) species takes, a second reduction must occur to yield Au(0). If the solvent is polar, such as methanol or water, and the Au(I) species is a ring or anionic chain, then a hydride can reduce the structure and create a gold-gold bond and dissociate a thiol from the structure. The gold atoms involved in the gold-gold bond would have a formal Au(0) oxidation state. However if the Au(I) species can be kept from forming rings or chains in the polar solvent or if the system is in a nonpolar solvent, then two Au(I) species in close proximity in the presence of hydride can react to yield a non-radical Au(0) species.

The oxidation of bare gold nanoclusters by thiol will also be examined, such as in the case of SMAD-produced gold nanoparticles. In this process, the gold nanoclusters are initially in the Au(0) oxidation state. However the SR-Au-SR "staple" motifs that are known to passivate gold nanoparticles contain Au(I) species. The adsorption of thiol on various sizes of gold clusters in several charge states will be calculated and the mechanism for the oxidation of Au_3 and three-dimensional Au_{12} will be modeled. The rate-limiting step is found to be the thiol hydrogen dissociation onto the gold cluster. Once this dissociation occurs, the hydrogen can move freely around the surface.

Finally, $Au_{25}(SH)_{18}^-$ will be investigated as a catalyst for selective hydrogenation of α,β-unsaturated aldehyde. The dependence of the energetics of hydrogen gas dissociation on

$Au_{25}(SH)_{18}^-$ on the functional and Grimme dispersion correction employed will also be examined.

Table of Contents

List of Figures

List of Tables

List of Charts

Dedication

I dedicate this thesis to my family, especially my wife who has been my support throughout my entire time in graduate school.

Chapter 1 - Introduction

1.1 Gold and nanoparticles

Gold has been of great interest to societies for many centuries as currency, medicine, or art. Bulk gold is inert and has a lustrous yellow color. However if gold is reduced to nanometer sizes, the resulting nanoparticles are reactive and red or other hues in color. Gold nanoparticles are used in a variety of applications such as drug delivery and therapy,[1,2] catalysts,[3] sensors,[4] electronics,[5] and optics.[6] Different nanoparticle morphologies such as spheres, cubes, wires, and rods have been synthesized and have diverse properties for these unique applications.[7] How were most of these morphologies synthesized? They have been synthesized through trial and error. Most groups find a synthesis method and modify it to meet their specific needs. Although these different morphologies and synthesis methods exist, until recently very little was known about their underlying growth mechanisms.

Noble metal nanoparticles have been of great interest ever since Michael Faraday created colloidal ruby gold.[8] Faraday found that by taking a precious noble metal salt, such as gold chloride, and treating it with a reducing agent, e.g. inorganic phosphorus, in diethyl ether that individual atoms or small clusters form with the assistance of stirring. The solution turns first brown, then grey, purple and red, and finally turns a deep ruby red color. The color change indicates the reduction of the gold precursor, from gold (III) to gold (0). This colloidal solution is stable for years; a sample survived until World War II when it was accidently destroyed.[9]

1.1.1 Turkevich (Citrate) synthesis

Turkevich and coworkers later confirmed the formation of gold nanoparticles by electron microscopy based on their synthesis, which is also called the citrate reduction method.[10] The standard citrate reduction synthesis is performed by taking tetrachloroauric acid ($HAuCl_4$) and

sodium citrate in boiling water and stirring for two minutes. In this synthesis method, citrate acts as the reducing agent and stabilizing ligand. This synthesis also creates mostly monodisperse particles that have a mean particle size of 200 Å with a deviation of 12.5 percent. Turkevich and coworkers also examined the effects of temperature, concentration of reagents, and dilution on the reaction time, mean particle size, and size deviation. They found that lowering the temperature increased the reaction time, but slightly decreased the mean particle size and size deviation (Table 1.1).

Table 1.1 The effect of temperature on reaction time, mean particle size, and size deviation. Reproduced from Ref. 4 with permission from The Royal Society of Chemistry.

Temp. °C	Approximate Time for the Completion of Reaction in min.	Mean Particle Size in Å	% Deviation
100 (standard)	5	200	12·5
80	25	165	8·1
70	45	180	8·6

They observed that decreasing the concentration of citrate (Table 1.2) had a major effect on the reaction time by reducing it from five minutes to 72 seconds. At concentrations lower than 3.75 mg of citrate, there is not enough citrate to keep the particles from aggregating and the solution becomes cloudy and clumped.

Table 1.2 The effect of citrate concentration on reaction time, mean particle size, and size deviation. Reproduced from Ref. 4 with permission from The Royal Society of Chemistry.

Citrate (mg.)	Approximate Time for the Completion of Reaction in min.	Mean Particle Size in Å	% Deviation
50 (standard)	5·0	200	12·5
25	5·0	145	9·4
10	2·0	165	11·8
5	1·2	240	12·1
3·75	2·0	dirty and clumped	
2·5	2·0	dirty and clumped	

They finally investigated the effects of dilutions of the solutions (Table 1.3) and found that the more concentrated solution resulted in smaller particle diameters, a faster reaction time, and smaller size deviation.

Table 1.3 The effect of dilution on reaction time, mean particle size, and size deviation. Reproduced from Ref. 4 with permission from The Royal Society of Chemistry.

Dilution	Approximate Time for the Completion of Reaction in min.	Mean Particle Size in Å	% Deviation
1/2	2	174	10·4
1 (standard)	5	200	12·5
2	6	235	12·6

The citrate synthesis has the advantages of rapid time of completion, that it takes place in a single phase, and that it can be adjusted to make slightly different size particles by changing temperature, concentration of citrate, and the dilution. The main disadvantage of the citrate synthesis is that it is unable to make particles smaller than about 14 nm. Another possible disadvantage is that the gold nanoparticles are capped and stabilized by citrate; therefore, ligand exchange becomes necessary for other applications where citrate is not desired.

1.1.2 Brust-Schiffrin synthesis

Another commonly used synthesis method is the Brust-Schiffrin (B-S) synthesis. Brust *et al.* synthesized gold nanoparticles by taking $HAuCl_4$ in an aqueous phase, and then phase transferring the gold precursor into toluene by the addition of tetraoctylammonium bromide (TOAB). Once in the toluene phase, dodecanethiol and sodium borohydride ($NaBH_4$) are introduced to reduce the Au(III) to Au(I) and then Au(0).[11] The ratio they used of starting material was four to one thiol to gold salt and a ten to one ratio of reducing agent to gold salt. This synthesis yields monodisperse thiolate-protected gold nanoparticles that are between one and three nanometers in diameter with the majority of them between two and two-and-half

nanometers. Both experimental and theoretical researchers have investigated the reduction of Au(III) to Au(I) because of the original hypothesis of Alvarez *et al.* that Au(I) oligomers formed and their further reduction led to growth into nanoparticles.[12] Goulet and Lennox were the first to suggest that a ratio of two thiols to one Au(III) was enough to cause the reduction to Au(I); however, they did not agree that a higher ratio of thiol to gold formed polymers in toluene.[13] As discussed in chapter 3, Barngrover and Aikens later confirmed by using density functional theory (DFT) that a two to one ratio of thiol to gold was enough to cause reduction.[14] However, they agreed with Alvarez *et al.* about the formation of Au(I) polymers in polar solvents and the possibility of further reduction leading to nanoparticle growth, as discussed in chapter 5. The debate on which Au(I) species are present is not completely resolved, but a 2014 paper by Luo *et al.* using time resolved UV-Visible absorption and electrospray ionization mass spectrometry (ESI-MS) and a mild reducing agent, CO, has shed a little light on what the Au(I) species could be.[15] Luo *et al.* were able to isolate the Au(I) species before the CO reduction occurred and were able to uniquely identify 12 species. The Au(I) species vary from $Au(SR)Cl^-$ and $Au(SR)_2^-$ up to larger anionic chains and rings (Figure 1.1.2.1). These species were previously identified by Barngrover and Aikens, as discussed in chapter 3.

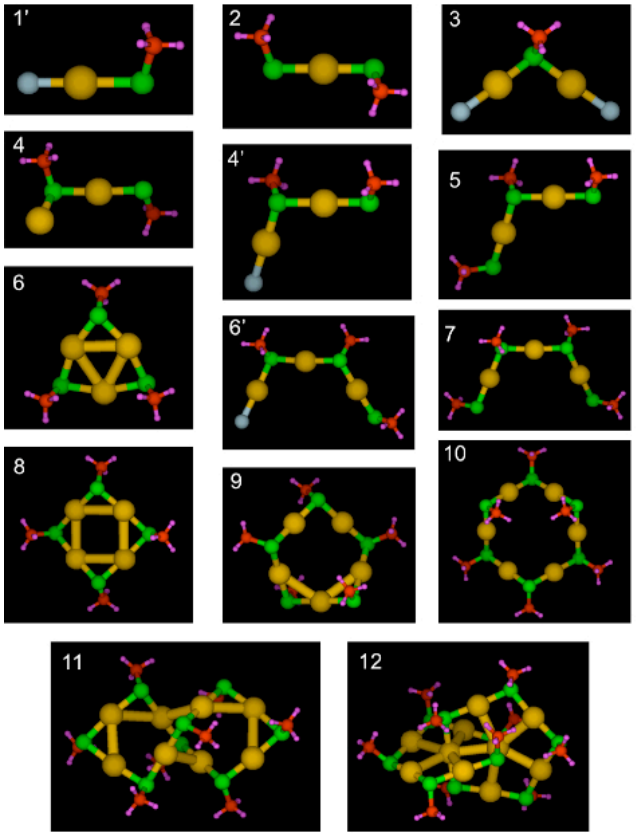

Complex precursors ($0\ e^-$)	
1'	$[Au(SR)Cl]^-$
2	$[Au(SR)_2]^-$
3	$[Au_2(SR)Cl_2]^-$
4	$Au_2(SR)_2$
4'	$[Au_2(SR)_2Cl]^-$
5	$[Au_2(SR)_3]^-$
6	$Au_3(SR)_3$
6'	$[Au_3(SR)_3Cl]^-$
7	$[Au_3(SR)_4]^-$
8	$Au_4(SR)_4$
9	$Au_5(SR)_5$
10	$Au_6(SR)_6$
11	$Au_8(SR)_8$
12	$Au_{10}(SR)_{10}$

Figure 1.1 Optimized DFT structures of the 12 unique precursors. Reprinted with permission from Ref. 15. Copyright 2014 American Chemical Society.

The debate on if the Au(I) species are single molecules, chains, or rings under all synthetic conditions is still unresolved. A further discussion of these precursors and their stabilities will be presented in chapters 4 and 5.

To gain other insights, researchers have made modifications to the original B-S synthesis including small changes such as the Au(III) salt used[16] and the ratio of thiol to Au(III) used,[13,17] to much more drastic changes like changing the number of phases from a two phase synthesis to a single phase synthesis,[17,18] changing the reducing agent from $NaBH_4$ to stronger reducing agents such as 9-BBN or lithium triethylborohydride (known as "superhydride"), or changing from thiols to thiolates. The thiolate variation is more dramatic because the thiolates are not in aqueous solutions and must be stabilized by long halogenated alkyl chains[19] or with electron withdrawing groups.[20] It has been suggested that the phase transfer agent can stabilize particles;

therefore it can both keep particles from forming polymers and can also be used as a capping agent.[21]

1.1.3 Nucleation of gold nanoparticles

Smoluchowski formulated equations to describe the coagulation process of individual atoms into clusters or small particles.[22] This is important for the formation of gold nanoparticles and has three defined steps: growth, nucleation, and coagulation. The first step, growth, is the coming together of individual atoms into small dimers, trimers, tetramers, etc. The second step, nucleation, is bringing the small clusters/polymers together to form stable nuclei. The final step, coagulation, is the aggregation of nuclei into the final stable particle size. The particle size depends on the synthesis method. In early synthesis of gold nanoparticles, nucleation was thought to occur because of impurities in the solution.[10] Turkevich and coworkers proposed what they called the "organizer" mechanism for nucleation. Their mechanism is similar to that of fluctuation theory; fluctuation theory assumes the solution is supersaturated and the statistical fluctuations of random atoms coalesce together to form a particle that is thermodynamically stable. The organizer mechanism assumes the gradual build up of small complexes that chemically bind to each other and undergo a rearrangement at a critical size. For the purpose of this thesis the small complexes would be the Au(I) species. Abécassis *et al.* and Perala *et al*. suggested that a stable nucleus contained ten gold atoms, which is similar to the smallest particle synthesized by the B-S method.[23,24]

1.1.4 Growth of gold nanoparticles

It is difficult to separate out the growth and nucleation components of nanoparticle synthesis; this is due to the fact that the reducing agent used usually contributes to both aspects. Perala *et al*. proposed a continuous nucleation-growth-passivation mechanism, where the nucleus

is formed, and the growth of the particle and the passivation of the particle continually occur until the particle reaches a stable size.[24] The reducing agent is typically the driving force that starts the gradual build up of precursor complexes. As previously stated, the Au(I) species are the main precursors; however as described in chapter 6 they generally have an aurophilic interaction with each other and do not progress the reaction without the kick start of the reducing agent. The exception is $AuClSR^-$; this particular Au(I) molecule can polymerize in polar solvents into larger anionic chains or neutral $Au_x(SR)_x$ rings as shown in chapter 3. Depending on the syntheses used, particles can grow into almost any desired size and shape, ranging from a few nanometers, typically called nanoclusters, up to a micron in diameter with shapes ranging from spheres to star-shaped rods.

1.1.5 Post processing of gold nanoparticles

Sometimes the desired size or shape of a gold nanoparticle cannot be obtained directly from the synthesis. Lin *et al*. first introduced digestive ripening in 2000.[25] Digestive ripening is a technique that takes polydisperse nanoparticles with the addition of excess thiol ligand and etches the particles down to a more desirable size and monodisperse shape. This method helps demonstrate the continuous nucleation-growth-passivation mechanism by showing that if particles are nonuniform that a post processing method can remove the outer layers of gold species and the nanoparticle can rearrange into a more homogeneous shape.

1.1.6 Solvated metal atom dispersion and self-assembled monolayers

So far in this introduction I have talked about the reductive property of thiols; however, they can also be used as an oxidant on Au(0) clusters. Two examples of this arise from the solvated metal atom dispersion (SMAD) method and self-assembled monolayers (SAMs), which both start from clusters or layers of Au(0). The Au(0) cluster or layer is oxidized on the surface

by the incoming thiol and forms oligomeric motifs referred to as "staple motifs".[26-29] These staple motifs are seen to passivate a wide variety of gold nanoparticles such as $Au_{25}(SR)_{18}^{-/0}$,[30-33] $Au_{36}(SR)_{24}$,[34] $Au_{38}(SR)_{24}$,[35,36] and $Au_{102}(SR)_{44}$.[37] There is recent work that suggests that other binding motifs may be possible for sterically demanding thiolates.[38,39]

Stoeva *et al.* introduced SMAD as a synthesis method for making thiolate-protected gold nanoparticles in 2002.[40] SMAD takes atoms from a metal vapor and traps them in a frozen solvent such as tetrahydrofuran (THF) at 77 K, then the system is allowed to warm up and the atoms wander together to yield clusters and colloids. After the cluster and colloids are formed, thiol is reacted with the system to form the nanoparticles ranging in diameter from 2 to 40 nanometers. Digestive ripening of the SMAD-produced particles yields a size of 4.5 ± 0.4 nm.

The gold atoms are in the zero valence oxidation state and the reacting thiol oxidizes the surface to the +1 state. A further discussion of thiols oxidizing gold clusters is provided in chapter 7.

1.2 Objectives and overview of the thesis

As previously discussed, nanoparticles are used in a wide variety of applications; however, the growth of the particles is not well understood. Groups have started to investigate the growth mechanism instead of simply using trial and error to obtain the desired nanoparticles at the end of the synthesis. The main objective of this thesis is to investigate the growth mechanism of gold thiolate nanoparticles starting from Au(III) and Au(0) precursors. A secondary objective is examining the mechanism of $Au_{25}(SH)_{18}^-$ as a selective hydrogenation catalyst for the formation of unsaturated alcohol or aldehyde from an α,β-unsaturated ketone.

Chapter 2 details the theory and computational methods used in this research. Chapter 3 (Barngrover, B. M.; Aikens, C. M. *J. Am. Chem. Soc.* **2012**, *134*, 12590) examines the reduction of gold(III) to gold(I) by the addition of methylthiol in methanol. In chapter 4 (Barngrover, B. M.; Aikens, C. M. *J. Phys. Chem. A* **2011**, *115*, 11818), the binding energies of gold(I) and silver(I) thiolate oligomers are analyzed. The reduction of gold(I) oligomer species by hydride and electron addition are investigated in chapter 5 (modified from Barngrover, B. M.; Aikens, C. M. *J. Phys. Chem. Lett.* **2011**, *2*, 990). The reduction of Au(I) species to Au(0) non-radical species are studied in chapter 6 (Barngrover, B. M.; Manges, T. J.; Aikens, C. M. *J. Phys. Chem. A* **2015**, *119*, 889). Chapter 7 (Barngrover, B. M.; Aikens, C. M. *J. Phys. Chem. A* **2013**, *117*, 5377) describes the oxidation of gold clusters by methylthiol. In chapter 8, the catalysis of acrolein or 2-propenal by $Au_{25}(SH)_{18}^-$ is examined.

Chapter 2 - Theory and Computational Methods

2.1 Quantum mechanics

2.1.1 The Schrödinger equation

Newton's laws of motion drive the macroscopic world and are described by classical mechanics. However, classical mechanics fails to describe the behavior of small particles such as the subatomic particles that make up the universe because the exact position and velocity of the subatomic particles cannot be known simultaneously, as shown by the Heisenberg uncertainty principle. However, the laws of quantum mechanics can describe the behavior of these small systems. In quantum mechanics, the basic knowledge that can be obtained for the system of interest is contained in the state function or wave function Ψ.[41] The time-dependent Schrödinger equation describes the state of a quantum mechanical system. In this thesis the systems of interest experience no time-dependent external forces, so the simpler time-independent Schrödinger equation is used, which is:

$$\hat{H}\psi(r) = E\psi(r) \tag{2.1}$$

where ψ is the time-independent wave function that depends only on position (**r**) and not time, E is the energy of the system, and $\hat{H}$ is the Hamiltonian defined as:

$$\hat{H}(r) = -\frac{\hbar^2}{2m}\nabla^2 + V(r) \tag{2.2}$$

In the system, $\hbar$ is defined as $h/2\pi$ where h is Planck's constant and the mass of the particle corresponds to m. The Laplacian operator ∇^2 refers to the second derivative with respect to the particle position. The first term of the Hamiltonian represents the kinetic energy of the particles. The second term corresponds to the potential energy of the particles.

2.1.2 The Born-Oppenheimer Approximation

The Schrödinger equation can be solved exactly with a full Hamiltonian for only a limited number of cases, including the harmonic oscillator, hydrogen atom, and particle in a box. However, for multi-electron systems this is not possible without making approximations. This is because the full Hamiltonian includes all the interactions of the electrons and nuclei in the system making the Schrödinger equation very complicated to solve. This full Hamiltonian for molecules may be written as:

$$\hat{H} = -\frac{\hbar^2}{2}\sum_{\alpha}\frac{1}{m_\alpha}\nabla_\alpha^2 - \frac{\hbar^2}{2m_e}\sum_i \nabla_i^2 + \sum_\alpha\sum_{\beta>\alpha}\frac{Z_\alpha Z_\beta e'^2}{r_{\alpha\beta}} - \sum_\alpha\sum_i\frac{Z_\alpha e'^2}{r_{i\alpha}} + \sum_j\sum_{i>j}\frac{e'^2}{r_{ij}} \quad (2.3)$$

where α and β denote the nuclei and *i* and *j* denote the electrons. The first term is the kinetic energy for the nuclei and the second term is the kinetic energy for the electrons. The third term is the potential energy arising from repulsion between the nuclei and $r_{\alpha\beta}$ is the distance between the two nuclei with atomic numbers Z_α and Z_β. The fourth term is the potential energy of attraction between the electrons and nuclei and $r_{i\alpha}$ is the distance between the electron *i* and nucleus α. The last term is the potential energy of repulsion between the electrons and r_{ij} is the distance between the two electrons.[41]

To make the full Hamiltonian more manageable to calculate for a wider range of systems, the electronic and nuclear parts can be separated. In addition, the nuclei are much heavier than the electrons; therefore, the nuclei can be treated as fixed points and thus the kinetic energy term for the nuclei in equation 2.3 can be neglected and the third term is a constant. This approximation is called the Born-Oppenheimer Approximation. The new Hamiltonian for electronic motion is:

$$\hat{H} = \hat{H}_{el} + V_{NN} \quad (2.4)$$

where the pure electronic Hamiltonian ($\hat{H}_{el}$) can be written as:

$$\hat{H}_{el} = -\frac{\hbar^2}{2m_e}\sum_i \nabla_i^2 - \sum_\alpha \sum_i \frac{Z_\alpha e'^2}{r_{i\alpha}} + \sum_j \sum_{i>j} \frac{e'^2}{r_{ij}} \qquad (2.5)$$

and the nuclear-repulsion term V_{NN} is:

$$V_{NN} = \sum_\alpha \sum_{\beta>\alpha} \frac{Z_\alpha Z_\beta e'^2}{r_{\alpha\beta}} \qquad (2.6)$$

Since V_{NN} is a constant for any set of nuclear coordinates, it can be omitted from the time-independent Schrödinger equation (eq. 2.1). This gives the equation:

$$\hat{H}_{el}\psi_{el} = E_{el}\psi_{el} \qquad (2.7)$$

Equation 2.7 can be solved for any number of nuclear configurations making the purely electronic energy (E_{el}) and electronic wave function (ψ_{el}) depend parametrically on the nuclear coordinates. The nuclear-repulsion term (eq. 2.6) can now be added to E_{el} to obtain the electronic energy including internuclear repulsion (U).

$$U = E_{el} + V_{NN} \qquad (2.8)$$

2.1.3 Relativistic effects

Relativistic effects are small corrections to the Schrödinger equation to deal with the increase of mass of electrons when they are traveling close to the speed of light. The equation for the relativistic mass of an electron is:

$$m_{rel} = \frac{m_e}{\sqrt{1-(\frac{v_e}{c})^2}} \qquad (2.9)$$

where m_e is the mass of an electron, v_e is the velocity of an electron, and c is the speed of light. If the Bohr radius given by the equation:

$$a_0 = \frac{4\pi\varepsilon_0\hbar^2}{m_e e^2} \tag{2.10}$$

where $\hbar$ is equal to $h/2\pi$ and h is Planck's constant, ε_0 is the permittivity of a vacuum, and e is the elementary charge, combining eqs. 2.9 and 2.10 gives the resulting equation:

$$a_{rel} = \frac{4\pi\varepsilon_0\hbar^2\sqrt{1-(v_e/c)^2}}{m_e e^2} \tag{2.11}$$

Equation 2.11 gives the relativistic Bohr radius in SI units. A ratio of the relativistic Bohr radius to the nonrelativistic Bohr radius can simplify the equation to:

$$\frac{a_{rel}}{a_0} = \sqrt{1-\left(\frac{v_e}{c}\right)^2} \tag{2.12}$$

If a hydrogen-like atom is considered, the velocity of an electron (v_e) can be simplified to:

$$v_e = \frac{Z}{n} \tag{2.13}$$

where Z is the atomic number and n is the principle quantum number. Substituting eq. 2.13 into eq. 2.12 results in:

$$\frac{a_{rel}}{a_0} = \sqrt{1-\left(\frac{Z}{nc}\right)^2} \tag{2.14}$$

Eq. 2.14 shows that for low n values and high Z values electrons will have a higher probability of being nearer to the nucleus. A nucleus with a large charge will cause an electron to have a high velocity. A higher electron velocity means an increased electron relativistic mass, and as a result the electrons will be near the nucleus more often. Since this thesis deals with gold and silver nanoparticles, relativistic effects are a major component to include in the calculations.

2.2 Computational methods

2.2.1 Density functional theory (DFT)

Density functional theory (DFT) is a popular method employed in physics and chemistry because of its ability to calculate ground state energies (E_0) reasonably accurately based on the density of that ground state (ρ_0). DFT, using the pure electronic Hamiltonian (eq. 2.2), contains only one and two electron spatial terms, meaning that only six spatial coordinates (x_1, x_2, y_1, y_2, z_1 and z_2) are needed for the integration to find the ground state energy unlike the electronic wave function of an n-electron molecule that depends on $3n$ spatial and n spin coordinates to find the ground state energy.

2.2.2 The Hohenberg-Kohn theorem

Hohenberg and Kohn proved that for nondegenerate ground states of molecules, the molecular ground state energy, wave function, and all other molecular electronic properties are unique and are only dependent on the ground state electronic probability density (ρ_0).[42] The ground state electronic wave function of an n-electron molecule is an eigenfunction of the pure electronic Hamiltonian (eq. 2.7) and the second term in DFT is called the external potential $v(\mathbf{r}_i)$, defined as:

$$v(\mathbf{r}_i) = -\sum_{\alpha} \frac{Z_\alpha}{r_{i\alpha}} \tag{2.15}$$

Once the external potential and the number of electrons are specified, the electronic Schrödinger equation is solved for the electronic wave function and energies of the molecule. Hohenberg and Kohn demonstrated that the ground state electronic probability density determines the external potential and the number of electrons. The ground state electronic energy is a functional of the ground state electronic probability density ($E_0 = E_0[\rho_0]$). The pure electronic Hamiltonian is the sum of all the electronic components: the electronic kinetic energy, the electron-nuclear attractions, and the electron-electron repulsions. Therefore, ρ_0 is the sum of the density contributions given by the equation:

$$E_0 = E_v\left[\rho_0\right] = \bar{T}\left[\rho_0\right] + \bar{V}_{Ne}\left[\rho_0\right] + \bar{V}_{ee}\left[\rho_0\right] \tag{2.16}$$

where E_v is the external potential energy, T is the kinetic energy, V_{Ne} is the nuclear-electron attraction, and V_{ee} is the electron-electron repulsion. The bars over the terms mean average. The external potential within the Born-Oppenheimer approximation gives a unique V_{Ne} for a determined number of electrons and nuclei. However, the electronic kinetic energy and the electron-electron repulsion terms are dependent on the external potential but have no known functional form, thus resulting in an impractical way to calculate E_0 from ρ_0.

2.2.3 The Kohn-Sham (KS) Method

To actually solve for E_0 from ρ_0, Kohn and Sham introduced a fictitious reference system of non-interacting particles, typically electrons, which generate the same density as any given system of interacting particles.[43] The Kohn–Sham (KS) equation is defined by a local effective

fictitious external potential, $v_s(\mathbf{r})$, in which the non-interacting particles move, called the Kohn–Sham potential. The Hamiltonian of the reference system is:

$$\hat{H}_s = \sum_{i=1}^{n}\left[-\frac{1}{2}\nabla_i^2 + v_s(r_i)\right] \equiv \sum_{i=1}^{n}\hat{h}_i^{KS} \tag{2.17}$$

where $\hat{h}_i^{KS}$ is the one-electron Kohn-Sham Hamiltonian. The reference Hamiltonian can be related to a real molecular Hamiltonian by:

$$\hat{H}_\lambda \equiv \hat{T} + \sum\nolimits_i v_\lambda(r_i) + \lambda\hat{V}_{ee} \tag{2.18}$$

where λ ranges from zero to one with zero being the reference system and one being the real system and v_λ is defined as the external potential that will equate the ground state electron density of the reference system and the real system. Since the reference system is defined as not having interacting particles and is required to be antisymmetric, the ground state wave function ($\psi_{s,0}$) is the Slater determinant of the lowest energy Kohn-Sham spin orbitals u_i^{KS}. The spatial part of the spin orbital ($\theta_i^{KS}(\mathbf{r}_i)$) is an eigenfucntion of the one electron operator $\hat{h}_i^{KS}$. They are related by the equation:

$$\psi_{s,0} = \left|u_1^{KS}u_2^{KS}...u_n^{KS}\right| \quad , \quad u_i^{KS} = \theta_i^{KS}(r_i)\sigma_i \tag{2.19}$$

where σ_i is a spin factor. The Kohn-Sham equation is defined as:

$$\hat{h}_i^{KS}\theta_i^{KS} = \varepsilon_i^{KS}\theta_i^{KS} \tag{2.20}$$

where ε_i^{KS} is the Kohn-Sham orbital energy. Kohn-Sham rewrote the Hohenberg-Kohn equation (eq. 2.16) by defining the unknown components as follows:

$$\Delta\bar{T}[\rho] \equiv \bar{T}[\rho] - \bar{T}_s[\rho] \tag{2.21}$$

$$\Delta\bar{V}_{ee}[\rho] \equiv \bar{V}_{ee}[\rho] - \frac{1}{2}\iint \frac{\rho(\mathbf{r}_1)\rho(\mathbf{r}_2)}{r_{12}}\, d\mathbf{r}_1 d\mathbf{r}_2 \quad (2.22)$$

Equation 2.21 is the difference in the average ground state electronic kinetic energy between the real system and the reference system. Equation 2.22 is the difference in the average ground state electron-electron repulsion of the real system and the classical electrostatic interelectronic repulsion energy if the electrons were smeared out. The new Kohn-Sham equation is:

$$E_0 = E_v[\rho] = \int \rho(r)v(r)dr + \bar{T}_s[\rho] + \frac{1}{2}\iint \frac{\rho(\mathbf{r}_1)\rho(\mathbf{r}_2)}{r_{12}}\, d\mathbf{r}_1 d\mathbf{r}_2 + \Delta\bar{T}[\rho] + \Delta\bar{V}_{ee}[\rho] \quad (2.23)$$

The last two terms are defined as the exchange-correlation energy functional $E_{xc}[\rho]$. The key to accurate KS DFT calculations of molecular properties is to get a good approximation to $E_{xc}[\rho]$. By varying the KS orbitals that determine the density by the equation:

$$\rho = \rho_s = \sum_{i=1}^{n} \left|\theta_i^{KS}\right|^2 \quad (2.24)$$

and defining the exchange-correlation potential (υ_{xc}) as $\delta E_{xc}/\delta\rho$, the Kohn-Sham Schrödinger equation (eq. 2.20) can be rewritten to include (υ_{xc}) and is defined as:

$$\hat{h}^{KS}(1)\theta_i^{KS}(1) = \varepsilon_i^{KS}\theta_i^{KS}(1) \quad (2.25)$$

KS equations are solved self-consistently:

1) Take initial guess of the KS orbitals θ_i^{KS}.

   Calculate ρ from equation 2.24.

2) Construct the KS operator $\hat{h}_i^{KS}$ using the potential given in equation 2.17.

3) Solve the KS equation 2.20 using the KS operator derived in step 2 to get new improved orbitals θ_i^{KS}.

4) Calculate the new ρ'. If E[ρ']–E[ρ] < Δ, where Δ is a preset convergence criterion, the calculation is converged. Otherwise, go back to step 1 with improved orbitals and repeat until converged.

2.2.4 Functionals

In 2000, John Perdew introduced the hierarchy or Jacob's ladder of DFT functionals (Table 2.1).[44] Climbing up the ladder typically increases precision of calculations but also increases the computational resources needed to complete the calculation. The first rung of the ladder is the local-density approximation (LDA), which as the name suggests only depends on the local density, which will be described in more detail below. The second rung is the generalized gradient approximation (GGA), which depends on the local density and the gradient of the density. The third rung called meta-GGA builds on the first two rungs and adds the kinetic energy density or the second derivative of the density gradient or both. The next rung is hybrid functionals; they are based on the lower rungs and incorporate exact HF exchange (eq. 2.26).

$$E_x = -\frac{1}{4}\sum_{i=1}^{n}\sum_{j=1}^{n}\left\langle \theta_i^{KS}(1)\theta_j^{KS}(2)\left|\frac{1}{r_{12}}\right|\theta_j^{KS}(1)\theta_i^{KS}(2)\right\rangle \qquad (2.26)$$

Table 2.1 Jacob's ladder of functionals

Functional category	Dependences	Common Examples
LDA	ρ	VWN[45]
GGA	$\rho, \nabla\rho$	BP86[46, 47], PBE[48]
Meta-GGA	$\rho, \nabla\rho, \nabla^2\rho$ and/or τ	TPSS[49]
Hybrid	$\rho, \nabla\rho, \nabla^2\rho$ and/or τ and *HF*	B3LYP[46, 50]

2.2.4.1 The Local-Density Approximation (LDA)

Hohenberg and Kohn showed that when ρ varies slowly with respect to position, the local-density approximation exchange-correlation energy functional ($E_{xc}^{LDA}[\rho]$) is given by:

$$E_{xc}^{LDA}[\rho] = \int \rho(r)\varepsilon_{xc}(\rho)\, d\mathbf{r} \tag{2.27}$$

where ***dr*** stands for integration over all space, and the $\varepsilon_{xc}(\rho)$ is the exchange and the correlation energy per electron in a jellium. A jellium or homogenous electron gas is a hypothetical electrically neutral, infinite volume system with a uniformly distributed infinite number of interacting electrons and positive charges moving continuously.[51] The quantity $\varepsilon_{xc}(\rho)$ can be separated into the sum of the exchange and correlation parts and for the Slater LDA the exchange functional is:

$$\varepsilon_x(\rho) = -\frac{3}{4}\left(\frac{3}{\pi}\right)^{1/3}\left(\rho(r)\right)^{1/3} \tag{2.28}$$

To make full use of LDA, a correlation part most be selected and added to the exchange functional.

2.2.4.2 The Generalized gradient approximation (GGA)

To improve upon LDA, the system must be uncoupled from the jellium and be able to handle a non-uniform electron gas. The development was the generalized gradient approximation (GGA) that includes not only the dependence on the local density but also the derivative of the density. Two popular GGA's were developed by Becke and Perdew (BP86)[16,17] and by Perdew, Burke, and Ernzerhof (PBE).[48] The exchange correlation correction by Becke is:

$$\varepsilon_x^{B88} = \varepsilon_x^{LDA} + \Delta\varepsilon_x^{B88}$$
$$\Delta\varepsilon_x^{B88} = -\beta\rho^{1/3}\frac{x^2}{1+6\beta x\sinh^{-1}x} \qquad (2.29)$$
$$x = \frac{|\nabla\rho|}{\rho^{4/3}}$$

where β is a parameter fit to known data for the rare gas atoms using the dimensionless gradient variable *x*. Becke's addition only corrects the exchange part and must be paired with a correlation correction; the one used in this thesis is the one of Perdew given by the equation:

$$\varepsilon_c = \int d^3n\varepsilon_c + \int d^3r d^{-1}e^{-\Phi}C(n)|\nabla n|^2 / n^{4/3} \qquad (2.30)$$

where

$$\Phi = 1.745\tilde{f}\left[\frac{C(\infty)}{C(n)}\right]\frac{|\nabla n|}{n^{7/6}} \qquad (2.31)$$

where ε_c is the correlation value from LDA and $\tilde{f}$ is the cutoff value set to 0.11 from the exact correlation energy of the neon atom.

The PBE functional contains both exchange and correlation functionals. The exchange part is given by the following equations:

$$\varepsilon_x^{PBE} = \varepsilon_x^{LDA}F(x)$$
$$F(x) = 1 + a - \frac{a}{1+bx^2} \qquad (2.32)$$

where *a* and *b* are constants. The correlation part is given by the following equations:

$$\varepsilon_c^{PBE} = \varepsilon_c^{LDA} + H\left(t\right)$$
$$H\left(t\right) = cf_3^3 \ln\left[1 + dt^2\left(\frac{1 + At^2}{1 + At^2 + A^2t^4}\right)\right]$$
$$A = d\left[\exp\left(-\frac{\varepsilon_c^{LDA}}{cf_3^3}\right) - 1\right]^{-1} \tag{2.33}$$
$$f_3\left(\zeta\right) = \frac{1}{2}\left[\left(1+\zeta\right)^{2/3} + \left(1-\zeta\right)^{2/3}\right]$$
$$t = \left[2\left(3\pi^3\right)^{1/3} f_3\right]^{-1} x$$

where c and d are constants and ζ is the relative spin polarization where $\zeta = (n_\alpha - n_\beta)/n$.

2.2.4.3 meta-GGA

A further advancement is to include the second derivative of the density ($\nabla^2\rho$) or the kinetic energy density (τ), which gives the meta-GGA functionals. The generalized equation for meta-GGA is:

$$E_{xc}^{mGGA}\left[\rho\right] = \int f\left(\rho, \nabla\rho, \nabla^2\rho, \tau\right)dr \tag{2.34}$$

where

$$\tau \equiv \frac{1}{2}\sum_i^n \left|\nabla\phi_i^{KS}\right|^2 \tag{2.35}$$

Most meta-GGA's use the kinetic energy density instead of the second derivative of the density. The kinetic energy density is numerically more stable than calculation of the second derivative of the density. A common meta-GGA used is TPSS which is a non-empirical functional.[49]

2.2.5 Basis Sets

Atomic orbitals are represented by basis functions. There are three types of basis functions commonly used; they are the Slater type orbitals (STO), Gaussian type orbitals (GTO) and plane waves. The STOs have the form of:

$$\chi_{\zeta,n,l,m} = NY_{l,m}(\theta,\varphi) r^{n-1} e^{-\zeta r} \tag{2.36}$$

where N is the normalization constant and $Y_{l,m}$ are the spherical harmonic functions. To model the behavior of a hydrogen atom orbital, the STOs have an exponential dependence. This dependence also helps to ensure rapid convergence.

The GTOs have the form of:

$$\chi_{\zeta,n,l,m} = NY_{l,m}(\theta,\varphi) r^{2n-2-l} e^{-\zeta r^2} \tag{2.37}$$

The GTO dependence on r^2 in the exponential leads to potential issues because it has a hard time modeling behavior near the nucleus since it has zero slope instead of a cusp like a STO. The GTO also falls off too quickly at distances far from the nucleus and the tail of the wave function is represented poorly. The STO is superior to the GTO based on the fact that it takes typically three times as many GTOs to represent a single STO to obtain the same level of accuracy. The reason Gaussian orbitals are often used is that the four-index integrals that have to be calculated can be expressed analytically as opposed to numerically with Slater functions. Both STOs and GTOs are localized basis sets; plane wave basis sets are delocalized and have a hard time describing small systems. However plane wave basis sets work well for periodic calculations because they need fewer functions to describe the system compared to STOs and GTOs. The plane wave function has the form

$$e^{i(kx+ly+mz)} \tag{2.38}$$

where k, l, and m are constants. A plane wave basis set scales with the size of the periodic cell and not the system described in the cell; however, larger cells typically require more basis functions. The number of STOs and GTOs scales linearly with the size of the system. To obtain highly accurate DFT calculations, a complete basis set is required; however this is not always practical so a basis set is chosen to balance accuracy and computational cost. A complete basis set is an infinite number of basis functions needed to describe a system completely. The other extreme is to choose a minimal basis set, which is a basis set that has the minimum number of functions to cover the number of atomic orbitals of each atom of interest. An improvement on the minimal basis set that is still smaller than the complete basis set is to add functions to each atomic orbital. Doubling the number of atomic orbitals is called double zeta, tripling the number of atomic orbitals is called triple zeta, quadrupling the number of atomic orbitals is called quadruple zeta, and so forth. Increasing the number of atomic orbitals continues until the complete basis set limit is reached. Because the core electron density does not change much during chemical bonding, having a large number of basis functions in the non-changing core does not typically increase the accuracy of the calculation. However the valence electron density changes and ideally can be described with more basis functions. This increase in valence basis functions but not the core basis functions is called a split valence basis. To increase the flexibility even further, additional functions can be added to include the polarizability of bonds. The use of frozen core orbitals can also be applied to speed up calculations. Frozen core orbitals occur when the core orbitals are fixed to a set value and do not interact in the bonding of the system.

2.2.6 Zeroth Order Regular Approximation (ZORA): Relativistic Effects

As mentioned previously, relativistic effects are important in this thesis; they are included by the zeroth order regular approximation (ZORA).[52,53] To make the Schrödinger equation include special relativity, Dirac expressed the one electron Hamiltonian as:

$$\hat{H} = \left(c\alpha p + \beta mc^2 \right) + V \tag{2.39}$$

where c is the speed of light, p is the momentum, and α and β are 4x4 Dirac matrices. Since the Dirac Hamiltonian contains 4x4 matrices, the Dirac wave function (Ψ^D) has four components, $\Psi^{L\alpha}$, $\Psi^{L\beta}$, $\Psi^{s\alpha}$, and $\Psi^{s\beta}$, where L is the large component or the electronic part of the wave function and s is the small component or the positronic part of the wave function. Only the large component is needed to describe electronic states but both components must be in relation to each other to avoid variational collapse. The large component wave function has the form:

$$\Psi^L = \left(\frac{1}{2c} k\sigma \cdot p \right) \Psi^s \tag{2.40}$$

where $k = \left(1 - \frac{V - E}{2c^2} \right)$. The parameter k is expanded in a power series that is cut off at the zeroth order to become ZORA. ZORA has the following form:

$$\left[\frac{c^2 p^2}{2mc^2 - V} + \frac{2c^2}{\left(2mc^2 - V \right)^2} - \frac{Zs \cdot l}{r^3} + V \right] \Psi^L = E\Psi^L \tag{2.41}$$

where s is the electron spin and l is the angular momentum operator.[51]

2.2.7 Continuum Solvation Models

Up to this point the discussion has focused on gas phase calculations, but not all reactions occur in the gas phase. Methods exist to include solvation into the calculations. One method is to include the solvent molecule directly into the calculation as part of the system; this method is called explicit solvation. This ensures that the solvent molecule is directly affecting the molecule of interest; however, the exact number of solvent molecules needed is unclear and computational requirements rise rapidly with the increased number of atoms. Another method is to use an implicit solvent or continuum solvent model. A continuum solvent treats the solvent as a uniform polarizable medium with a dielectric constant and the solute is contained inside a cavity. The cavity for the solute is usually made to match the shape but it can vary. The continuum solvent energy is calculated by the summation of the cavity energy plus the dispersion energy plus the electronic energy.[51] In this thesis, the Amsterdam Density Functional (ADF)[54] program is used and the continuum solvent is implemented by the Conductor-like Screening Model (COSMO).[55] COSMO involves a Green function dielectric operator acting on an arbitrary shape. The shape or cavity is made from taking the Van der Waals radius of the atom and adding the solvation radius to yield the effective solvation radius. The dielectric screening is polarized over the cavity with the majority of the screening occurring between the solvation radius and the effective solvation radius. The cavity electron density is calculated along with the density matrix of the molecule and is added as either an additional term if it does not depend on the density matrix or it is added into the Hamiltonian if it does depend on the density matrix.[55]

Chapter 3 - The Golden Pathway to Thiolate-Stabilized Nanoparticles: Following the Formation of Gold(I) Thiolate from Gold(III) Chloride

Reproduced with permission from:

Barngrover, B. M.; Aikens, C. M. *J. Am. Chem. Soc.* **2012**, *134*, 12590.

3.1 Abstract

Pathways for the formation of gold thiolate complexes from gold(III) chloride precursors $AuCl_4^-$ and $AuCl_3$ are examined. This work demonstrates that two distinct reaction pathways are possible; which pathway is accessible in a given reaction may depend on factors such as the residue group R on the incoming thiol. Density functional theory calculations using the BP86 functional and a polarized triple-ζ basis set show that the pathway resulting in gold(III) reduction is favored for R=methyl. A two-to-one ratio of thiol or thiolate to gold can reduce Au(III) to Au(I), and a three-to-one ratio can lead to polymeric Au(SR) species, which was first suggested by Schaaff *et al.* [*J. Phys. Chem. B*, **1997**, 101, 7885] and later confirmed by Goulet and Lennox [*J. Am. Chem. Soc.*, **2010**, 132, 9582]. Most transition states in the pathways examined here have reasonable barrier heights around 0.3 eV; we find two barrier heights that differ substantially from this which suggest the potential for kinetic control in the first step of thiolate-protected gold nanoparticle growth.

3.2 Introduction

Gold thiolate nanoparticles have been synthesized for many years without a good understanding of the reaction pathway between the gold(III) chloride species and the thiols. Gold nanoparticles are often synthesized using the Brust-Schiffrin method[11] or a modified version.[13,19,56,57] Until now, a limited number of studies have examined the synthesis mechanism. The Brust-Schiffrin synthesis is a two-phase synthesis that starts with tetrachloroaurate in water, which is phase-transferred into toluene where the thiol ligands are then introduced in a three-to-one ratio. The reducing agent, in this case sodium borohydride, is then added resulting in 1-3 nm diameter gold particles. This synthesis method is often chosen for the reliability of the resulting monodisperse gold thiolate nanoparticles. Modified versions of the Brust-Schiffrin synthesis include changes in the ratio of thiol ligands to gold halide salt[17] and in the number of phases that the reaction takes place in, usually a change from two phases to a single phase.[17,18] The use of the original Brust-Schiffrin or a modified version depends on the desired size and morphology of the synthesized gold thiolated nanoparticles, because these characteristics affect the physical and chemical properties of the nanoparticles.[58,59]

A three-to-one thiol to gold ratio was first suggested by Schaaff *et al.* to cause the formation of gold-thiolate oligomers.[60] Later Goulet *et al.* verified that a three-to-one ratio does form oligomers of gold thiolate.[13] They also concluded in their work that a two-to-one ratio of thiol ligands to gold salt causes reduction of the gold salt from Au(III) to Au(I) and forms a disulfide.[13]

Anionic chain oligomers of $Au(SR)_2^-$ and $Au_2(SR)_3^-$ are of significant interest since they are attached to the outside of many gold nanoparticles including $Au_{25}(SR)_{18}^-$, $Au_{38}(SR)_{24}$, and $Au_{102}(SR)_{44}$.[56,61-65] They have also been predicted to passivate $Au_{144}(SR)_{60}$[66] and are observed on

self-assembled monolayers (SAMs).[67-70] Longer chains of $Au_3(SR)_4^-$ are suggested by Zeng *et al*. and Jiang *et al.* to passivate $Au_{20}(SR)_{16}$ and by Garzón *et al.* to passivate $Au_{18}(SR)_{14}$.[71-73] In addition, some anti-arthritis drugs are helical or ring-like gold-thiolate oligomers that have been characterized with x-ray crystallography.[1,74] These chains or rings could be involved in the growth of nanoparticles. Barngrover and Aikens recently demonstrated that hydride addition in the second step of the Brust-Schiffrin synthesis reduces the chains and rings and forms gold-gold bonds, which could represent the start of gold nanoparticle growth.[75] Zeng *et al.* determined that reduced rings could be interlocked to form catenane ring structures and could be brought together to form $Au_{20}(SR)_{16}$.[76]

Other modified Brust-Schiffrin syntheses use different Au(III) precursor molecules; for example, $AuCl_3$ can be substituted in place of $AuCl_4^-$.[16] Futhermore, thiolates can be employed instead of thiols in the pursuit of synthesizing gold thiolate nanoparticles. Thiolates allow the synthesis to occur in fewer steps, since removal of the thiol proton is not necessary during the chloride ligand replacements. However, due to their unstable nature in aqueous solutions thiolates must be stabilized with long halogenated alkyl chains[19] or with electron withdrawing groups.[20]

3.3 Computational Details

All calculations are performed with the Amsterdam Density Functional (ADF)[5430] package, using density functional theory with the Becke Perdew (BP86)[46,47] functional and a frozen-core polarized triple-ζ (TZP) basis set. We include scalar relativistic effects by employing the Zero Order Regular Approximation (ZORA).[53] We incorporate the methanol solvent using the Conductor-like Screening Model (COSMO), which represents the solvent by its dielectric constant. [55,77-79]

Calculations described in this work employ the methyl group on the thiol or thiolate ligand unless otherwise stated. All intermediates and transition states are fully optimized; Hessian calculations have been performed to verify the existence of one imaginary frequency for the transition states. Energies reported in this work include zero-point energy corrections, which are typically on the order of hundredths of an eV.

3.4 Results and Discussion

3.4.1 First Thiol Reaction

In this work, we investigate the step-wise addition of methylthiol to gold(III) chloride in

Pathway A

$AuCl_4^- + HSCH_3 \rightarrow AuCl_3HSCH_3 + Cl^-$ (1)

$AuCl_3HSCH_3 + Cl^- \rightarrow AuCl_3SCH_3^- + HCl$ (1')

$AuCl_3SCH_3^- + HSCH_3 \rightarrow AuCl_2HSCH_3SCH_3 + Cl^-$ (2A)

$AuCl_2HSCH_3SCH_3 + Cl^- \rightarrow AuCl_2(SCH_3)_2^- + HCl$ (2A')

$AuCl_2(SCH_3)_2^- + HSCH_3 \rightarrow AuClHSCH_3(SCH_3)_2 + Cl^-$ (3A)

$AuClHSCH_3(SCH_3)_2 + HSCH_3 \rightarrow Au(HSCH_3)_2(SCH_3)_2^+ + Cl^-$ (4A)

$Au(HSCH_3)_2(SCH_3)_2^+ + Cl^- \rightarrow Au(HSCH_3)(SCH_3)_3 + HCl$ (4A')

Pathway B

$AuCl_4^- + HSCH_3 \rightarrow AuCl_3HSCH_3 + Cl^-$ (1)

$AuCl_3HSCH_3 + Cl^- \rightarrow AuCl_3SCH_3^- + HCl$ (1')

Scheme 3.1 Overall reaction of four thiol additions to $AuCl_4^-$.
Pathway A leads to Au(III) product while pathway B leads to Au(I) product.

a methanol solvent. The entire pathway involving four thiol additions is shown in Scheme 1. The first addition proceeds through a bipyramidal transition state with a calculated barrier height of 0.34 eV and results in the dissociation of a chloride ion with a reaction energy of -0.03 eV (Figure 3.1). The chloride ion can subsequently react with the thiol proton to cause the proton to

dissociate and bind to the chloride. The proton dissociation has an energy of -0.14 eV. These two steps may be summarized as

$$AuCl_4^- + HSCH_3 \rightarrow AuCl_3HSCH_3 + Cl^- \quad (1)$$

$$AuCl_3HSCH_3 + Cl^- \rightarrow AuCl_3SCH_3^- + HCl \quad (1')$$

where the prime denotes the proton dissociation step. In neutral solution, the Cl^- species is more likely to perform this acid-base reaction than the solvent or free thiol (Appendix Table A1). The two steps that occur during the first thiol addition have not yet been observed experimentally.

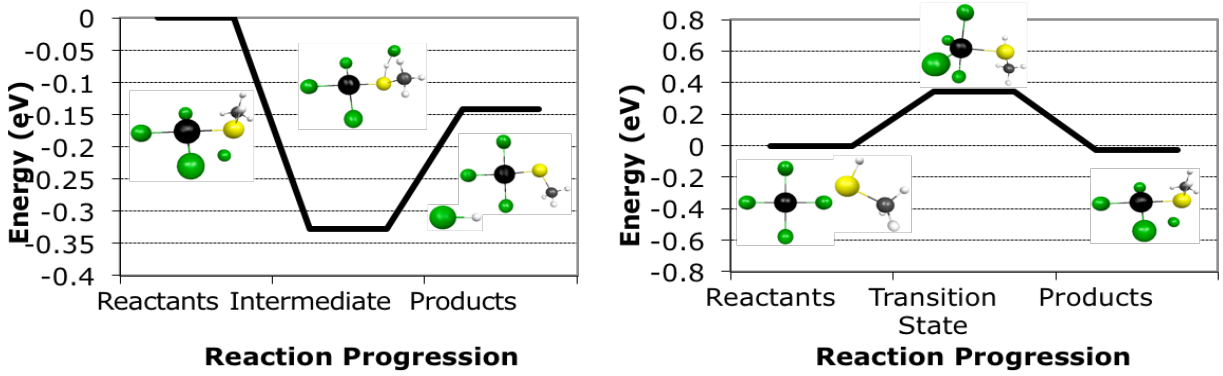

Figure 3.1 Reaction pathway for the first thiol addition to $AuCl_4^-$ and subsequent proton dissociation.

3.4.2 Second Thiol Reaction

The second addition of thiol to the now monosubstituted gold complex has two different potential reaction pathways. The first pathway 2A is the less kinetically favored pathway for the methyl ligand, where the thiol reacts through another bipyramidal transition state with a barrier height of 0.37 eV and ejects a chloride ion off the monosubstituted gold to form a disubstituted Au(III) complex (Figure 3.2a) according to:

$$AuCl_3SR^- + HSR \rightarrow AuCl_2(HSR)(SR) + Cl^- \quad (2A)$$

In this pathway the trans configuration is preferred over the cis configuration with reaction energies of 0.03 and 0.04 eV, respectively. In step 2A', the recently ejected chloride ion

is able to react with the proton attached to the newly added thiol, which causes the proton to dissociate analogously to step 1'. This proton dissociation has a reaction energy of -0.09 eV.

$$AuCl_2(HSR)SR + Cl^- \rightarrow AuCl_2(SR)_2^- + HCl \qquad (2A')$$

In the second, more kinetically favored pathway 2B, the thiol reacts with the thiolate and forms a protonated disulfide (Figure 3.2b). When the protonated disulfide forms, the remaining gold chloride complex is reduced to a gold(I) species and a chloride ion is released.

$$AuCl_3SR^- + HSR \rightarrow AuCl_2^- + HRSSR^+ + Cl^- \qquad (2B)$$

This reaction has a barrier height of 0.14 eV. The overall reaction energy is computed to be 0.16 eV for infinitely separated products; since this does not account for various molecular interactions and basis set superposition error, a single point energy calculation for all three products is performed, and the overall reaction energy is computed to be 0.11 eV. Although this reaction (which forms the protonated disulfide) has a positive reaction energy, the overall reaction energy can be lowered by -0.58 eV if a chloride ion deprotonates the protonated disulfide (Figure 3.2b) according to

$$HRSSR^+ + Cl^- \rightarrow RSSR + HCl \qquad (2B')$$

Goulet and Lennox found that one equivalent of thiol led to half of an equivalent of the Au(I) complex;[2] this suggests that the second thiol addition step occurs faster than the first step, which is in agreement with the barrier heights found in our current work.

Although we have focused the above discussion on the two most preferred pathways, other products could potentially be formed from the addition of two thiols to $AuCl_4^-$; the overall energies for these additional reactions are shown in Table 3.1. In general, reduction of Au(III)-containing species to Au(I)-containing species is thermodynamically favored. The formation of free anions is also thermodynamically favored over the formation of the related diatomic gas.

The proton from the incoming thiol can transfer to the disulfide making it a singly or doubly protonated species, bind with chloride to form HCl, or remain on the thiol. The most thermodynamically favored option is for the proton to bind with chloride resulting in HCl and an unprotonated disulfide and gold complex. The option of protonating the disulfide is the least favored.

a.

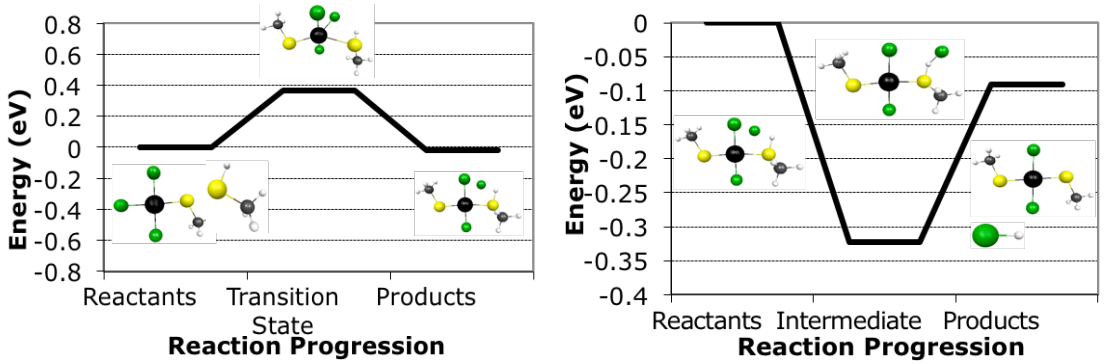

b.

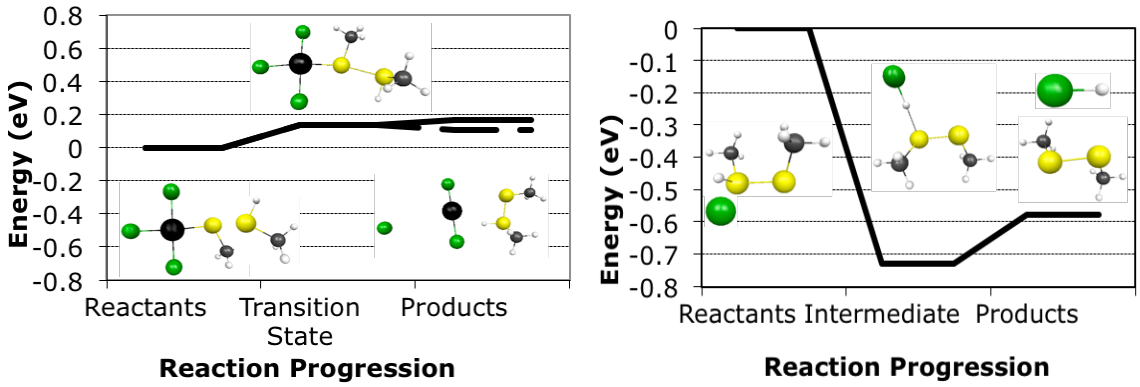

Figure 3.2 a) Reaction pathway A for second thiol addition leading to Au(III) product followed by proton dissociation. b) Reaction pathway B leading to Au(I) product followed by proton dissociation from the disulfide. The dotted line in figure b is the single point energy of the dissociated products, whereas the solid line represents the energy of the infinitely separated products; the discrepancy may be due to interactions between the species or basis set superposition error.

Table 3.1 Overall Reaction Energies of Two Thiol Additions

Products	Reaction Energies (eV)
$2HCl + RSSR + AuCl_2^-$	-0.58[b]
$2HCl + AuCl_2(SR)_2^-$	-0.01[a]
$2HCl + Cl_2 + Au(SR)_2^-$	1.70
$HCl + Cl^- + RSSRH^+ + AuCl_2^-$	-0.01
$HCl + Cl^- + AuCl_2(HSR)(SR)$	0.33
$HCl + Cl^- + Cl_2 + Au(HSR)(SR)$	1.25
$2Cl^- + HRSSRH^{2+} + AuCl_2^-$	1.53
$2Cl^- + AuCl_2(HSR)_2^+$	0.11
$2Cl^- + Cl_2 + Au(HSR)_2^+$	1.15
$H_2 + Cl_2 + RSSR + AuCl_2^-$	1.56
$H_2 + Cl_2 + AuCl_2(SR)_2^-$	2.14
$H_2 + 2Cl_2 + Au(SR)_2^-$	3.85

a. Pathway A. b. Pathway B.

3.4.3 Third Thiol Reaction

Now we turn to the addition of the third thiol in pathways A and B. In the third addition step 3A, we see the continuing trend of chloride ion removal and the formation of a trisubstituted gold(III) complex; however, this chloride does not dissociate the thiol proton. This reaction energy is less than -0.01 eV and the barrier height is 0.62 eV (Figure 3.3a).

$$AuCl_2(SR)_2^- + HSR \rightarrow AuCl(HSR)(SR)_2 + Cl^- \quad (3A)$$

In pathway 3B the thiol also reacts and ejects a chloride ion to form a monosubstituted gold(I) complex with a reaction energy of -0.10 eV and a barrier height of 0.26 eV (Figure 3.3b).

$$AuCl_2^- + HSR \rightarrow AuClHSR + Cl^- \quad (3B)$$

For the methyl ligand examined in this work, pathway 3B is both kinetically and thermodynamically favored over pathway 3A. The proton does not dissociate upon subsequent interaction with the chloride ion. Since the barrier height of pathway 3B is higher than for pathway 2B, the second thiol addition is likely to complete before pathway 3B becomes operative, which again agrees with the results of Goulet and Lennox that $AuCl_2^-$ is formed after addition of two equivalents of thiol.[2]

a.

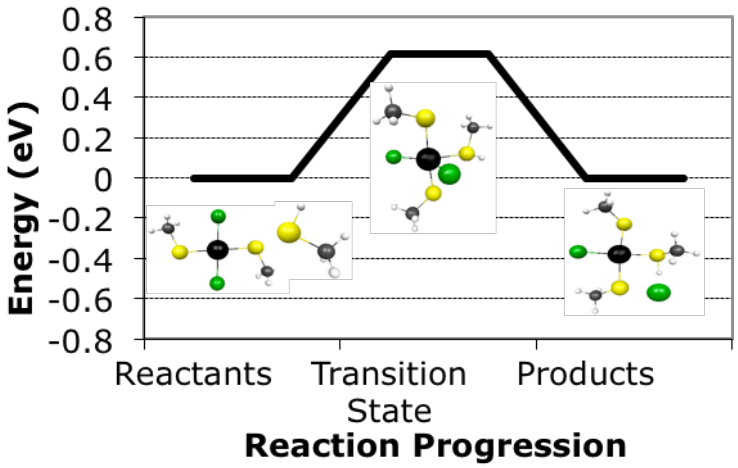

b.

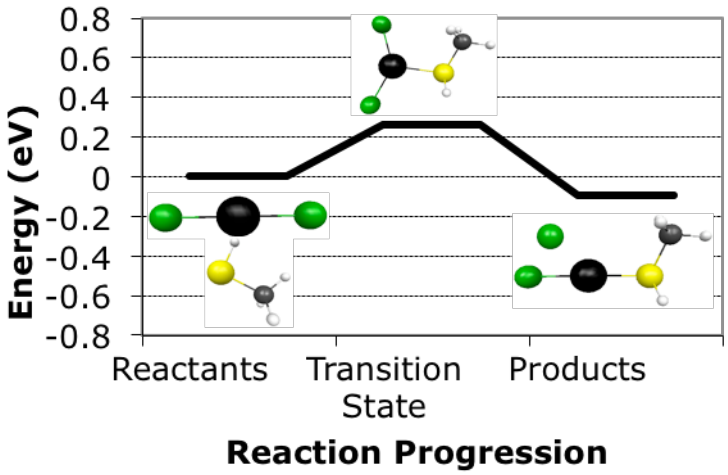

Figure 3.3 Third thiol addition in a) pathway A with Au(III) species, and b) pathway B with Au(I) species.

3.4.4 Fourth Thiol Reaction

The fourth addition to pathways A and B causes the removal of the remaining chloride ligand, resulting in a fully substituted gold complex. The barrier height for the gold(III) pathway 4A is 0.34 eV with a reaction energy of -0.20 eV (Figure 3.4a). Proton dissociation lowers the overall reaction by -0.19 eV.

$$AuCl(HSR)(SR)_2 + HSR \rightarrow Au(HSR)_2(SR)_2^+ + Cl^- \quad (4A)$$

$$Au(HSR)_2(SR)_2^+ + Cl^- \rightarrow Au(HSR)(SR)_3 + HCl \quad (4A')$$

The gold(I) pathway 4B has a barrier height of 0.18 eV and a corresponding reaction energy of 0.14 eV (Figure 3.4b). The proton dissociation is not favored thermodynamically.

$$AuClHSR + HSR \rightarrow Au(HSR)_2^+ + Cl^- \quad (4B)$$

The overall energy for pathway A is -0.02 eV, and the overall energy for pathway B is -0.54 eV. These pathways are summarized in Scheme 3.1. Table 3.2 displays the overall reactions possible for the addition of four thiols. Many products can form from the addition of four thiols to $AuCl_4^-$. However, only the two most likely pathways are discussed in detail in this paper. The most thermodynamically favored products are disulfide and the doubly protonated Au(I) complex. The singly protonated Au(I) species is the second most favored product. The related doubly and singly protonated Au(III) species are also thermodynamically favored compared to the other Au(III) complexes but not as much as the Au(I) complexes for the $R=CH_3$ ligand. Although the chloride ion often accepts a proton in the first two steps of the reaction, the thiol proton can remain attached to the gold complex in the last two steps.

a.

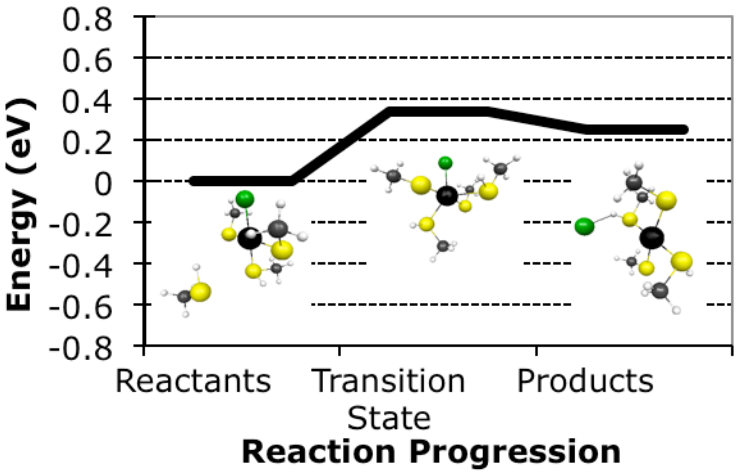

b.

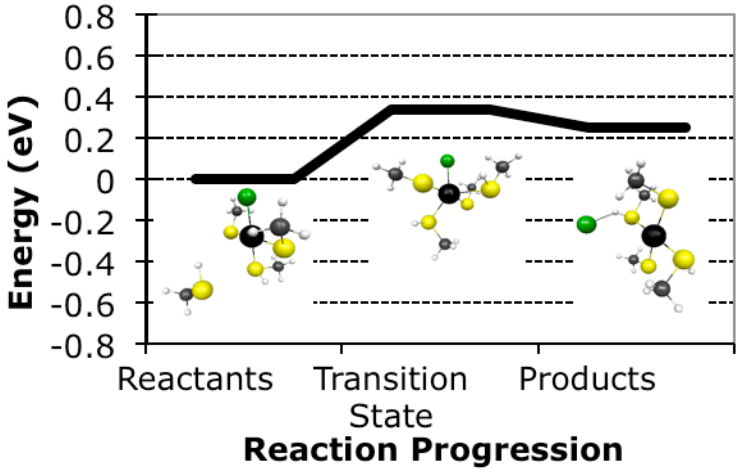

Figure 3.4 Fourth thiol addition in a) pathway A (Au(III) species) and b) pathway B (Au(I)).

Table 3.2 Overall Reactions Energies of Four Thiol Additions

Products	Reaction Energies (eV)
$4Cl^- + HRSSRH^{2+} + Au(HSR)_2^+$	1.58
$4Cl^- + Au(HSR)_4^{3+}$	1.66
$3Cl^- + HCl + RSSRH^+ + Au(HSR)_2^+$	0.04
$3Cl^- + HCl + Au(HSR)_3(SR)^{2+}$	0.62
$2Cl^- + 2HCl + RSSR + Au(HSR)_2^+$	-0.54[b]
$2Cl^- + 2HCl + RSSRH^+ + Au(HSR)(SR)$	0.14
$2Cl^- + 2HCl + HRSSRH^{2+} + Au(SR)_2^-$	2.13
$2Cl^- + 2HCl + Au(HSR)_2(SR)_2^+$	0.17
$1Cl^- + 3HCl + RSSR + Au(HSR)(SR)$	-0.44
$1Cl^- + 3HCl + RSSRH^+ + Au(SR)_2^-$	0.59
$1Cl^- + 3HCl + Au(HSR)(SR)_3$	-0.02[a]
$4HCl + RSSR + Au(SR)_2^-$	0.01
$4HCl + Au(SR)_4^-$	0.08

a. Pathway A. b. Pathway B.

3.4.5 R Group Dependence

Methyl as the residue group does not lead to proton dissociation from $AuClHSCH_3$. A more electron-withdrawing group could cause the thiol proton to become quite acidic and dissociate. We see a significant change in reaction energy of chloride ion induced proton dissociation from AuClHSR depending on the R group. When the residue group is phenyl this reaction has an overall reaction energy of less than 0.01 eV, compared to methyl as a residue group which has an overall reaction energy of 0.32 eV. Another option is for the reaction to take place in a basic solution, which will help dissociate the proton. Energies for other bases used to

remove the thiol proton can be found in the Appendix A, Table A1. This is important because the removal of the proton allows for the formation of chains and rings as described below, which may be the precursor to gold thiolate nanoparticles.

It should also be noted that Bachman *et al.* demonstrated that if electron withdrawing ligands are used the Au(III) complex can be obtained instead of the Au(I) species.[20] This suggests that variation of the R group may be used to provide kinetic and/or thermodynamic control of pathways A and B.

3.4.6 Thiolate vs. Thiol Addition

One-step additions can occur if thiolates are used instead of thiols. Thiolate additions proceed in either one of the two pathways through the gold(III) species or the gold(I) species. The gold(I) pathway with the reduction to $Au(SCH_3)_2^-$ and the formation of the disulfide is slightly more favored with a reaction energy of -4.63 eV compared to the gold(III) analog which has a reaction energy of -4.56 eV (Table 3.3). The thiolate additions are much more thermodynamically favored than their thiol analogs. This could be advantageous or could be a hindrance due to the spontaneity of the reaction, leaving little control of the reaction.

Table 3.3 Overall Reaction Energies of Four Thiolate Additions

Products	Reaction Energy (eV)
$4Cl^- + RSSR + Au(SR)_2^-$	-4.63
$4Cl^- + Au(SR)_4^-$	-4.56

3.4.7 Effect of Thiol Ratio

Varying the ratio of thiol to tetrachloroaurate allows for different degrees of ligand substitution. A one-to-one ratio usually results in a single substitution of ligands, the removal of chloride ion and the addition of thiol. Increasing the ratio to two-to-one can result in either a

second ligand exchange or can result in in the formation of a disulfide and reduction of the gold(III) to gold(I) which is in agreement with Goulet *et al*.[13] Note that control over the barrier heights of steps 1 and 2 is needed to lead to monosubstituted products since current procedures instead lead to half of an equivalent of disubstituted products.[13] This could potentially be achieved with the use of various residue groups such as electron withdrawing groups. Further increasing the ratio to three-to-one results in either the trisubstituted gold(III) complex or the first substitution on the gold(I) complex. A final increase of the ratio to four-to-one produces the gold(III) thiol(ate) complex or the gold(I) thiol complex; the gold(III) thiol(ate) species is possible with electron withdrawing ligands.[20]

3.4.8 Reactions Starting from $AuCl_3$

Tetrachloroaurate is the most common starting material although $AuCl_3$ is occasionally used as well.[16] The only difference occurs in the first thiol addition; addition of thiol to $AuCl_4^-$ causes the ejection of a chloride ion whereas reactions with $AuCl_3$ do not eject this ion. Addition to $AuCl_3$ results in a greater overall reaction energy (Table 3.4). The product, $AuCl_3HSR$, can then react in the same manner as described above.

Table 3.4 Reaction Energies of $AuCl_4^-$ and $AuCl_3$ with Thiol and Thiolate

	$AuCl_4^-$	$AuCl_3$
Thiol	-0.17 eV*/-0.03 eV$^+$	-2.54 eV
Thiolate	-1.33 eV	-3.84 eV

*Thiol proton dissociated to chloride and $^+$No thiol proton dissociation

3.4.9 Formation of Gold-Thiolate Chains and Rings

Removal of the thiol proton after the third addition of thiol is important because sulfur will then have two lone pairs, which allows it to react with another gold atom. This leads to the dimerization of two $AuClSCH_3^-$ (Figure 3.5). When the two monomers react, the internal

chlorine is ejected to form a chloride ion, allowing the sulfur and gold to form a bond; this dimerization has a reaction energy of -0.37 eV and a barrier height of 0.33 eV. The new subunit has a terminal chlorine, which can be used to initiate further monomer additions to form a long chain. We investigated trimers, tetramers, and octomers. The trimer can be formed from the dimer and a monomer with an overall reaction energy of -0.35 eV. The tetramer can be formed from the previous trimer and a monomer with an overall energy of -0.36 eV. The octomer investigated in this work is formed from two tetramers to demonstrate that longer chains could be made in this manner instead of adding monomers to the progressively growing chains; this reaction has an energy of approximately -0.3 eV (not including zero-point energy). Once a chain is formed, it can also cyclize. An example of cyclization is illustrated in Figure 3.6; this process has an overall reaction energy of -0.22 eV and a barrier height of 0.36 eV. A TΔS correction value has been calculated for the cyclization process with an energy of 0.026 eV, which suggests that the entropy change is not significant for this process. Cyclized products such as $(AuSR)_4$ have been observed experimentally by various mass spectrometry methods by multiple groups including Gies *et al.,* Dass and co-workers, and Negishi *et al.*[80-85] In addition, these oligomers may be involved in the second step of gold nanoparticle growth.[75]

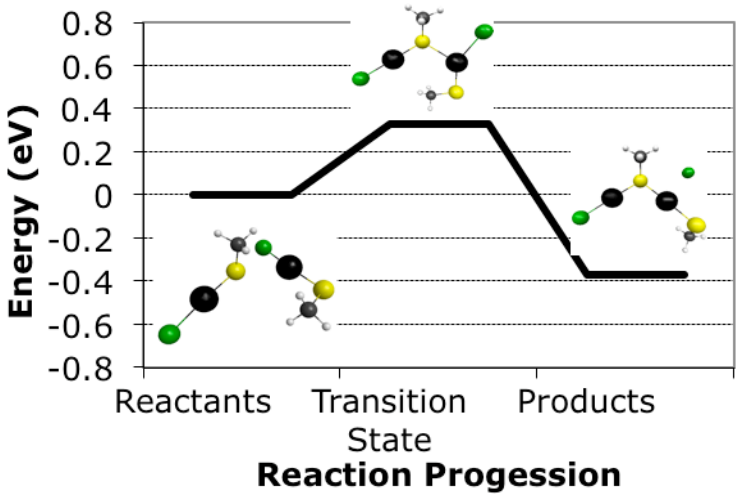

Figure 3.5 Dimerization of $AuClSCH_3^-$.

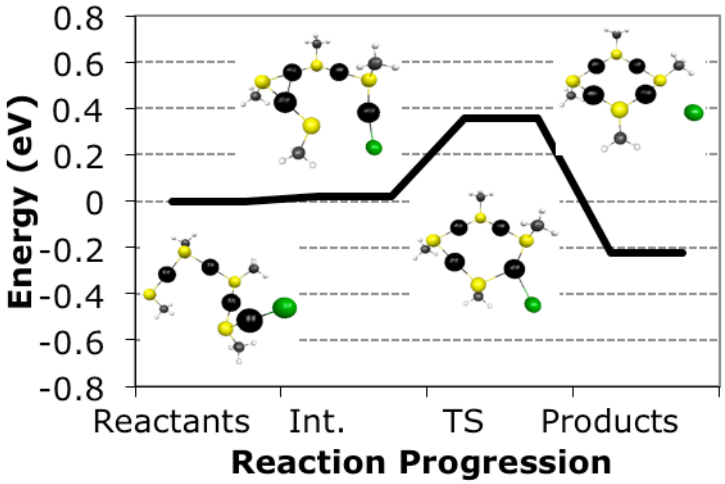

Figure 3.6 Cyclization of $Au_4(SCH_3)_4Cl^-$.
Int. = Intermediate and TS = Transition State

3.5 Conclusions

Gold(I) thiolate nanoclusters and nanoparticles have been synthesized for many years with little understanding of the mechanism that is responsible for their formation. This work suggests a mechanism for the first step of the Brust-Schiffrin synthesis method. Our calculations with a two-to-one ratio of methylthiol to gold salt show that reduction of gold(III) to gold(I) and the formation of a disulfide is thermodynamically favored which agrees with previous experimental work. The fate of the thiol proton is determined and it does not have to remain on

the thiol; it is actually thermodynamically favored to dissociate to bind with the chloride ion. We have also demonstrated that a three-to-one ratio of thiol to gold salt can lead to polymeric chains of AuSR, an idea first proposed by Schaaff *et al.* in 1997 and later confirmed by Goulet *et al.* These polymeric chains can grow to various sizes or cyclize into rings such as $(AuSR)_4$ which have been seen experimentally in mass spectrometry work. Those chains and rings could then be reduced in the second step of the Brust-Schiffrin synthesis as discussed previously in Ref. 75. Our investigation also examined the transition states for the thiol additions to the gold species and revealed that the gold(III) structures go through a trigonal bipyramidal transition state with reasonable barrier heights of about 0.3 eV. Two distinct pathways were examined; one that leads to the reduction of gold(III) to gold(I) or the other that exchanges all of the halide ligands on Au(III) for sulfur containing ligands. Either pathway can be potentially relevant depending on the type of residue groups attached to the sulfur, such as long halogenated alkyl chains or electron withdrawing groups. In addition, reactions with thiolates and with a $AuCl_3$ precursor have been studied in this work.

3.6 Acknowledgements

The authors would like to thank the Alfred P. Sloan Foundation for a Sloan Research Fellowship (2011-2013) and the Camille and Henry Dreyfus Foundation for a Camille Dreyfus Teacher-Scholar Award (2011-2016). The authors would also like to thank Kansas State University for additional funding that supported this research.

Chapter 4 - Incremental Binding Energies of Gold(I) and Silver(I) Thiolate Clusters

Reproduced with permission from:

Barngrover, B. M.; Aikens, C. M. *J. Phys. Chem. A* **2011**, *115*, 11818.

4.1 Abstract

Density functional theory is used to find incremental fragmentation energy, overall dissociation energy, and average monomer fragmentation energy of cyclic gold(I) thiolate clusters and anionic chain structures of gold(I) and silver(I) thiolate clusters as a measure of the relative stability of these systems. Two different functionals, BP86 and PBE, and two different basis sets, TZP and QZ4P, are employed. Anionic chains are examined with various residue groups including hydrogen, methyl, and phenyl. Hydrogen and methyl are shown to have approximately the same binding energy, which is higher than phenyl. Gold-thiolate clusters are bound more strongly than corresponding silver clusters. Lastly, binding energies are also calculated for pure $Au_{25}(SR)_{18}^-$, $Ag_{25}(SR)_{18}^-$, and mixed $Au_{13}(Ag_2(SH)_3)_6^-$ and $Ag_{13}(Au_2(SH)_3)_6^-$ nanoparticles.

4.2 Introduction

The precious metals of gold and silver have held special value to us since their discovery. Historically they were used as currency; now, however, they are used in many more applications, especially when employed on the nanoscale level with ligands. Some of the applications for gold(I) thiolate clusters are in antiarthritic and antitumor drugs as well as protein labeling, drug delivery, and sensing.[1,2,74] Silver thiolate clusters have applications as biosensors.[86]

In 2006, two groups independently studied the structures for cyclic metal methylthiolate clusters using density functional theory and found essentially the same lowest energy configurations.[87,88] Howell investigated $M_n(SR)_n$ (M = Cu, Ag, Au and n = 2-6) rings and found that the strain on the system is relieved at n = 4.[87] Grönbeck et al. studied the structures and fragmentation energies of cyclic $(AuSR)_n$ ($R = CH_3$, n = 2-12) using PBE.[88] They found that the smallest systems had planar structures while the larger structures went to a crown-like zigzag configuration.[88] The fragmentation energies of the systems converged at n = 4.[88] They showed that larger ligands such as hexylthiolate, benzenthiolate, and glutathionate have minor differences on the Au-S framework structure but no negligible effects on the HOMO-LUMO gap.[88]

More recent work by Zeng and coworkers suggested helical and catenane structures for the larger systems (n = 6-12).[89] A later study by Kacprzak et al. agreed that catenane structures are preferred for n = 10-12 but found crown structures to be lower energy that helical structures for n = 6-9.[90] They also examined fragmentation energy as function of the metal and found Cu > Au > Ag.[90]

Experimentally, gold(I) complexes have been crystallized and observed by many different groups.[74,91-93] The gold(I) crystals seen by Bau are helical in nature.[74] Simpson et al.,

LeBlanc and coworkers, and Wiseman et al. have all observed cyclic ring structures of gold(I) complexes.[91-93] Wiseman et al. also observed catenane structures for larger gold(I) clusters (n = 10, 12).[93]

Silver(I) complex crystals have also been synthesized and characterized by many groups.[94-98] Ahmed and coworkers have performed X-ray crystallography and observed tetrameric ring structure for a large silver (I) complex, whereas smaller structures adopt a chair-like configuration.[94] Dance et al. have studied many different silver(I) complexes by using X-ray crystallography and NMR and have seen cyclic clusters, bridged-linked monocyclic clusters, and layered silver(I) clusters.[95-98]

In addition, anionic chains such as $Au(SR)_2^-$ and $Au_2(SR)_3^-$ are observed on the outside of the core of many different size nanoparticles such as $Au_{25}(SR)_{18}^-$, $Au_{38}(SR)_{24}$, and $Au_{102}(SR)_{44}$.[56,61-65] They have been predicted to passivate $Au_{144}(SR)_{60}$[66] and are observed on self-assembled monolayers (SAMs).[67-70] A longer $Au_3(SR)_4^-$ chain was predicted by Zeng et al. and by Jiang et al. to passivate $Au_{20}(SR)_{16}$.[71,72] Moreover, these motifs could be precursors in nanoparticle growth.[57] In this work we calculate the binding energies of anionic chains since these could affect the sizes and structures of nanoparticles. The electronic structure and optical absorption of pure $Au_{25}(SH)_{18}^-$, $Ag_{25}(SH)_{18}^-$, and mixed $Au_{13}(Ag_2(SH)_3)_6^-$ and $Ag_{13}(Au_2(SH)_3)_6^-$ systems have previously been studied by Aikens,[99] so binding energies of the $M_2(SR)_3^-$ chains to the 13 atoms icosahedral cores are also studied in this work.

4.3 Computational Methods

The fragmentation energies for the gold and silver clusters are determined by using density functional theory with Becke Perdew (BP86)[46,47] and Perdew-Burke-Ernzerhof (PBE)[48] functionals and polarized triple zeta (TZP) and quadruple zeta (QZ4P) basis sets. A few energies

have also been calculated with the Tao-Perdew-Staroverov-Scuseria (TPSS) functional.[49] All calculations are performed using the Amsterdam Density Functional (ADF)[54] package. We include scalar relativistic effects by incorporating Zero Order Regular Approximation (ZORA)[53] The cluster sizes range from one to four metal atoms with corresponding thiolate ligands, which have hydrogen, methyl, or phenyl groups. Both functionals were also used to find the fragmentation energies of the cyclic gold thiolate clusters ranging from two to nine metal atoms.[88-90] Energies for both functionals are compared. The energies of interest are the incremental fragmentation energy, calculated as $E_{inc} = E[RS(MSR)_n^-] - E[MSR] - E[RS(MSR)_{n-1}^-]$ (M = Au, Ag and R = H, CH_3, Ph), and the overall dissociation energy which is calculated as $E_{total} = E[RS(MSR)_n^-] - (n+1)E[SR^-] - nE[M^+]$. In addition, an average monomer fragmentation energy is computed for cyclic systems as $E_{av} = [E[(AuSR)_n] - nE[AuSR]]/n$. The incremental and overall dissociation energies for the gold and silver clusters are calculated to determine the stability of the clusters. The same calculations are done on the mixed metal core nanoparticles for comparison with overall binding energy calculated as $E_{overall} = E[M_{13}(M_2(SR)_3)_6^-] - E[M_{13}^{+5}] - 6E[M_2(SR)_3^-]$ and average binding energy calculated as $E_{average} = E_{overall}/6$.

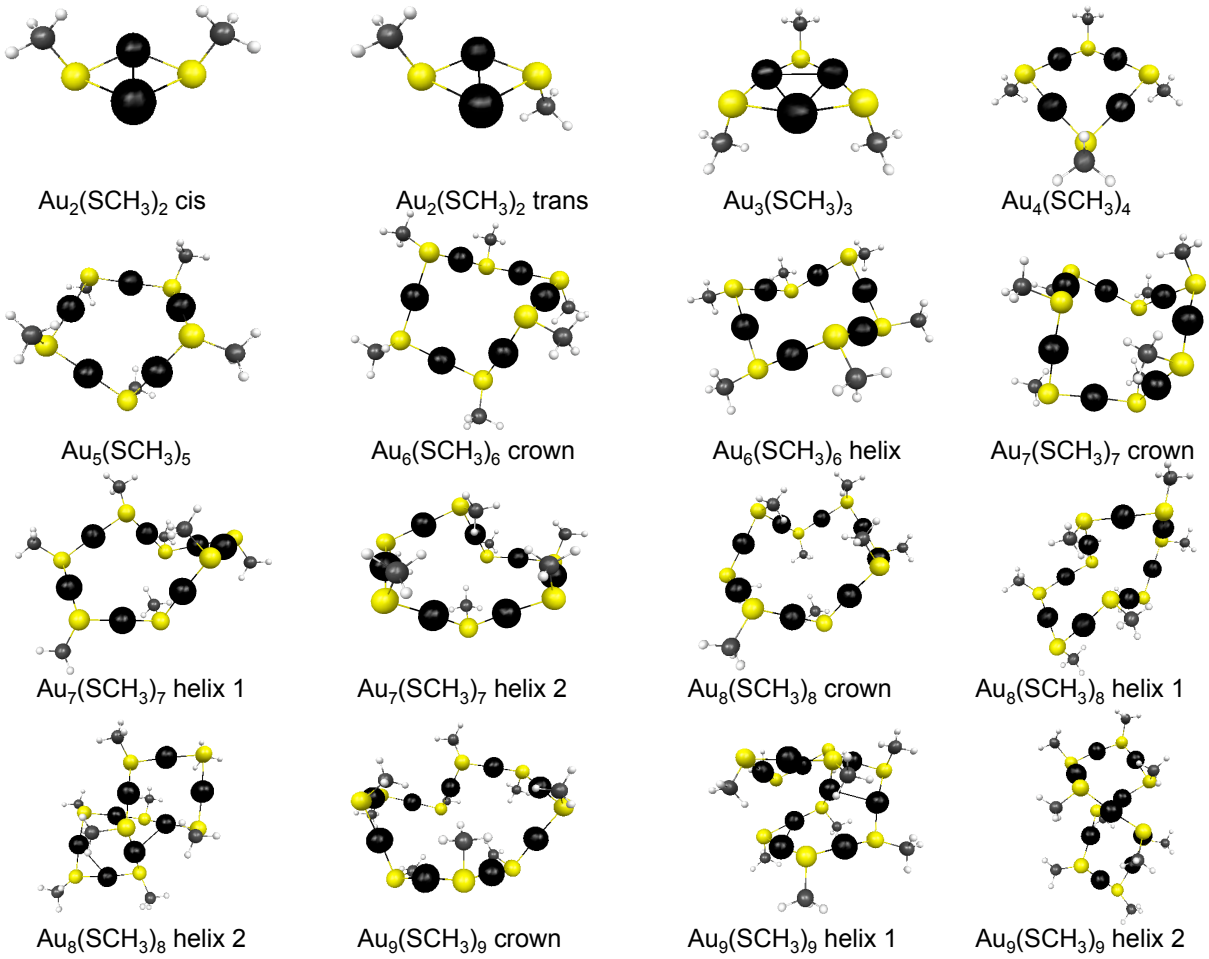

Figure 4.1 Optimized cyclic structures for $Au_x(SCH_3)_x$ (x = 2-9). Key: Au: black; S: yellow; C: grey; H: white

4.4 Results and Discussion

We performed calculations on cyclic methylthiolate gold clusters (Figure 4.1) and their anionic chain analogs. The values we calculated for E_{inc} and E_{av} shown in Table 4.1 are in agreement with Häkkinen, Grönbeck, and coworkers.[88,90] Our cyclic clusters are also in agreement with experimentally known gold structures found by Bau,[74] Simpson et al.,[91] LeBlanc et al.,[92] and Wiseman et al.[93] with sulfur-gold-sulfur bond angles of approximately 180 degrees, and gold-sulfur bond lengths of approximately 2.3 Å. The DFT calculations of the cyclic clusters showed that the dimers have BP86 monomer fragmentation energies of 1.07 eV for the cis configuration and 1.09 eV for the trans configuration. In comparison, the PBE monomer

fragmentation energies of the dimers are 1.17 eV for the cis configuration and 1.18 eV for the trans configuration. At the TPSS/TZP level of theory, these fragmentation energies are predicted to be 1.11 eV and 1.13 eV, respectively. These systems also have average binding energies of 0.54 eV and 0.55 eV for BP86 and 0.58 eV and 0.59 eV for PBE. The trimer is much higher in both monomer fragmentation and average binding energies than the dimers. The monomer fragmentation energy is 4.00 eV for BP86 and 4.07 eV for PBE, and average binding energy is 1.69 eV and 1.75 eV for BP86 and PBE, respectively. The monomer fragmentation energy at the TPSS level of theory is 4.06 eV, so both BP86 and PBE are in good agreement with this functional. As shown in Table 4.1, the cyclic clusters converge from four to six metal atoms with monomer energies about 1.90 eV for BP86 and about 2.00 eV for PBE, and average binding energies of 1.92 eV for BP86 and about 2.00 eV for PBE. Convergence is achieved when the incremental binding energies do not vary significantly from those of the next smaller sized cluster. Our values are in good agreement with data from Häkkinen.[88]

Table 4.1 Binding Energies of Cyclic Gold Methylthiolate Clusters

	BP86/TZP			PBE/TZP			PBE Ref. 88	
Group size	E_{inc} (eV)	E_{av} (eV)	E_{total} (eV)	E_{inc} (eV)	E_{av} (eV)	E_{total} (eV)	E_{inc} (eV)	E_{av} (eV)
Dimer cis	1.07	0.54	21.59	1.17	0.58	21.69	1.16	0.58
Dimer trans	1.09	0.55	21.61	1.18	0.59	21.70		
Trimer	4.00	1.69	35.86	4.07	1.75	36.04	4.07	1.74
Tetramer	2.58	1.91	48.69	2.65	1.98	48.95	2.61*	1.96
Pentamer	1.95	1.92	60.91	2.02	1.99	61.23	1.97	1.97
Hexamer-crown	1.89	1.92	73.06	1.96	1.98	73.45	2.01	1.98
Hexamer-helix	1.89	1.92	73.06	2.05	2.00	73.55		
Heptamer-helix 1	1.95	1.92	85.27	2.03	2.00	85.84		
Heptamer-helix 2	1.96	1.92	85.27	2.00	2.00	85.80		
Heptamer-crown	1.93	1.92	85.25	2.08	2.00	85.79	1.96	1.98
Octomer-helix 1	1.93	1.92	97.46	1.99	2.00	98.09		
Octomer-helix 2	1.91	1.92	97.45	2.05	2.00	98.11		
Octomer-crown	2.01	1.93	97.52	2.03	2.00	98.08	2.01	1.98
Nonomer-helix 1	1.83	1.91	109.55	1.99	2.00	110.35		
Nonomer-helix 2	1.95	1.92	109.66	2.05	2.01	110.43		
Nonomer-crown	1.89	1.93	109.68	1.97	2.00	110.31	1.96	1.97

*Corrected value (originally reported as 1.96)

Incremental energies for both the cyclic clusters and the anionic chains converge after four metals. The cyclic clusters are less stable than the anionic chains. For the cyclic clusters the incremental binding energies converge at 1.92 eV and 1.97 eV (Table 4.2) compared to the anionic chains that converge at 2.01 eV and 2.10 eV with the BP86 and PBE functionals, respectively.

Table 4.2 Binding Energies of Gold- and Silver- Thiolate Anionic Chains

	BP86/TZP		PBE/TZP	
	E_{inc} (eV)	E_{total} (eV)	E_{inc} (eV)	E_{total} (eV)
$Au(SH)_2^-$	3.24	13.21	3.30	13.30
$Au_2(SH)_3^-$	2.40	25.59	2.46	25.75
$Au_3(SH)_4^-$	2.14	37.70	2.18	37.93
$Au_4(SH)_5^-$	2.03	49.70	2.07	49.99
$Au_5(SH)_6^-$	2.00	61.68	2.08	62.07
$Au(SCH_3)_2^-$	3.22	13.48	3.29	13.57
$Au_2(SCH_3)_3^-$	2.32	26.07	2.36	26.20
$Au_3(SCH_3)_4^-$	2.13	38.46	2.23	38.70
$Au_4(SCH_3)_5^-$	2.02	50.74	2.09	51.06
$Au_5(SCH_3)_6^-$	2.01	63.01	2.10	63.43
$Au(SPh)_2^-$	2.99	12.45	3.01	12.40
$Au_2(SPh)_3^-$	2.15	23.97	2.15	23.94
$Au_3(SPh)_4^-$	1.94	35.36	2.07	35.40
$Au_4(SPh)_5^-$	1.83	46.64	1.99	46.78
$Ag(SH)_2^-$	2.84	11.01	2.88	11.09
$Ag_2(SH)_3^-$	2.06	21.25	2.10	21.40
$Ag_3(SH)_4^-$	1.86	31.28	1.92	31.50
$Ag_4(SH)_5^-$	1.76	41.21	1.81	41.52
$Ag_5(SH)_6^-$	1.77	51.16	1.71	51.44
$Ag(SCH_3)_2^-$	2.84	11.15	2.89	11.22
$Ag_2(SCH_3)_3^-$	2.05	21.51	2.10	21.66
$Ag_3(SCH_3)_4^-$	1.90	31.72	1.96	31.96
$Ag_4(SCH_3)_5^-$	1.81	41.83	1.85	42.15
$Ag_5(SCH_3)_6^-$	1.82	51.96	1.89	52.37
$Ag(SPh)_2^-$	2.61	10.18	2.61	10.13
$Ag_2(SPh)_3^-$	1.82	19.57	1.88	19.53
$Ag_3(SPh)_4^-$	1.73	28.86	1.83	28.87
$Ag_4(SPh)_5^-$	1.67	38.02	1.75	37.99
	MUE	0.056	MAD	0.061

Since both gold and silver nanoparticles are of interest experimentally, we examined binding energies of both gold and silver anionic clusters (Figure 4.2). The two types of metal clusters have substantially different incremental energies. As seen in Table 4.2, the gold clusters have higher energy than the silver clusters. The Mean Unsigned Error (MUE) and Mean

Absolute Deviation (MAD) between gold and silver clusters are the same at 0.29 eV, meaning that the gold clusters always have higher binding energies than the silver clusters. Thus, the gold thiolate chains are predicted to be more stable than the silver thiolate chains. A similar trend was observed for cyclic clusters.[90]

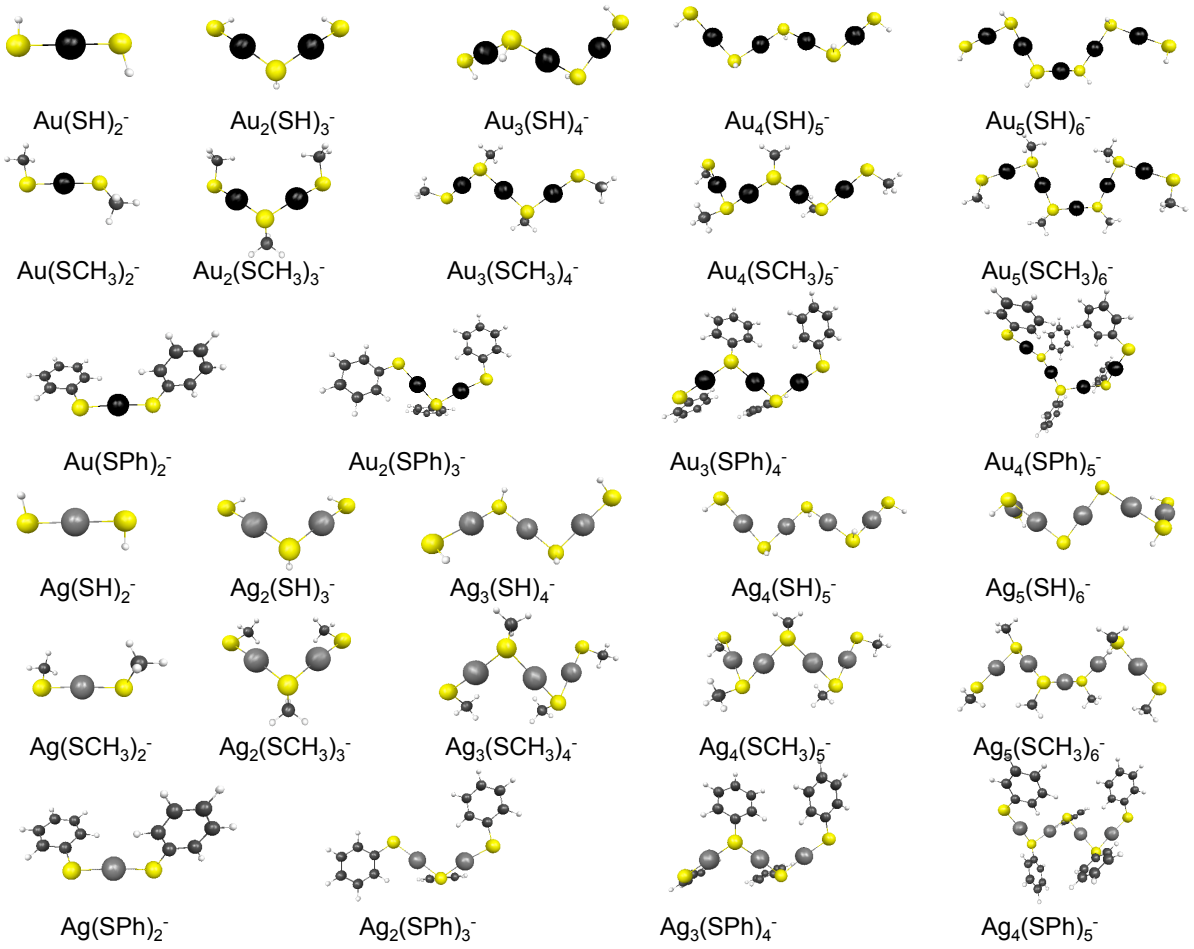

Figure 4.2 Optimized anionic chain structures for $M_x(SR)_y^-$ (M = Au and Ag; R = H, CH_3, and Ph; x = 1-5; y = 2-6). Key: Au: black; Ag: silver; S: yellow; C: grey; H: white.

We also looked at the effect of different residue groups attached to the sulfur. With the attachment of hydrogen we see incremental binding energies of 3.24 eV for the $Au(SH)_2^-$ and 2.84 eV for $Ag(SH)_2^-$ at the BP86/TZP level of theory. As the cluster size increases we see a decrease in incremental energy, from approximately 3.24 eV and 2.84 eV for systems with one metal atom to 2.00 eV and 1.77 eV for $Au_5(SH)_6^-$ and $Ag_5(SH)_6^-$ respectively. The incremental

fragmentation energy appears to converge approximately for clusters with four to five metal atoms.

Changing residue groups to methyl does not change the energies by a significant amount: $Au(SCH_3)_2^-$ and $Ag(SCH_3)_2^-$ have incremental fragmentation energies of 3.22 eV and 2.84 eV at the BP86/TZP level of theory. The same trend for increasing cluster size holds true: $Au_5(SCH_3)_6^-$ and $Ag_5(SCH_3)_6^-$ both have lower energies than their smaller counterparts with E_{inc} energies of 2.01 eV and 1.82 eV. Again, the incremental fragmentation energies converge at four to five metal atom clusters.

The change to phenyl as the residue group shows different results than observed with the other two residue groups. The smallest phenyl clusters have E_{inc} energies of 2.99 eV for gold and 2.61 eV for silver. The E_{inc} energies also decrease with the growth of the clusters. $Au_4(SPh)_5^-$ has incremental energies of 1.83 eV for BP86 and 1.99 eV for PBE and $Ag_4(SPh)_5^-$ has energies of 1.67 eV for BP86 and 1.75 eV for PBE. We expect that the E_{inc} values for this system also converge after four metal atoms, which suggests that additional AuSPh and AgSPh units will bind with E_{inc} values of approximately 1.83 eV and 1.99 eV for gold with BP86 and PBE, respectively, and 1.67 eV and 1.75 eV for silver with BP86 and PBE. This suggests that the energies of formation are significantly different for aliphatic and aromatic ligands. As the clusters grow in size their incremental energies decrease but their total energy increases in a linear fashion. The increase in total energy is expected because larger molecules have a greater overall binding energy.

Based on the DFT calculations that we have performed on the gold and silver thiolate anionic chain clusters, the BP86 functional generally resulted in a slightly lower energy than the PBE functional, with a MUE of 0.056 eV and a MAD of 0.061 eV. The slight difference in

values comes from the reversal of the trend on a few of the phenylthiolate clusters. Energies can be specifically compared in Table 4.2. TPSS incremental binding energies for $Au(SCH_3)_2^-$ and $Au_2(SCH_3)^-$ are predicted to be 3.22 and 2.31 eV, respectively, which are in very good agreement with the BP86 results and only differ slightly from the PBE values.

BP86 calculations with a quadruple-zeta basis set are employed to determine the effects of larger basis sets. Fragmentation energies calculated with the Triple Zeta Polarized (TZP) basis set are generally lower than energies calculated with the Quadruple Zeta Polarized (QZ4P) basis set. The MUE between the TZP and QZ4P is 0.022 and has a MAD of 0.029. The difference in MUE and MAD values comes from some of the small methylthiolate silver clusters that have lower energy with QZ4P than TZP as seen in Table 4.3.

Table 4.3 Basis Set Effects on the Binding Energies of Gold- and Silver- Thiolate Anionic Chains

	BP86/QZ4P	
	E_{inc} (eV)	E_{total} (eV)
$Au(SH)_2^-$	3.26	13.38
$Au_2(SH)_3^-$	2.45	25.94
$Au_3(SH)_4^-$	2.19	38.25
$Au(SCH_3)_2^-$	3.24	13.67
$Au_2(SCH_3)_3^-$	2.36	26.44
$Au_3(SCH_3)_4^-$	2.17	39.03
$Au(SPh)_2^-$	3.08	12.67
$Au_2(SPh)_3^-$	2.17	24.42
$Au_3(SPh)_4^-$	2.02	36.03
$Ag(SH)_2^-$	2.84	11.03
$Ag_2(SH)_3^-$	2.07	21.29
$Ag_3(SH)_4^-$	1.85	31.33
$Ag(SCH_3)_2^-$	2.82	11.18
$Ag_2(SCH_3)_3^-$	2.03	21.56
$Ag_3(SCH_3)_4^-$	1.88	31.79
$Ag(SPh)_2^-$	2.61	10.24
$Ag_2(SPh)_3^-$	1.83	19.69
$Ag_3(SPh)_4^-$	1.77	29.08
MUE	0.022	
MAD	0.029	

For both of the functionals and basis sets compared in this work, differences between various levels of theory are less than the differences obtained by changing metal atoms or residue groups. The change in the functionals account for about three percent of the total E_{inc} and the basis sets are about one percent of the total E_{inc} which means that they account for only a small fraction of the total. In seeing this comparison and with the thought of cost and run time in mind,

a calculation using either functional will give a reasonable value with a MUE again of 0.022 and 0.056 and a MAD of 0.029 and 0.061 for the basis set and functionals respectively. For our calculations the smaller basis set yields answers with about 0.02 to 0.03 eV of those of the quadruple basis set, and this level of accuracy is sufficient for this work.

In addition to examining anionic chains, we have also studied the binding energies of the $[M_2(SH)_3]^-$ units to icosahedral metal cores to form $M_{25}(SH)_{18}^-$ nanoparticles. We investigate the pure gold, pure silver, and mixed systems that were previously studied in Ref. 99. The 13-atom core metal nanoclusters of gold and silver show the same trends that the other clusters studied show. The gold core binds stronger to the ligands than the silver core; however, both cores bind stronger to the silver ligands than the gold ligands, as seen in Table 4.4. The silver cores have overall binding energies of 63.88 eV for the gold motifs and 65.15 eV for the silver motifs and the corresponding gold cores have overall binding energies of 69.97 eV for the gold motifs and 71.33 eV for the silver motifs. The average binding energies show the same trend: the silver core with the gold motifs has an average binding energy of 10.65 eV and with the silver motifs it has an average energy of 10.86 eV. The gold core with gold motifs has an average energy of 11.66 eV and with the silver motifs it has an average energy of 11.89 eV. This could be explained in two ways: that the silver ligands are unstable by themselves in solution or that the cores are very strongly bound to the silver ligands.

Table 4.4 BP86/TZP Overall and Average Binding Energies of $M_2(SH)_3^-$ to the Icosahedral core of $M_{25}(SH)_{18}^-$ Nanoclusters

Cluster sizes	$E_{overall}$ (eV)	$E_{average}$ (eV)
$Ag_{13}(Au_2(SH)_3)_6^-$	63.88	10.65
$Au_{13}(Ag_2(SH)_3)_6^-$	71.33	11.89
$Ag_{13}(Ag_2(SH)_3)_6^-$	65.15	10.86
$Au_{13}(Au_2(SH)_3)_6^-$	69.97	11.66

4.5 Conclusions

In this body of work, we have shown that the incremental binding energies of cyclic clusters and anionic chains converge after four metal atoms, and that the cyclic clusters are less stable than their anionic analogs. Our cyclic cluster models are in agreement with experimentally known structures and calculations.

We have also shown that there is no significant difference between the BP86 and PBE functionals as well as between the triple zeta and quadruple zeta basis sets. Both contribute very little to the total monomer fragmentation energy; the choice of functional affects the energy by about three percent and the basis set yields differences of only about one percent. A larger factor for energy change comes from the changing of residue groups. The hydrogen and methyl groups showed similar energies, whereas the phenyl group showed lower binding energies.

The icosahedral core metal nanoparticles show the same trends as the smaller clusters. The gold cores have higher overall binding and average binding energies than the silver cores. However, the silver thiolate motifs have higher energies in both categories than the gold thiolate motifs.

4.6 Acknowledgements

The authors thank the Air Force Office of Scientific Research (AFOSR) for funding under grant FA9550-09-1-0451. C.M.A. is a 2011 Alfred P. Sloan Research Scholar.

Chapter 5 - Electron and Hydride Addition to Gold(I) Thiolate Oligomers – Implications for Gold Thiolate Growth Mechanism

5.1 Abstract

In this work we examine the possible second step of the Brust-Schiffrin synthesis by employing density functional theory and investigating the addition of electrons and hydrides to gold(I) thiolate oligomers. Electron affinities (EAs) are calculated for the addition of 1 to 4 electrons for cyclic and chain-like structures. The addition of solvent makes the EAs more favorable than in gas phase. The addition of electrons results in the dissociation of Au^- and anionic chains. Hydride was added to the cyclic clusters instead of direct electron addition results in the dissociation of thiol and the formation of a gold-gold bond where the thiol was. The resulting structures can react together to form larger clusters that may be possible precursors to larger stable thiolate-protected gold nanoparticles.

5.2 Introduction

Gold(I) thiolate oligomer formations have been of great interest since they were suggested by Alvarez *et al*. to form during nanoparticle growth particularly during the Brust-Schiffrin synthesis.[11,12] However, Goulet and Lennox do not agree that polymers are formed in the Brust-Schiffrin synthesis.[13] Barngrover and Aikens performed density functional theory (DFT) calculations and found that a three to one ratio of thiol ligands to Au(III) can form Au(I)SR polymers, especially in polar solvents under slightly basic conditions.[14] Other groups have examined the synthesis of thiolate-protected gold nanoparticles by making modifications to the Brust-Schiffrin synthesis. Modifications such as changing the number of phases from two to one,[18,60,85,100] changing the ratio of thiol ligand to gold precursor,[13,60] or changing the reducing agent from sodium borohydride to 9-BBN,[101] lithium triethylborohydride ("superhydride"),[18] or

electrodes[102] have been examined. Luo *et al*. modified the Brust-Schiffrin synthesis by using CO as the reducing agent and utilizing time resolved UV-Visible absorption and electrospray ionization mass spectrometry (ESI-MS) was able to identify 12 precursors ranging from small Au(I) species to larger rings and anionic polymers.[15]

Not only are gold(I) thiolate oligomers possible precursors in nanoparticle growth, but they also passivate nanoparticles. When the oligomers are present on the surface of gold thiolate nanoparticles, they are often called "staple" motifs. They are found on various sizes of nanoparticles including $Au_{25}(SR)_{18}^{-,0}$, $Au_{38}(SR)_{24}$, and $Au_{102}(SR)_{44}$.[61-65,103,104] Staple motifs can also be formed in self-assembled monolayers (SAMs).[67-70]

The Brust-Schiffrin synthesis of gold thiolate nanoparticles involves the phase transfer of Au(III) chloride precursor into toluene followed by the addition of dodecanethiol and sodium borohydride ($NaBH_4$).[11] The equations written by Brust *et al*. to describe their synthesis have the reducing agent replaced with a number of electrons. Previous work in our group on the growth of gold phosphine nanoparticles shows that the addition of one electron facilitates the formation of a gold-gold bond.[105] In this body of work we will extend this previous work into gold thiolate clusters and examine the addition of electrons as well as the addition of hydrides, which act as a two-electron donor.

5.3 Computational Details

All calculations were performed using the Amsterdam Density Functional (ADF)[54] package. We used the Becke-Perdew (BP86)[46,47] functional with a triple-ζ polarized basis set. Scalar relativistic effects are included by the use of Zero Order Regular Approximation (ZORA).[53] Solvents of water and toluene are included as continuum solvents by use of the conductor-like screening model (COSMO).[55] When calculating electron affinities, structures

were allowed to fully optimize after the addition of each electron; EAs are calculated by $X + e^- \rightarrow X^-$. Unrestricted calculations were employed for open shell systems. To assign partial charges of dissociating fragments, both Mulliken and Voronoi Deformation Density methods have been considered.

5.4 Results and Discussion

To examine the second part of the growth mechanism of gold thiolate nanoparticles, cyclic clusters ranging from $Au_3(SCH_3)_3$ to $Au_7(SCH_3)_7$ were optimized (Figure 5.1); these are the same structures optimized in Chapter 4.[106] One to four electrons were added to each of the cyclic clusters and allowed to relax. The addition of one electron resulted in the flattening of the ring structures and no dissociation occurred. The addition of the second electron resulted in the dissociation of the smallest ring $Au_3(SCH_3)_3$ into $Au_2(SCH_3)_3^-$ and Au^- (Figure 5.2a). Adding the third electron caused the dissociation of most of the larger ring structures into $Au_n(SCH_3)_{n+1}^-$ and Au^- where n = 3-6. A subset of structures was examined for the fourth electron addition that resulted in two anionic chains and 2 Au^- and not neutral gold.

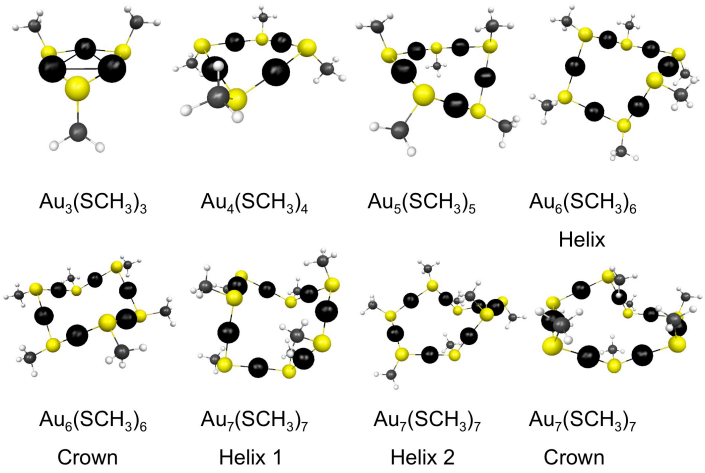

Figure 5.1 Cyclic $Au_n(SCH_3)_n$ (n=3-7) clusters. Gold: black; sulfur: yellow; carbon: grey; hydrogen: white.

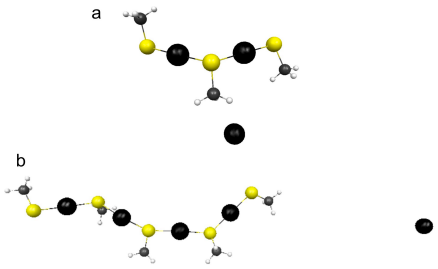

Figure 5.2 (a) Dissociation of Au^- from $Au_3(SCH_3)_3$ after addition of two electrons. (b) Dissociation of Au^- from $Au_5(SCH_3)_5$ after addition of three electrons.

For each electron added to the cyclic clusters, electron affinities are calculated (Table 5.1). The first electron affinities are exothermic and range from -0.20 to -0.78 eV meaning that the clusters can easily accept the addition of one electron. However the acceptance of the second electron is much less favorable ranging from 1.49 to 2.39 eV. The third electron acceptance is even less favorable than the second with values ranging from 3.62 to 5.60 eV. We also examined a few chain like structures including $Au_2(SCH_3)_3^-$, $Au_3(SCH_3)_4^-$, and gold-capped $Au_3(SCH_3)_3$ (Figure 5.3a-c). The gold-capped chain had the most favored EA examined at -2.63 eV. However, the two anionic chains had the least favored first EAs at 3.51 and 2.90 eV. The second EA for all three structures were less favorable and the neutral second EA falls within the range of the neutral cyclic clusters. Upon relaxation of the gold-capped chain, the terminal gold dissociated as Au^- and the remaining chain is the commonly observed $Au_2(SCH_3)_3^-$ oligomer. The only time thiolate dissociation has been seen in this work is after the second electron addition to $Au_2(SCH_3)_3^-$ (Figure 5.3d); however, it is paired with Au^- dissociating from the same structure. Overall, we find that the addition of electrons to Au(I)SR oligomers leads to the dissociation of Au^- and not neutral Au and anionic chains or thiolates.

Table 5.1 Vertical EAs in eV for Gold-Thiolate Oligomers in the Gas Phase

	First EA	Second EA	Third EA
cyclic			
$Au_3(SCH_3)_3$	-0.30	1.49	[a]
$Au_4(SCH_3)_4$	-0.20	2.39	5.60
$Au_5(SCH_3)_5$	-0.31	1.93	4.89
$Au_6(SCH_3)_6$ crown	-0.78	1.55	4.30
$Au_6(SCH_3)_6$ helix	-0.53	1.55	4.24
$Au_7(SCH_3)_7$ crown	-0.69	1.68	[a]
$Au_7(SCH_3)_7$ helix 1	-0.56	1.65	3.62
$Au_7(SCH_3)_7$ helix 2	-0.56	1.54	3.71
chain-like			
$Au_3(SCH_3)_3$ gold-capped	-2.63	2.06	[a]
$Au_2(SCH_3)_3^-$	3.51	5.81	[a]
$Au_3(SCH_3)_4^-$	2.90	4.68	[a]

a. Gold dissociated after second electron addition

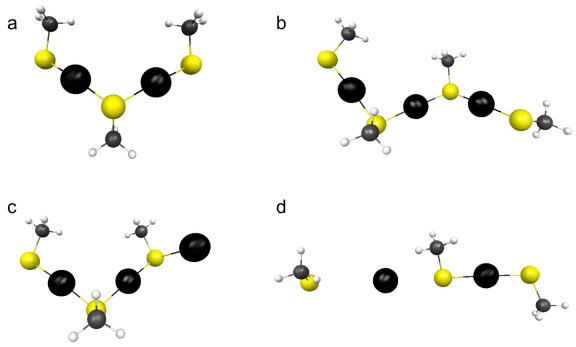

Figure 5.3 (a) $Au_2(SCH_3)_3^-$. (b) $Au_3(SCH_3)_4^-$. (c) Gold-capped $Au_3(SCH_3)_3$. (d) $Au_2(SCH_3)_3^-$ dissociation into Au^- ion, SCH_3^- ligand, and $Au(SCH_3)_2^-$ complex.

We also calculated electron affinities in water and toluene solvents to model the conditions of actual nanoparticle growth. The inclusion of solvent greatly stabilized the structures and led to much more favorable EA values (Table 5.2). In water, the first EA ranges

from -1.85 to -2.19 eV. In toluene, the first EA ranges from -1.16 to -1.40 eV. The addition of the second electron is also favorable, ranging from -2.32 to -3.87 eV in water and -0.28 to -1.53 eV in toluene. The second electron addition is more favored than the first in water; however, toluene mostly keeps the same trend of the first EA being more favorable than the second EA like the gas phase calculations. The exception for toluene is $Au_3(SCH_3)_3$. In water, similar to the gas phase, the addition of two electrons is enough to dissociate $Au_3(SCH_3)_3$ into Au^- and $Au_2(SCH_3)_3^-$. Unlike the gas phase calculations, the addition of two electrons is able to dissociate almost all of the larger structures in water. The exceptions are $Au_7(SCH_3)_7$ crown and helix 1 isomers; this is probably because the larger structures can handle the larger charge accumulation. Toluene is similar to the gas phase calculations in that the third EAs are the least favored and the majority of the structures do not dissociate. Again no free thiolate dissociated without being accompanied by Au^-.

Table 5.2 Vertical EAs in eV of Cyclic $Au_n(SCH_3)_n$ in Water and Toluene

	Water			Toluene		
	First EA	Second EA	Third EA	First EA	Second EA	Third EA
$Au_3(SCH_3)_3$	-2.19	-3.87	[a]	-1.35	-1.53	[a]
$Au_4(SCH_3)_4$	-1.92	-2.36	[a]	-1.16	-0.28	0.95
$Au_5(SCH_3)_5$	-1.97	-2.45	[a]	-1.17	-0.51	1.08
$Au_6(SCH_3)_6$ crown	-2.01	-2.48	[a]	-1.40	-0.71	0.72
$Au_6(SCH_3)_6$ helix	-1.98	-2.49	[a]	-1.33	-0.69	0.68
$Au_7(SCH_3)_7$ crown	-1.93	-2.32	-1.62	-1.39	-0.49	0.51
$Au_7(SCH_3)_7$ helix 1	-1.85	-2.44	-2.20	-1.25	-0.52	0.33
$Au_7(SCH_3)_7$ helix 2	-1.92	-2.50	[a]	-1.33	-0.63	0.37

a. Gold dissociated after second electron addition

Since the addition of electrons did not yield reliable precursors to the growth of nanoparticles, we examined the addition of hydride to the clusters. We first found out that the

products depend on the angle of attack of the incoming hydride. If the hydride comes in at 180 degrees to the S-C-H, a ligand exchange occurs with the hydride and the CH_3^- resulting in $Au_nSH(SCH_3)_{n-1}$. If the hydride instead comes in at an angle of 120 degrees, dissociation of $HSCH_3$ occurs and a gold-gold bond forms where the new thiol was bound (Figure 5.4a). The new structure has a -1 overall charge. This $Au_4(SCH_3)_3^-$structure is unique in the fact that it has a staple motif consisting of $Au_2(SCH_3)_3^-$ surrounding two gold atoms bound together that can be considered to be in the Au(0) oxidation state. After the formation of $Au_4(SCH_3)_3^-$, two of these oligomers can be combined to form a larger cluster of $Au_8(SCH_3)_6^{2-}$ (Figure 5.4b). This structure has 4 Au(0) atoms surrounded by two staple motifs.

The addition of a second hydride to $Au_4(SCH_3)_3^-$ results in the breaking of the ring but no thiol dissociation (Figure 5.4c). This is because the system is too small to handle the addition of electrons provided by the hydride. Larger systems such as $Au_6(SCH_3)_6$, however, can handle the extra electrons and, depending on the location of the addition of the extra hydride, leads to different isomers (Figure 5.5).

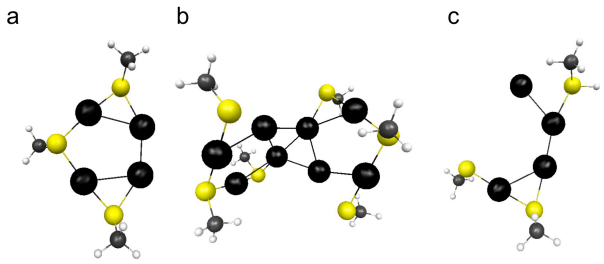

Figure 5.4 (a) $Au_4(SCH_3)_3^-$ product from hydride addition to $Au_4(SCH_3)_4$. (b) $Au_8(SCH_3)_6^{2-}$ formed from two $Au_4(SCH_3)_3^-$ complexes. (c) Second hydride addition to n = 4 product.

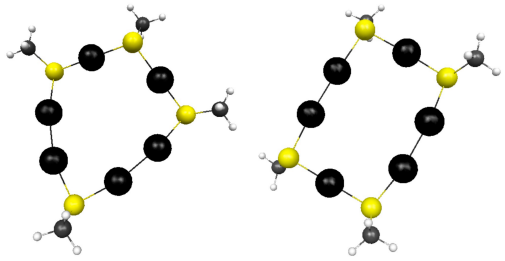

Figure 5.5 Two products formed after the addition of two hydrides to $Au_6(SCH_3)_6$.

5.5 Conclusions

In conclusion, we have demonstrated a possible secondary step in gold thiolate nanoparticle growth especially in polar solvents. The first addition of electrons is favored in any solvent or phase examined. The inclusion of solvent makes the second addition of electrons favored where water is even more favorable than toluene. The second electron addition to water is almost two times more favorable than the first addition. Most structures, except crown and helix $Au_7(SCH_3)_7$, dissociated after the second electron addition in water, whereas in gas phase and toluene this did not occur until the addition of the third electron. For all of the electron additions to cyclic structures, the structures dissociated into Au^- and $Au_n(SCH_3)_{n+1}^-$, where n=3-6. The electron addition to the chain-like structures resulted in smaller anionic chains and Au^- except for $Au_2(SCH_3)_3^-$, which dissociated into Au^-, SCH_3^-, and $Au(SCH_3)_2^-$. The addition of hydride to cyclic clusters results in the dissociation of thiol; the formation of a gold-gold bond and the ring shape is maintained. The second addition of hydride to the smaller clusters does not result in the dissociation of a second thiol; however, in the larger clusters this is possible. The larger clusters can handle the additional electrons provided by hydride whereas the smaller clusters cannot. Once the clusters have been reduced with a hydride, they can be combined together to form larger clusters. This may lead to the possible growth of larger stable nanoparticles.

5.6 Acknowledgements

The authors thank the Air Force Office of Scientific Research for funding under grant FA9550-09-1-0451. C.M.A. is a 2011 Alfred P. Sloan Research Scholar.

Chapter 6 - Prediction of Non-radical Au(0)-containing Precursors in Nanoparticle Growth Processes

Reproduced with permission from:

Barngrover, B. M.; Manges, T. J.; Aikens, C. M. *J. Phys. Chem. A* **2015**, *119*, 889.

6.1 Abstract

This density functional theory (DFT) investigation examines the formation of non-radical Au(0) species from the reduction of Au(I) species. The Au(I) complexes of interest are $AuCl_2^-$, $AuBr_2^-$, AuI_2^-, $AuClPH_3$, and $AuCl(H)SCH_3^{(-)}$, which are precursors for gold nanoparticle and cluster formation. Reaction of two of the Au(I) species with a hydride results in the ejection of two of the ligands and the formation of Au_2 with two ligands still attached. AuX_2^- (where X = Cl, Br, or I) reactions eject two halides and form $Au_2X_2^{2-}$. $AuClL^{(-)}$ (where L = PH_3, $HSCH_3$, or SCH_3^-) reactions can either eject chloride, HCl, PH_3, $HSCH_3$, or SCH_3^- and form $Au(0)L_2^{q-}$ or $Au(0)ClL^{q-}$ (q = 0, 1, 2). The $Au_2Cl_2^{2-}$ complex can further react with $AuCl_2^-$, which forms $Au_3Cl_3^{2-}$ and a chloride anion. The new $Au_3Cl_3^{2-}$ species can then react with $AuCl_2^-$ or $Au_2Cl_2^{2-}$ or with another $Au_3Cl_3^{2-}$. Larger clusters can be formed from these precursors. In this work, reactions in both methanol and benzene solvents are considered as models for one-phase and two-phase gold nanoparticle growth processes. Overall, this investigation shows how Au(0)-containing species can be formed without assuming the formation of Au(0) atoms (radical species).

6.2 Introduction

Applications for gold nanoparticles include drug delivery and therapy,[1,2] catalysts,[3] sensors,[4] electronics,[5] and optics.[6] Different nanoparticle morphologies such as spheres, cubes, wires, and rods have been synthesized and have diverse properties for these unique applications.[7] Yet, how are these different morphologies created? Although some general principles are known, many syntheses rely on trial and error. A better understanding is needed of the growth mechanisms of nanoparticles, and in this work we examine the initial steps of nanoparticle growth in order to gain a better picture of how gold nanoparticles form.

Brust and Schiffrin first published a synthesis of stable gold thiolate nanoparticles in 1994.[11] The Brust-Schiffrin (B-S) synthesis starts with tetrachloroauric acid ($HAuCl_4$) or tetrachloroaurate ($AuCl_4^-$), which is phase-transferred into toluene by the use of tetraoctylammonium bromide (Equation 6.1). Once in the organic phase, the ligand, such as dodecanethiol ($C_{12}H_{25}SH$), and reducing agent, which is typically sodium borohydride ($NaBH_4$), are added to the solution (Equation 6.2). In equation 6.2, Brust and Schiffrin use the expression $3me^-$ for the addition of electrons instead of explicitly considering $NaBH_4$.

$$AuCl_{4\,(aq)}^- + N(C_8H_{17})_{4\,(toluene)}^+ \rightarrow N(C_8H_{17})_4^+AuCl_{4\,(toluene)}^- \quad (6.1)$$

$$mAuCl_{4\,(toluene)}^- + nC_{12}H_{25}SH_{(toluene)} + 3me^- \rightarrow 4mCl_{(aq)}^- + Au_m(C_{12}H_{25}SH)_{n(toluene)} \quad (6.2)$$

Brust, Schiffrin, and co-workers later described a related one-phase synthesis using methanol.[107] Since the introduction of the Brust-Schiffrin synthesis, several implicit assumptions about the growth mechanism have appeared in the literature, but scientific investigations into the precise growth mechanism have only appeared in the last few years. Two of these assumptions are that the formation of Au(I)-thiolate polymers precedes the final reduction to gold-thiolate nanoparticles, and that Au(0) atoms can form and aggregate during the growth process.

The role of the formation of gold-thiolate polymers was first questioned in 2010, when Goulet and Lennox demonstrated that changing the thiol ligand to Au(III) salt ratio from 4:1 to 2:1 caused reduction to $Au(I)X_2^-$ (X = halide) but did not lead to the formation of Au(I)-thiolate oligomers.[13] Barngrover and Aikens supported the hypothesis regarding the initial formation of $Au(I)X_2^-$ species using density functional theory (DFT) calculations.[14] However, they also demonstrated with DFT that reaction of $Au(I)X_2^-$ with the thiol ligand can potentially lead to $AuCl(H)SR^{(-)}$ species, at least in a polar solvent such as methanol.[14] Furthermore, they showed that deprotonated Au(I) units ($AuClSR^-$) can react with each other and grow longer ClAuSR-$(AuSR)_n$- oligomers. They also demonstrated that these oligomers can be reduced with hydrides to form possible nanoparticle precursors, although they did not discount growth mechanisms based on the reduction of AuX_2^- or $Au(SR)_2^-$ species.[108] Nonetheless, Goulet and Lennox suggested that a three to one ratio of ligand to Au(III) salt does not form polymeric Au(I) species; instead the $Au(I)X_2^-$ species remain in solution.[13] Tong *et al.* also agreed with Goulet and Lennox that the $Au(I)X_2^-$ species remained in solution in the presence of the phase-transfer agent.[109] However, Zhu *et al*. later showed that $AuSRX^-$ and $Au(SR)_2^-$ can be formed experimentally depending on the concentration of reactants and suggested that polymeric Au(I) can form under certain conditions.[110] Even so, the debate still exists regarding under what conditions Au(I) polymers can be formed during reduction and the importance of these species in the growth mechanism. Nevertheless, all groups agree that reduction occurs from Au(III) and that Au(I) is the primary species formed after reduction by thiol ligands, making it an important precursor in the growth of nanoparticles.

The starting ligands can be changed or introduced after the reduction has occurred. The typical ligand is a long chain alkanethiol; however, other ligands can be used. Fluorinated

thiolates can be employed as ligands as shown by Gentilini *et al.*[19] In addition, phosphines can be used as demonstrated by Hudgens *et al.*[111] Fink *et al.* and Petroski *et al.* showed that "bare" gold nanoparticles could form without the addition of a ligand; in this case, the nanoparticles are thought to be stabilized by the phase-transfer agent.[112,113] As shown in our current work, these nanoparticles are likely stabilized at the surface by halide ligands remaining from the gold salt and/or the counterion of the phase transfer agent. Recently, Tong and co-workers suggested that even in the B-S two-phase synthesis in which thiol ligands are present, the growth mechanism first proceeds via reduction of $Au(I)X_2^-$ (X = halide) units to form metal clusters/nanoparticles prior to ligand exchange to form the metal-chalcogen bonds.[109,114] Thus, understanding the reduction of $Au(I)X_2^-$ units will provide necessary insights into gold nanoparticle growth processes. Tong and co-workers proposed that the phase-transfer agent could act as a reverse micelle and transport the gold precursor salt into the toluene phase, where it would then be reduced inside the reverse micelle.[109,114] The phase-transfer agent acting as a transport vehicle has been recently studied by Joshi and Bigioni for larger nanoparticles.[115] By utilizing optical microscopy, they observed that a single ionic surfactant, dihexadecyldimethylammonium bromide (DHAB), could transport an aggregate of gold nanoparticles from water and inject it into toluene through capillary force created by the hydrophobicity of the aggregate in the aqueous phase.[115]

A reducing agent such as sodium borohydride, lithium triethylborohydride, or triethylsilane[18,112,113,116] is needed to cause complete reduction to Au(0). A common interpretation in the literature is that Au(0) is initially formed as an isolated gold atom without any ligands attached, which then cluster to form larger particles.[24,111] This interpretation may possibly arise from addition of electrons leading to removal of the anionic ligands such as

chlorides; however, isolated atoms of gold are radicals and would be expected to be highly reactive if formed. In addition, this assumption implicitly treats $NaBH_4$ as a one-electron donor instead of a two-electron (hydride) donor, yet it has been known to be a two-electron donor since its discovery in 1942.[117]

As demonstrated by the above discussion, the underlying growth mechanism of nanoparticles is still under some debate. Currently, researchers agree that the first step is the formation of Au(I) species from the reduction of the Au(III) salt no matter what synthetic method is employed. However, formation of the Au(0)-containing species is still not understood. In this work, we examine how Au(I) species are reduced to form Au(0)-containing nanoparticles. We investigate possible precursors in the one-phase method (using a methanol solvent) as well as in the organic phase of a two-phase B-S approach (represented by benzene). We consider the hydride reduction of Au(I) species protected by various ligands including chloride, phosphine, and thiol(ate) to show that this leads to a dimeric Au(0)-containing species without formation of gold radicals. We also examine the growth of gold-chloride nanoparticles, which are applicable to understanding the growth mechanisms of "bare" gold nanoparticles and to the B-S synthesis in the "reverse micelle" hypothesis of Tong and co-workers. Although not discussed in this present work, thiolate-for-chloride ligand exchange is known to occur with low barrier heights (~0.35 eV in methanol),[14] so the gold-chloride nanoparticle precursors could easily undergo ligand exchange to form gold-thiolate nanoparticles. In addition, the physical insights gained here can be extended to the growth of gold-thiolate nanoparticles originating from reduction of $Au(SR)_2^-$.

6.3 Computational Details

All calculations are performed with the Amsterdam Density Functional (ADF)[54] package, using density functional theory with the Becke Perdew (BP86)[46,118] functional and a frozen-core

polarized triple-ζ (TZP) basis set. BP86-D calculations including the Grimme dispersion correction[119] are considered where noted in the text. We include scalar relativistic effects by employing the Zeroth Order Regular Approximation (ZORA).[53] We incorporate methanol and benzene solvents using the Conductor-like Screening Model (COSMO), which represents the solvent by its dielectric constant.[55,78,79]

All intermediates and transition states are fully optimized; Hessian calculations have been performed to verify the existence of one imaginary frequency for the transition states. Absorption spectra, vibrational frequencies, and Raman tensor strengths have been calculated at the BP86/TZP level of theory.

6.4 Results and Discussion

6.4.1 Reduction of AuX_4^- to AuX_2^- (X = Cl, Br, or I)

$AuCl_4^-$ is the most common starting gold(III) salt for nanoparticle growth. However, other halides can be substituted into $AuCl_4^-$. The reaction energy to substitute a bromide ion into $AuCl_4^-$ is -0.22 eV in methanol at the BP86/TZP level of theory. Thus, it is possible that bromide from the phase-transfer agent may substitute into $AuCl_4^-$ prior to reduction. Iodide can also replace chloride in $AuCl_4^-$ with a reaction energy of -0.96 eV in methanol.

$AuCl_4^-$ can be reduced by two thiol ligands to form $AuCl_2^-$ and a disulfide.[13,14] This reaction in methanol with methylthiol ligands has an energy of -0.58 eV.[14] The analogous $AuBr_4^-$ and AuI_4^- reactions have reaction energies of 0.07 eV and 0.48 eV, respectively. $AuCl_4^-$ can also be reduced by a reducing agent such as sodium borohydride ($NaBH_4$) to form $AuCl_2^-$. The reaction energy with a hydride ion as the reducing agent in methanol is -3.43 eV. The reaction energies to reduce $AuBr_4^-$ and AuI_4^- with hydride in methanol are -3.08 eV and -2.63 eV, respectively. The reduction of AuX_4^- is a key step in nanoparticle growth due to the fact that

AuX_4^- does not react with itself. Instead, an aurophilic interaction, or a non-covalent attractive interaction, is present between AuX_4^- complexes. A further discussion on aurophilic interactions and dispersion corrections can be found in Appendix C.

6.4.2 Reduction of AuX_2^- (X = Cl, Br, or I)

$AuCl_2^-$ is an important species because it is the primary precursor available after the reduction of $AuCl_4^-$. Properties of these precursors including their calculated vibrational frequencies and absorption spectra are provided in the SI. $AuCl_2^-$ also has an aurophilic interaction with a second $AuCl_2^-$ molecule as previously mentioned for $AuCl_4^-$. Again, a more in-depth investigation of this interaction can be found in Appendix C. A chemical reaction can occur between two $AuCl_2^-$ species to form a $Au_2Cl_3^-$ chain and a chloride ion (Chart 6.1). In methanol, the reaction energy is calculated to be 0.48 eV and the barrier height is 0.72 eV. In water, these values are slightly lower; however, this reaction is predicted to be endothermic and is less favorable to occur compared to the formation of the $ClAuSCH_3AuSCH_3$ chain from Ref. 14 (Chart 6.1).

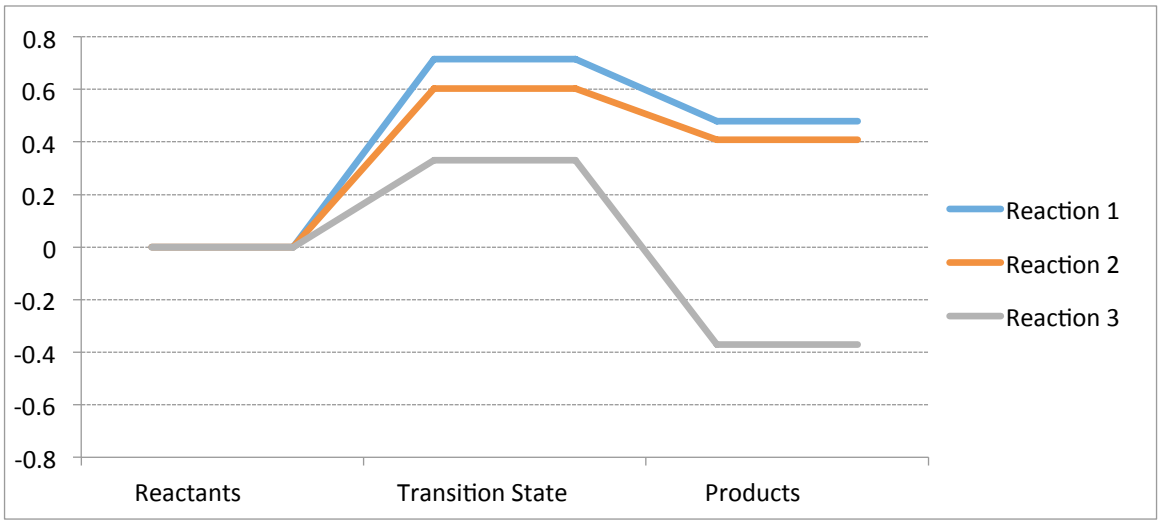

Chart 6.1 The formation of $Au_2Cl_3^-$ chain in methanol (Reaction 1) and water (Reaction 2) compared to the formation of $ClAu_2(SR)_2^-$ in methanol (Reaction 3).

Like AuX_4^-, bromide or iodide analogs of AuX_2^- can be made. AuX_2^- typically does not react with itself or with AuX_4^- to form covalent bonds. However, if one or more electrons are introduced either from a reducing agent or electric current,[102] AuX_2^- can react. In this work, we find that two AuX_2^- in close proximity will react with hydride to produce $Au_2X_2^{2-}$ and eject HX and X^- (Figure 6.1a). In methanol with hydride as the reducing agent, the reaction of two $AuCl_2^-$ has an energy of -1.32 eV and a barrier height of 1.03 eV. This barrier height is notably low considering a total of three negative charges are present in the system. The reaction energies for $AuBr_2^-$ and AuI_2^- reduction are -1.04 eV and -0.71 eV, respectively. $Au_2X_2^{2-}$ is an important species because it contains fully reduced gold and is a closed shell (non-radical) species. This molecule represents the first likely Au(0)-containing precursor under B-S synthesis conditions. Its characterization (UV-Vis, IR, and Raman) is presented in Appendix C for future experimental identification.

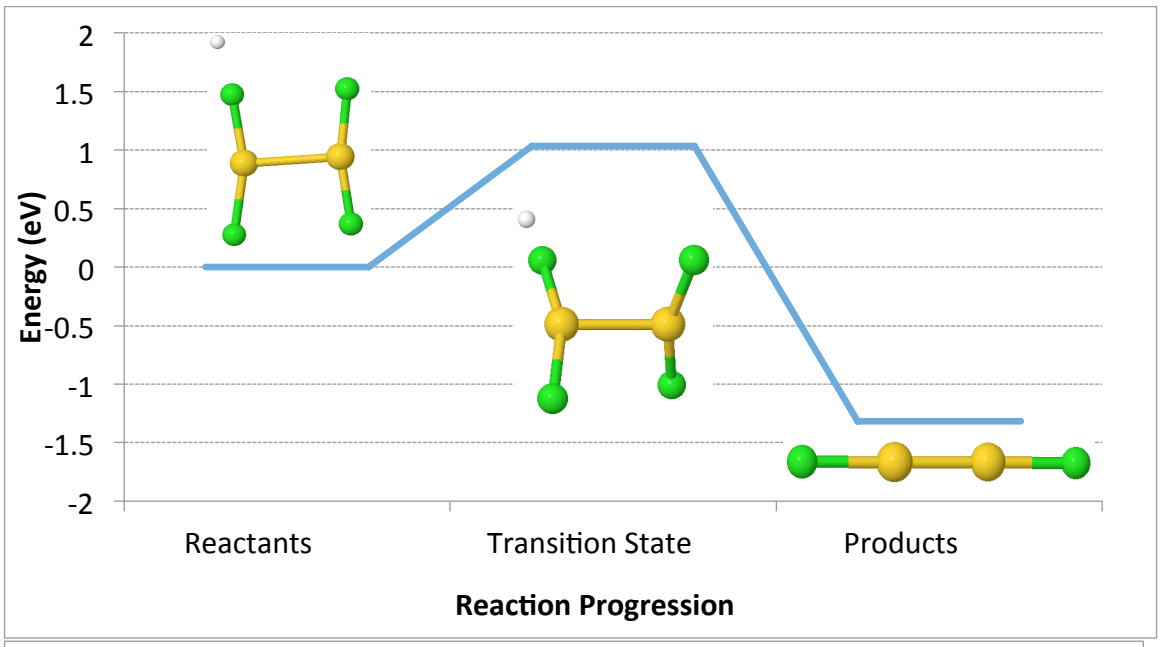
2
1.5
1
0.5
0
-0.5
-1
-1.5
-2
Energy (eV)
Reactants
Transition State
Products
Reaction Progression

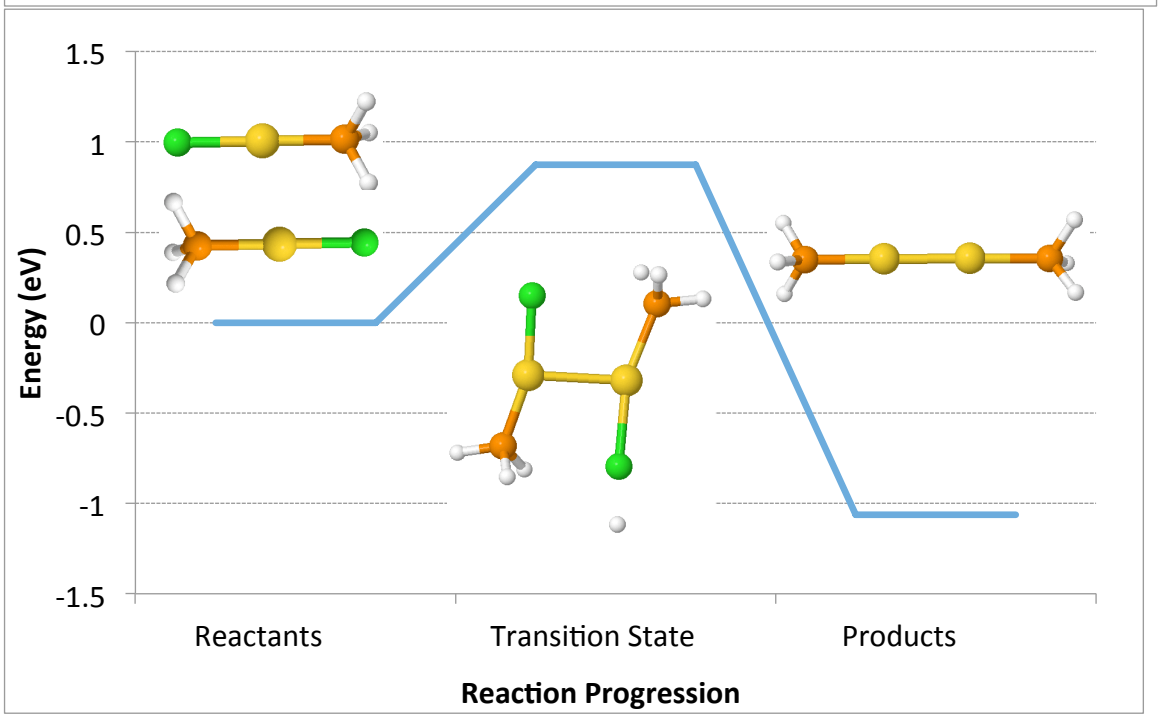
1.5
1
0.5
0
-0.5
-1
-1.5
Energy (eV)
Reactants
Transition State
Products
Reaction Progression

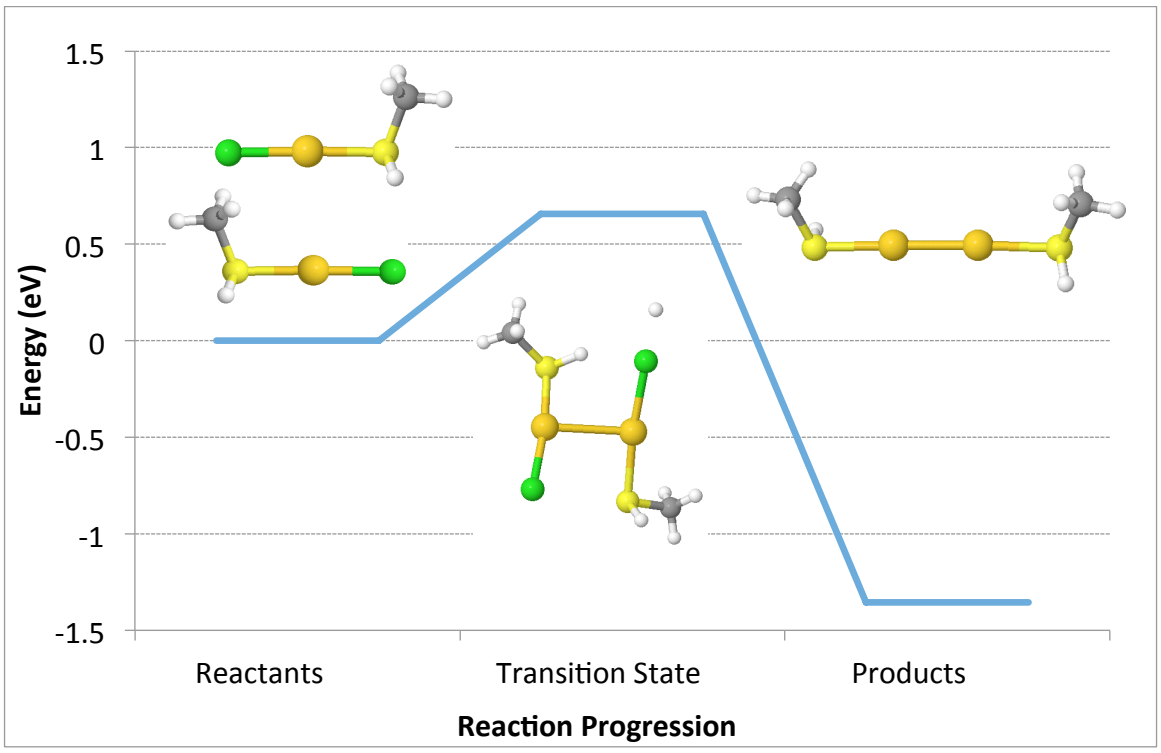

Figure 6.1 Hydride addition to a. $2AuCl_2^-$ b. $2AuClPH_3$ c. $2AuClHSCH_3$. Gold = gold, chloride = green, phosphorus = orange, sulfur = yellow, carbon= gray, and hydrogen = white

6.4.3 Reduction of $AuClL^{(-)}$ (L = PH_3, $HSCH_3$, or SCH_3)

Other ligands have been investigated to grow nanoparticles such as phosphines, thiols, and thiolates.[11,13,14,18,19,75,105,111] We have examined the reduction of these species and find that they react similarly to AuX_2^-. Hydride reduction reactions using $AuClPH_3$ as a precursor can lead to the formation of Au-Au bonds and the detachment of Cl^-, HCl, or PH_3. The reaction energy to form $Au_2(PH_3)_2$ from $AuClPH_3$ in methanol is -1.06 eV with a barrier height of 0.88 eV (Figure 6.1b) and the energy to form $Au_2ClPH_3^-$ is -0.73 eV. $AuClHSCH_3$ reactions are similar to the phosphine reactions, where a chloride, HCl, or a thiol ligand can be expelled. It is more favorable to form $Au_2(HSCH_3)_2$ than $Au_2ClHSCH_3$ with reaction energies of -1.36 eV and -1.21 eV, respectively (Figure 6.1c). The barrier height for formation of $Au_2(HSCH_3)_2$ is 0.66 eV. $AuClSCH_3^-$ can also be used as a precursor and it has the option to lose chloride, HCl, thiol, or

thiolate. The most favored reaction is the formation of $Au_2ClSCH_3^{2-}$ plus a thiol and a chloride with a reaction energy of -1.21 eV. The next favored reaction is the formation of $Au_2(SCH_3)_2^{2-}$ plus a chloride and HCl with a reaction energy of -0.52 eV. The least favored reaction is the creation of $Au_2ClSCH_3^{2-}$ and a thiolate and HCl with a reaction energy of 0.009 eV. We have been unable at this time to find a transition state with a single imaginary frequency for hydride reduction of any of the thiolate species.

6.4.4 Reactions of $Au_2Cl_2^{2-}$

For the remainder of the paper, we only discuss gold-chloride complexes; however, we expect similar reactions with other ligands. Once the Au(0)-containing $Au_2Cl_2^{2-}$ precursor has been formed, it can react with species present in the reaction mixture. The reaction of two $Au_2Cl_2^{2-}$ containing precursors is unfavorable, which is likely due to Coulomb repulsion of the two dianionic species; reaction energies can be found in Appendix C. However, $Au_2Cl_2^{2-}$ is unique in that it will react with $AuCl_2^-$. This reaction forms $Au_3Cl_3^{2-}$ and spontaneous ejection of a chloride occurs with a reaction energy in methanol of -0.57 eV with a barrier height of 0.31 eV (Figure 6.2). $Au_3Cl_3^{2-}$ is not a true Au(0) species: it is more accurate to describe it as two electrons delocalized over three gold atoms. For the purposes of this paper, we will refer to this cluster as a Au(0) species although the formal charges on Au are (+1/3). The characterization of $Au_3Cl_3^{2-}$ is also presented in Appendix C.

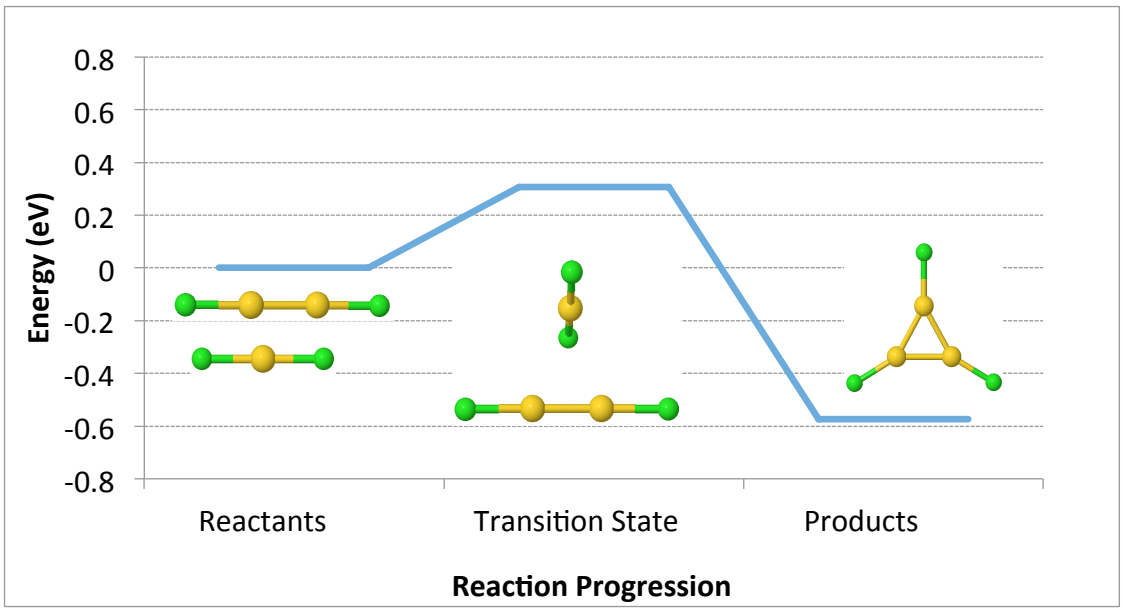

Figure 6.2 $AuCl_2^-$ addition to $Au_2Cl_2^{2-}$. Gold = gold and chloride = green

6.4.5 Growing Larger Clusters

Larger clusters can be grown incrementally by adding $AuCl_2^-$ to the previously mentioned Au(0) species. For example, $Au_3Cl_3^{2-}$ and $AuCl_2^-$ react to form $Au_4Cl_5^{3-}$ in methanol with a reaction energy of 0.09 eV. It is favorable to lose a chloride from $Au_4Cl_5^{3-}$ to yield $Au_4Cl_4^{2-}$ and Cl^- with an energy of -0.23 eV and a transition state energy of 0.09 eV (Figure 6.3). $Au_4Cl_4^{2-}$ has a tetrahedral gold core with two delocalized electrons similar to known gold-phosphine clusters.[105,111,120-122] This cluster could be a building block for the core of nanoparticles.[61,62,65,123] Characterization of this cluster is also presented in the Appendix C. The reaction of $Au_4Cl_4^{2-}$ with $AuCl_2^-$ results in a $Au_5Cl_6^{3-}$ structure with a reaction energy of 0.06 eV. In this case the removal of a chloride does not make the reaction exothermic but even more endothermic, with a chloride dissociation energy of 0.26 eV.

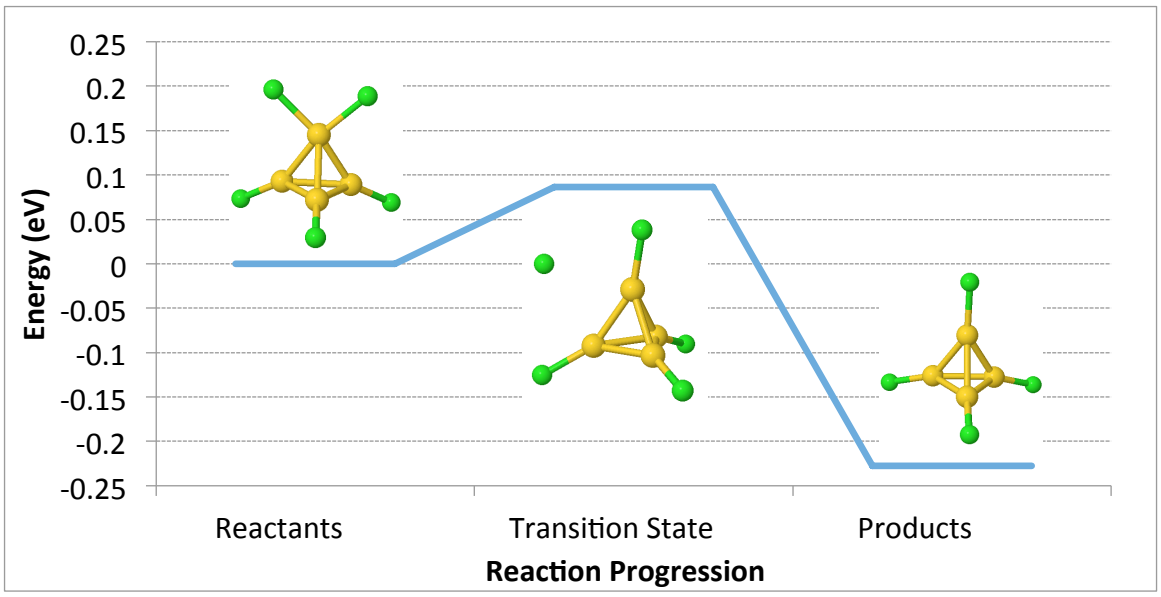

Figure 6.3 $AuCl_2^-$ addition to $Au_3Cl_3^{2-}$ and subsequent chloride removal. Gold = gold and chloride = green

Addition of $AuCl_2^-$ units does not lead to an increase in the electron count of the core, so in order to increase the number of electrons in the core, larger clusters can be grown by combining some of the Au(0) species. As noted above, $Au_2Cl_2^{2-}$ does not react with itself. However, $Au_2Cl_2^{2-}$ and $Au_3Cl_3^{2-}$ can react with each other. If the interaction occurs on the edge of $Au_3Cl_3^{2-}$, it forms $Au_5Cl_5^{4-}$ with a reaction energy of -0.06 eV in methanol (Figure 6.4a). If the interaction occurs at the vertex of $Au_3Cl_3^{2-}$, the reaction can form $Au_5Cl_4^{3-}$ plus chloride in methanol with a reaction energy of -0.50 eV (Figure 6.4b). The reaction of $Au_4Cl_4^{2-}$ and $Au_2Cl_2^{2-}$ result in $Au_6Cl_6^{4-}$ with a reaction energy of -0.45 eV (Figure 6.5a). Dimers of $Au_3Cl_3^{2-}$ and $Au_4Cl_4^{2-}$ can combine to form $Au_6Cl_6^{4-}$ and $Au_8Cl_8^{4-}$ respectively (Figure 6.5b and 6.5c). In methanol, $Au_6Cl_6^{4-}$ forms with a reaction energy of -0.08 eV and $Au_8Cl_8^{4-}$ forms with a reaction energy of -0.18 eV.

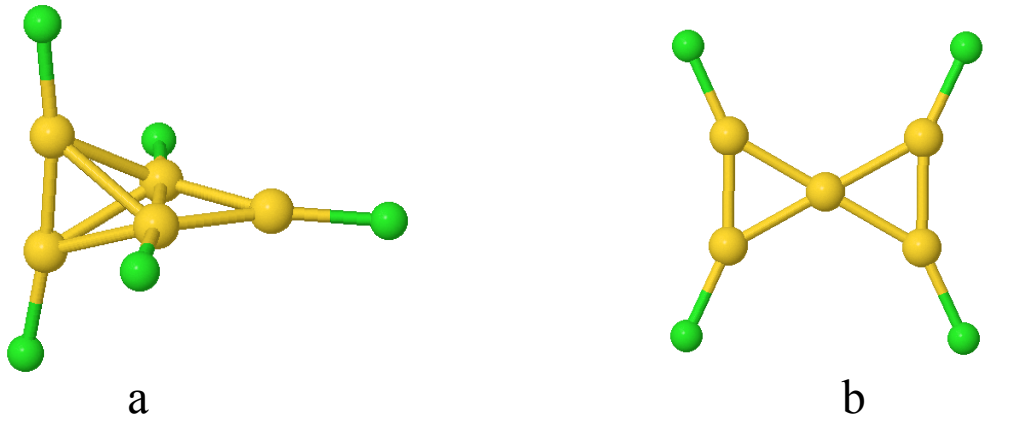

Figure 6.4. $Au_2Cl_2^{2-}$ addition to $Au_3Cl_3^{2-}$ a. at the edge and b. at the vertex. Gold = gold and chloride = green

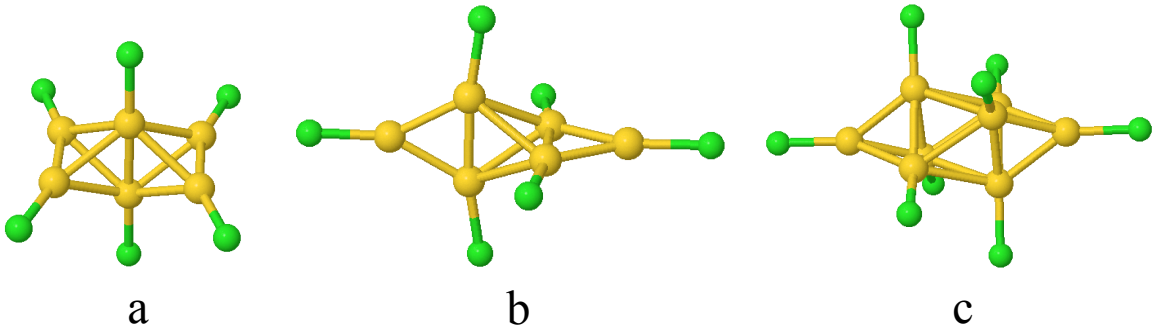

Figure 6.5 a. $Au_2Cl_2^{2-}$ addition to $Au_4Cl_4^{2-}$ b. $Au_3Cl_3^{2-}$ addition to $Au_3Cl_3^{2-}$ c. $Au_4Cl_4^{2-}$ addition to $Au_4Cl_4^{2-}$. Gold = gold and chloride = green

6.4.6 Benzene

To understand the original B-S synthesis, we also examined the reaction in a representative organic solvent (benzene) since nanoparticles are often grown in the organic phase. The reduction of the starting gold salt, $AuCl_4^-$, with hydride in benzene has a reaction energy of -3.46 eV and forms $AuCl_2^-$. Two $AuCl_2^-$ in the presence of a hydride can react as in methanol; however; this forms Au_2Cl^-, HCl, and two chloride ions with a reaction energy of -0.43 eV. The reaction of two Au_2Cl^- together yields $Au_4Cl_2^{2-}$; several isomers exist for this system. The formation of trans, Y, and linear isomers of $Au_4Cl_2^{2-}$ have reaction energies of 0.68 eV, 0.18 eV, and 0.07 eV, respectively, which suggests that these isomers are unlikely to form.

The reaction of two $AuCl_2^-$ to yield $Au_2Cl_2^{2-}$ is calculated to have a reaction energy of only -0.07 eV in benzene compared to -1.32 eV in methanol. The less favorable reaction energy is likely due to the buildup of two negative charges, which is unfavorable in nonpolar solvents such as benzene. In addition, it is important to note that the two $AuCl_2^-$ have to be in close proximity to react. In methanol, the aurophilic interaction of the Au(I) species is predicted to be 0.073 eV at the BP86/TZP level of theory, but is -0.148 eV at the BP86-D/TZP level of theory. The dispersion correction is required in order to predict an aurophilic interaction for this system. The aurophilic interaction in benzene is much weaker than the corresponding aurophilic interaction in methanol. If the dispersion correction is included in benzene, the aurophilic interaction has an energy of 0.966 eV, so the dimer is unlikely to form; if dispersion is not included, repulsive Coulombic interactions dominate and no local minimum with close intermolecular distances exists. If the two Au(I) species do not come close enough, the hydride will react with only one of the $AuCl_2^-$ molecules and can either exchange the hydride for a chloride to form $HAuCl^-$ or reduce $AuCl_2^-$ to Au^-, HCl, and Cl^-. In this case, Au(0)-containing species are not formed.

For the benzene reaction to yield reasonable Au(0)-containing precursors similar to the methanol reaction, we find that the introduction of tetramethylammonium (TMA) is required. We believe that the TMA helps balance the buildup of charge on the small gold cluster and enables the Au(I) precursors to approach each other. This was also observed in a recent study examining thiol substitution into $AuCl_2^-$ in benzene.[124] Without dispersion, the interaction between the two TMA-$AuCl_2$ complexes has an energy of -0.31 eV; with the dispersion correction, this interaction has an energy of -0.96 eV. With BP86-D, the two TMA and $AuCl_2^-$ units construct a system with an inner layer of $AuCl_2^-$ and an outer layer of TMA (Figure 6.6a). Hydride added to this system forms $Au_2Cl_2^{2-}$ (Figure 6.6b), unlike the addition of hydride to two

isolated $AuCl_2^-$ in benzene that yields Au_2Cl^-. With dispersion, the calculated gold-gold distance between $AuCl_2^-$ units is 3.73 Å. The reaction energy is -2.02 eV. If dispersion effects are not included in the calculations, the $AuCl_2^-$ units are computed to have a gold-gold distance of 6.21 Å, and no reaction occurs when hydride is added. The addition of a third TMA and $AuCl_2^-$ leads to a geometry with the three gold species in the inner layer and the three TMAs in the outer layer (Figure 6.6c). We do not believe this constitutes a reverse or inverse micelle but more of a counter-ion interaction, although much larger TMA-$AuCl_2^-$ systems would need to be studied to investigate this. The introduction of a fourth TMA and $AuCl_2^-$ expands the sphere of the layers, so all four Au(I) species are in the center and the four TMAs are on the outside (Figure 6.6e). The insertion of hydride into the systems containing three and four $AuCl_2^-$ units leads to the reduction of two Au(I) species to Au(0) and the formation of $Au_2Cl_2^{2-}$ as reported earlier in methanol (Figure 6.6d and 6.6f) with reaction energies of -2.33 eV and -1.48 eV, respectively. This suggests that the phase-transfer agent plays a crucial role in the formation of small gold clusters in benzene. Once $Au_2Cl_2^{2-}$ is formed, growth can occur by addition of $AuCl_2^-$. The formation of $Au_3Cl_3^{2-}$ from the reaction of $Au_2Cl_2^{2-}$ and $AuCl_2^-$ has a favorable reaction energy of -0.56 eV in benzene without considering the effect of TMA. $Au_3Cl_3^{2-}$ can further react with $AuCl_2^-$ to form $Au_4Cl_4^{2-}$ with a reaction energy of -0.06 eV, again without TMA.

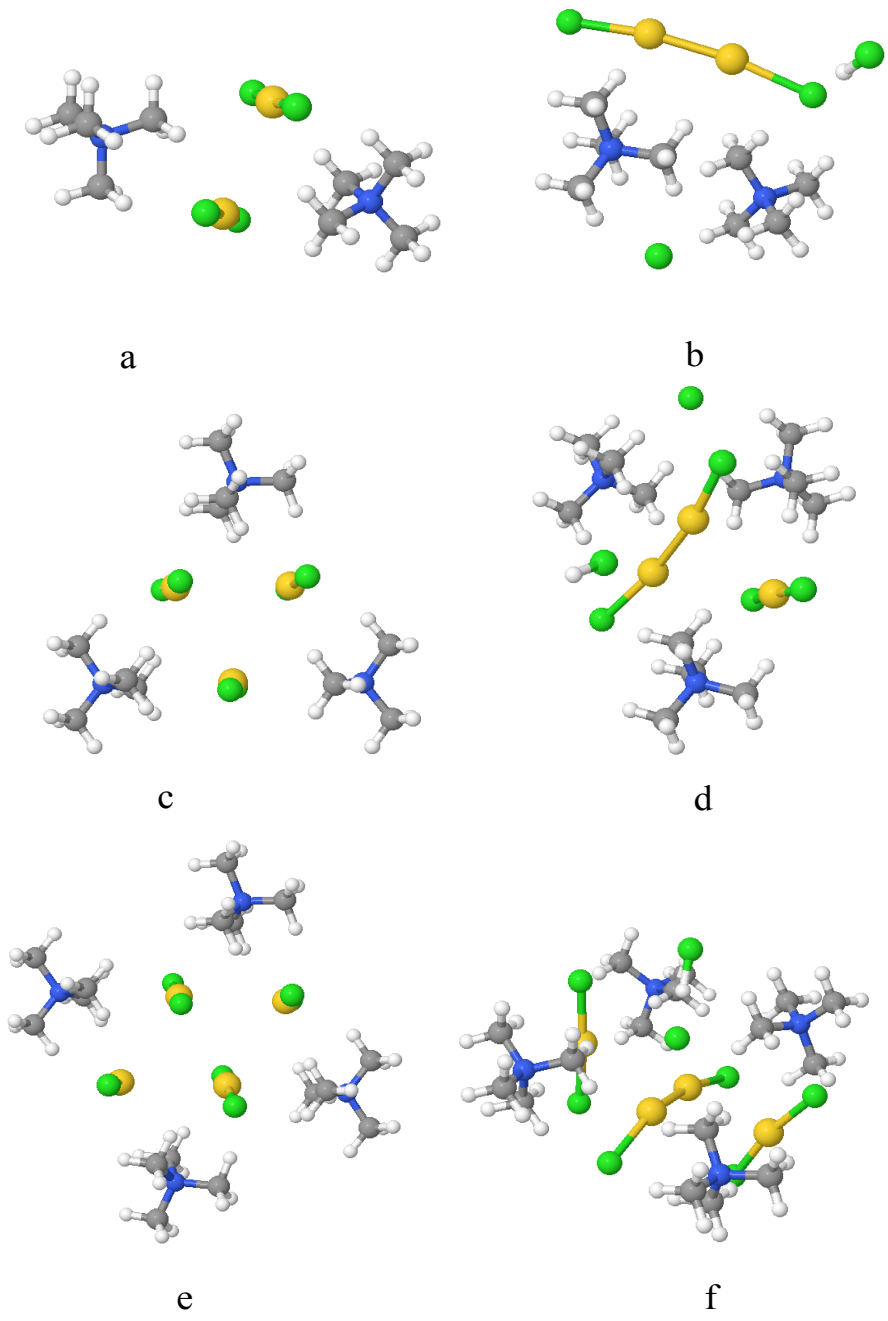

Figure 6.6 a. 2 Tetramethylammonium (TMA^+) and 2 $AuCl_2^-$ b. Hydride added to 6a. c. 3 TMA-$AuCl_2$ d. Hydride added to 6c. e. 4 TMA-$AuCl_2$ f. Hydride added to 6e. Gold = gold, chloride = green, nitrogen = blue, carbon = gray, and hydrogen = white

6.5 Conclusions

In this work we have demonstrated that closed-shell Au(0) species can be formed from hydride reduction of two Au(I)L_2 for a wide variety of ligands including halides, thiols, thiolates,

and phosphines. AuX_2^- (where X = Cl, Br, or I) hydride reduction reactions eject two halides and form $Au_2X_2^{2-}$. $AuClPH_3$ reactions can eject chloride, HCl, or PH_3 resulting in either $Au_2(PH_3)_2$ or $Au_2ClPH_3^-$. $AuClHSCH_3$ reactions are similar to the phosphine reactions, where a chloride, HCl, or a thiol can be ejected. The possible gold-containing products from the reaction are $Au_2(HSCH_3)_2$ or $Au_2ClHSCH_3$. $AuClSCH_3^-$ reactions behave similarly to both of the previous reactions; these molecules have the option to eject chloride, HCl, thiol, or thiolate. The reactions result in the formation of $Au_2ClSCH_3^{2-}$, $Au_2(SCH_3)_2^{2-}$, or $Au_2ClSCH_3^{2-}$. The Au(0) species can react to form larger clusters either through incremental addition of $AuCl_2^-$ or reactions with other Au(0) species. Some of the growth reactions become more favorable after the removal of a chloride such as $Au_4Cl_5^{3-}$ to form $Au_4Cl_4^{2-}$.

Reactions in benzene initially do not behave like the corresponding ones in methanol; hydride reduction of two $AuCl_2^-$ units favors the formation of Au_2Cl^-. However, Au_2Cl^- does not react favorably to form products. The introduction of TMA makes the benzene reactions perform similar to the methanol reactions. Dispersion corrected calculations are needed to account for the aurophilic interaction of the gold(I) molecules so that they are in close proximity to react when hydride was added. The TMA-$AuCl_2^-$ systems were found to form layered structures with $AuCl_2^-$ on the inside.

6.6 Acknowledgments

This material is based on work supported by the National Science Foundation under grant no. CHE-1213771. C.M.A. is grateful to the Alfred P. Sloan Foundation for a Sloan Research Fellowship (2011-2013) and the Camille and Henry Dreyfus Foundation for a Camille Dreyfus Teacher-Scholar Award (2011-2016).

Chapter 7 - Oxidation of Gold Clusters by Thiols

Reproduced with permission from:

Barngrover, B. M.; Aikens, C. M. *J. Phys. Chem. A* **2013**, *117*, 5377.

7.1 Abstract

The formation of gold-thiolate nanoparticles via oxidation of gold clusters by thiols is examined in this work. Using the BP86 density functional with a triple ζ basis set, the adsorption of methylthiol onto various gold clusters Au_n^Z (n = 1-8, 12, 13, 20; Z = 0, -1, +1) and Au_{38}^{4+} is investigated. The rate-limiting step for the reaction of one thiol with the gold cluster is the dissociation of the thiol proton; the resulting hydrogen atom can move around the gold cluster relatively freely. Addition of a second thiol can lead to H_2 formation and the generation of a gold-thiolate staple motif.

7.2 Introduction

Gold-thiolate nanoparticles and self-assembled monolayers (SAMs) are important for a variety of applications.[125-127] Recent structural studies using x-ray crystallography, scanning tunneling microscopy (STM), and/or density functional theory (DFT) on nanoparticles and SAMs have demonstrated that these systems have a core-shell-like arrangement in which gold-thiolate oligomers –SR-(Au-SR-)$_n$- (where the gold atom is formally considered to be in the +1 oxidation state) can cover a gold core or surface (which primarily contains Au(0)). For example, oligomeric motifs (often called "staples") are seen on a wide variety of nanoparticles such as $Au_{25}(SR)_{18}^{-/0}$,[30-33] $Au_{36}(SR)_{24}$,[34] $Au_{38}(SR)_{24}$,[35,36] and $Au_{102}(SR)_{44}$,[37] although recent work suggests that other binding motifs may be possible for sterically demanding thiolates.[38,39] These staples are also present on SAMs.[26-29]

The growth of gold-thiolate nanoparticles is often accomplished by the Brust-Schiffrin synthesis, in which a gold(III) salt reacts with thiol (HSR) and $NaBH_4$ and is consequently reduced to form $Au_n(SR)_m$ nanoparticles.[128] An alternative method of formation is through the use of solvated metal atom dispersion (SMAD), in which atoms from a metal vapor are trapped in frozen solvent such as tetrahydrofuran (THF) at 77K, warmed to yield clusters and colloids, and subsequently reacted with thiol.[129] These two synthetic methods can yield different sizes of gold-thiolate nanoparticles.[130]

Because the properties of a gold nanoparticle depend on its size and morphology, understanding its growth mechanism is of interest since this can potentially lead to control over these aspects. Several experimental[131-133] and theoretical[108,134] studies have begun to examine the Brust-Schiffrin synthesis and determine whether or not thiols are able to play a role in reducing the Au(III) salt to a nanoparticle containing Au(0) and Au(I). However, little is known about the oxidative synthesis in which thiols oxidize bare gold clusters in order to yield $Au_n(SR)_m$ nanoparticles. Two experimental studies have shown that H_2 is released in this process.[135,136] A very recent theoretical study used ab initio molecular dynamics with DFT to examine the interaction of two thiols with an Au_4 cluster; they found that H_2 is produced in the reaction and a staple is formed on the gold cluster.[137] Methylthiolates adsorbed on bare Au_{38} clusters have also been observed by Jiang et al. to form staple motifs in dynamic simulations.[138] In this work, we examine reaction pathways for the interaction of small gold clusters Au_n (n = 1-8, 12, 13, 20, 38) with one and two thiols in order to determine the preferred adsorption sites for thiols, the rate-limiting step of hydrogen atom dissociation and transfer, and the thermodynamics of H_2 production and staple formation in order to provide a greater understanding of the oxidative growth mechanism of gold nanoparticles.

7.3 Computational Details

All calculations are performed with the Amsterdam Density Functional (ADF)[54] package, using density functional theory with the Becke Perdew (BP86)[46,118] functional and a frozen-core polarized triple-ζ (TZP) basis set. We include scalar relativistic effects by employing the Zero Order Regular Approximation (ZORA).[53] We incorporate the tetrahydrofuran solvent using the Conductor-like Screening Model (COSMO), which represents the solvent by its dielectric constant.[55,78,79]

Initial structures for the small gold clusters Au_n (n = 1-8, 12, 13, 20, 38) are obtained from the literature;[139-144] both two-dimensional (2D) and three-dimensional (3D) structures for Au_{12} and Au_{13} are considered since these sizes are near the 2D-3D crossover point for gold.[143,144] Neutral, anionic, and cationic charge states for the gold clusters are examined as discussed in the following section. Calculations described in this work employ the methyl group on the thiol or thiolate ligand. All intermediates and transition states are fully optimized; Hessian calculations have been performed to verify the existence of one imaginary frequency for the transition states.

7.4 Results and Discussion

Table 7.1 Thiol adsorption energies for $Au_n^{(0,-,+)}$ (n = 1-8, 12, 13, 20) and Au_{38}^{4+}.

Neutral Clusters	Energy (eV)	Anion Clusters	Energy (eV)	Cation Clusters	Energy (eV)
Au_1	-0.68	Au_1	0.04	Au_1	-2.52
Au_2	-1.34	Au_2	NA	Au_2	-1.97
Au_3	-1.43	Au_3	NA	Au_3	-1.66
Au_4	-1.43	Au_4	-0.68	Au_4	-1.50
Au_5	-0.96	Au_5	-0.90	Au_5	-1.66
Au_6	-0.89	Au_6	-0.67	Au_6	-1.46
Au_7	-0.97	Au_7	-0.87	Au_7	-1.27
Au_8	-1.03	Au_8	-0.64	Au_8	-1.36
Au_{12} 2D	-0.90	Au_{12} 2D	-0.62	Au_{12} 2D	-1.21
Au_{12} 3D	-0.88	Au_{12} 3D	-0.55	Au_{12} 3D	-1.17
Au_{13} 2D	-0.98	Au_{13} 2D	-0.61	Au_{13} 2D	-1.40
Au_{13} 3D	-1.02	Au_{13} 3D	-0.63	Au_{13} 3D	-1.37
Au_{20}	-0.77	Au_{20}	-0.73	Au_{20}	-1.16
				Au_{38}^{4+}	-1.07

7.4.1 One Thiol Adsorption

Adsorption energies for one thiol on various gold clusters can be found in Table 7.1 and adsorption structures are shown in Figure 7.1. Binding of thiols to all unique gold coordinates were considered; only the lowest energy thiol adsorption sites are presented here. In almost all cases, thiol adsorption is exothermic. The first exception is the Au_1 anion, which is the only gold system examined here on which thiol adsorption is endothermic. Thiol adsorption on the neutral Au atom is exothermic with an adsorption energy (E_{ads}) of -0.68 eV, and adsorption on the Au_1^+ cation is the most favored with an adsorption energy of -2.52 eV. Thiol adsorption on all larger clusters is exothermic with the exception of Au_2^- and Au_3^- for which the thiol did not bind, which

is in agreement with Varganov et al. who observed the same phenomenon with hydrogen on these clusters.[145] Since the thiol binds via lone pair donation to the gold cluster, it appears that the Au_n^- (n = 1-3) anions are too small to favorably accommodate this binding (possibly due to a high electron density). For Au_1 through Au_3, all of the charge states have the same lowest energy structure for a given cluster size. Au_4 has two different low energy structures depending on charge: the neutral and anion share the same Y-shaped structure, whereas the cation has a diamond shape. As observed for Au_1, the cation is the charge state for which thiol adsorption is the most favored, followed by the neutral state, and lastly the anionic charge state. Au_5 also has two different low energy structures: Au_5^0 and Au_5^+ share the same W-shaped structure, whereas Au_5^- has a branched Y-shaped structure for its low energy structure. The lowest energy structures for Au_1-Au_8 are indicated in Figure 7.1 with their corresponding charge states. The gold clusters with one thiol adsorbed have the same core structures as the bare systems. Even though various charge states have different lowest energy structures, the trend for favored adsorption continues with $|E_{ads}(\text{cation})| > |E_{ads}(\text{neutral})| > |E_{ads}(\text{anion})|$.

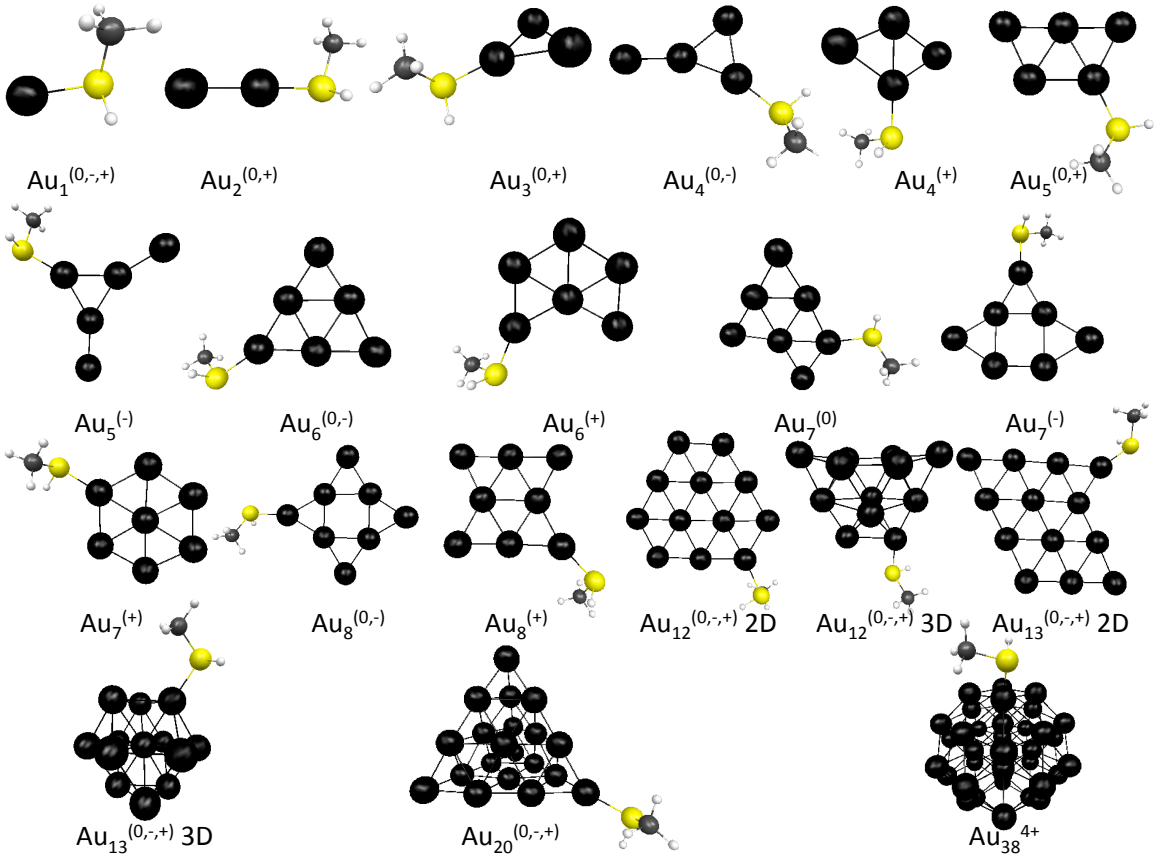

Figure 7.1 Lowest energy adsorption of methylthiol onto $Au_n^{(0,-,+)}$ (n = 1-8, 12, 13, 20) and Au_{38}^{4+}. Gold = black, sulfur = yellow, carbon = grey, and hydrogen = white

For Au_{12}, both two-dimensional (2D) and three-dimensional (3D) structures were considered with three different charge states, since this cluster size is approximately where the 2D to 3D crossover occurs. At the BP86/TZP level of theory, the 2D structure is lower in energy than the 3D structure. The adsorption energy trend as a function of charge state continues even with the change in dimension. Au_{13} 2D and 3D structures have also been examined. For this system, we have investigated the cuboctahedral structure, which is not the lowest energy 3D structure but is of interest due to its high symmetry. Previous studies have examined binding of the thiolate ion to the cuboctahedral Au_{13} cluster.[146,147] It should be noted that the Au_{13} 2D structure is lower in energy than this cuboctahedral structure. For Au_{20}, the tetrahedral structure is the lowest energy structure.[140] Again, the adsorption energy of the cation is the greatest,

followed by the neutral and then the anion. The last cluster we examined was octahedral Au_{38}^{4+}. The +4 charge state was examined because the neutral cuboctahedral cluster distorts due to a Jahn-Teller distortion.[123,148] This +4 charge leads to a cluster with an electronic magic number of 34 electrons. The octahedral cluster has two unique gold coordination sites: one is an edge atom joining two hexagonal faces and one square face, and the other is the face site in the center of each hexagonal face. The edge site is the more favored thiol adsorption site compared to the face site, which is logical since it has a lower coordination number.

7.4.2 Reaction Pathway

Next, we investigated the reaction pathway from the adsorption of one thiol on Au_3 and Au_{12} 3D to the formation of $HAu_x(SCH_3)$ in order to determine which step is the rate-limiting step. The reaction pathways for Au_3 and Au_{12} are shown in Charts 7.1 and 7.2. The first transition state is calculated for the dissociation of the thiol proton onto the gold cluster. For Au_3, this transition state lies 0.83 eV above the adsorbed complex; for Au_{12} 3D, the barrier height is 0.78 eV. When the thiol proton dissociates it gains partial charge from the gold cluster and behaves more like a hydrogen atom. Once the hydrogen is on the gold surface, it is free to move around the gold surface with relative ease, as shown by the barrier heights for the subsequent steps; for Au_3, the next largest barrier height is 0.03 eV. This ease of movement has been observed by other groups.[145,149] Au_{12} has a stable second intermediate, with the stability possibly due to the hydrogen bridging the two gold atoms, making the subsequent barrier height rather high at 0.71 eV; however this barrier height is still smaller than the previously mentioned one for the thiol proton dissociation.

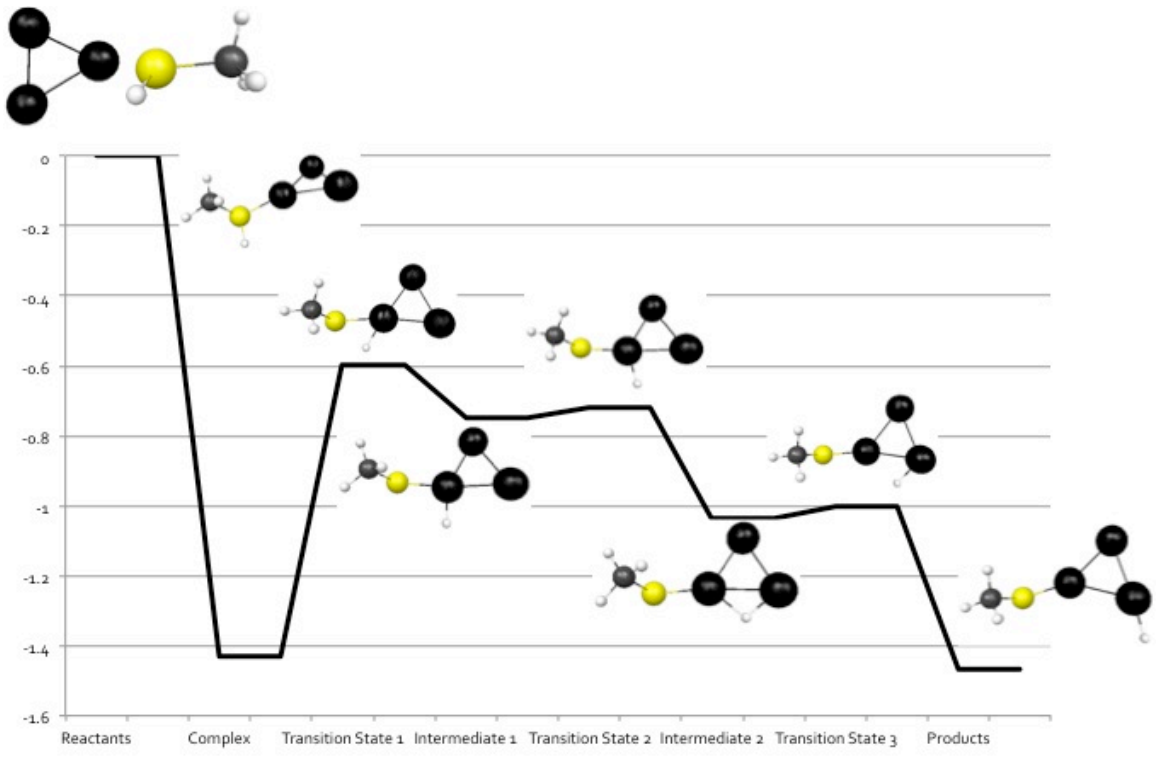

Chart 7.1 Reaction pathway of thiol adsorption on Au_3 and subsequent hydrogen movement on the gold cluster. Gold = black, sulfur = yellow, carbon = grey, and hydrogen = white

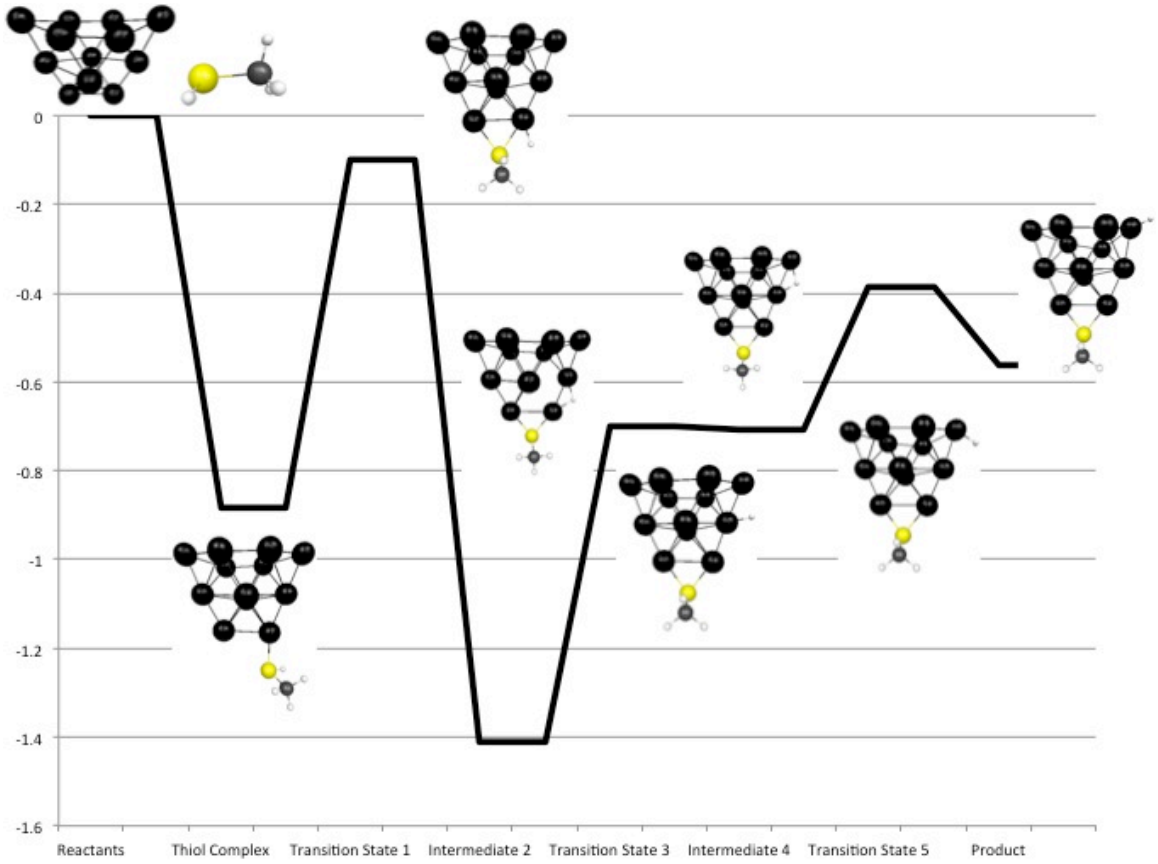

Chart 7.2 Reaction pathway of thiol adsorption on Au_{12} 3D and subsequent hydrogen movement on the gold cluster. Gold = black, sulfur = yellow, carbon = grey, and hydrogen = white

In Charts 7.1 and 7.2, the first transition state lies significantly below the energy of the separated reactants; in consequence, if energy transfer to metal vibrational modes or to solvent is slow enough, this reaction will proceed easily. Because the gold clusters are not bare under experimental conditions, we have considered the effects of solvent (in this case, THF) adsorption on the reaction energies. THF binds to the Au_3 and Au_{12} 3D clusters with E_{ads} of -0.69 and -0.28, respectively. The reaction for the replacement of THF by a thiol (leading to the first intermediates shown in Charts 7.1 and 7.2) yields reaction energies of -0.74 and -0.60, respectively; the energy released in these reactions is not quite enough to overcome the thiol dissociation barrier, so an effective activation energy barrier should be observed under experimental conditions.

Since the proton removal step is the rate-limiting step for Au_3 and Au_{12} 3D, a further investigation into this barrier height for all of the neutral gold-thiol clusters has been performed. Proton removal barrier heights are presented in Table 7.2. Thiol proton dissociation on Au_1 through Au_8 is found to have barrier heights of 0.87, 1.26, 0.83, 1.18, 1.10, 1.61, 0.86, and 1.38 eV, respectively. An overall odd-even effect is observed, which we believe is due to the unpaired electron in the odd size clusters which more easily allows the cluster to provide an electron to the incoming hydrogen, thus lowering the barrier height. On closer examination, the barrier height on Au_7 is significantly lower than clusters of neighboring sizes; this is because Au_7 undergoes an isomer change (Figure 7.2). For the remaining larger clusters the pattern appears to hold true. Au_{12} 3D is also an interesting case to examine closer. The Au_{12} 3D structure forms a thiolate bridge between two gold atoms when the thiol proton is removed. This is only observed in this structure and Au_7.

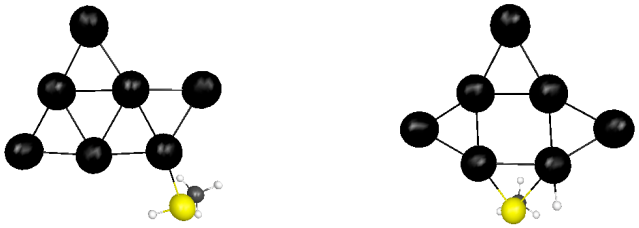

Figure 7.2 The isomer shift of Au_7 after the removal of the thiol proton and the formation of thiolate and hydrogen. Gold = black, sulfur = yellow, carbon = grey, and hydrogen = white

7.4.3 Second Thiol Addition

The crux of this investigation is to develop an understanding of the formation of gold thiolate nanoclusters and hydrogen gas. To explore this, a second thiol is required. Structures resulting from the addition of a second thiol to $HAu_3(SCH_3)$ and $HAu_{12}(SCH_3)$ 3D have been optimized. There are three sites for the incoming thiol to bind to on the Au_3 complex: where the thiolate is coordinated, where the hydrogen is coordinated, or on the uncoordinated gold (Figure

7.3). The favored adsorption site for the incoming thiol is the uncoordinated site (**1**) with an adsorption energy of -0.84 eV. The next favored adsorption site (**2**) is where the first hydrogen is coordinated with an adsorption energy of -0.41 eV. The least favored adsorption site (**3**) is where the first thiolate is coordinated with an adsorption energy of -0.14 eV. This trend makes sense because the incoming thiol would not have to compete with any other molecule or atom to bind to the uncoordinated site. The reaction energy for the production of hydrogen gas and a gold cluster with thiolates on different gold atoms (structure **4**) is -0.02 eV from structure **2** or 0.41 eV from structure **1**; the reaction energy is endothermic for the latter reaction because the initial structure has a high binding energy for the thiol. The least favored reaction is the production of H_2 from structure **3** where the thiol and thiolate are coordinated to the same gold; this process has a reaction energy of 0.83 eV.

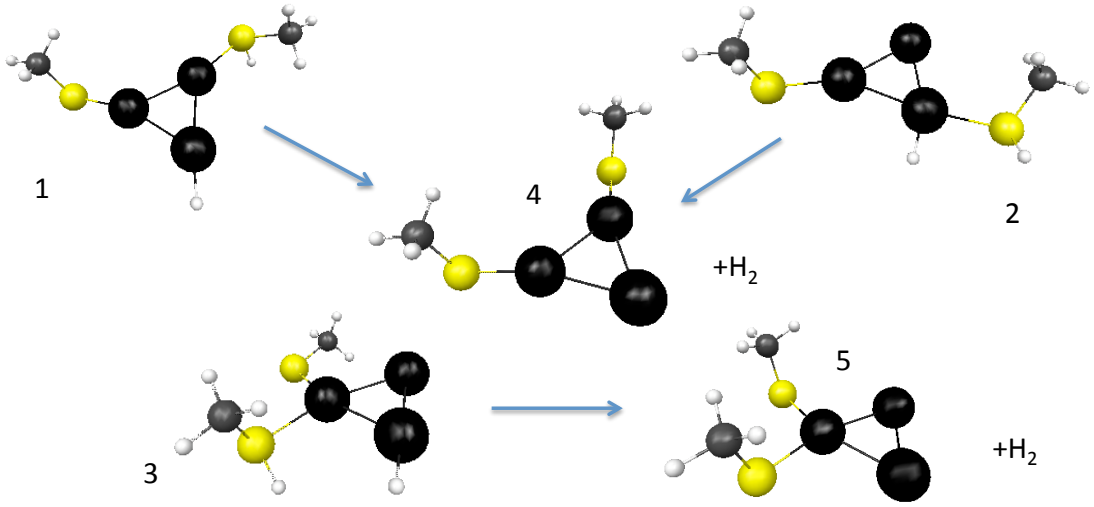

Figure 7.3 The second thiol adsorption to the vertices of Au_3.
Structure 1. Second thiol uncoordinated gold site
Structure 2. Second thiol coordinated to hydrogen site
Structure 3. Second thiol coordinated to thiolate site
Structure 4. Evolution of hydrogen gas and thiolate formation from structures 1 and 2.
Structure 5. Evolution of hydrogen gas and thiolate formation from structure 3.
Gold = black, sulfur = yellow, carbon = grey, and hydrogen = white

Compared to Au_3, Au_{12} 3D has many additional sites that the second thiol could adsorb to; in this work we focus on the low energy sites, which are the other vertices. Unlike the Au_3 case, the thiol adsorbing to the vertex that was not coordinated to the thiolate or hydrogen (structure **1** in Figure 7.4) is not the most favored structure for Au_{12} 3D (E_{ads} = -1.02 eV). Instead, the lowest energy structure is structure **2** in which the incoming thiol adsorbs to the gold atom where the hydrogen is coordinated (E_{ads} = -1.27 eV). The least favored adsorption site is structure **3** where the thiolate is already adsorbed (E_{ads} = -0.81 eV). For both structures **1** and **2**, evolution of hydrogen gas is thermodynamically unfavorable; reaction energies to produce H_2 and structures **4** and **5** are 0.62 and 0.95 eV, respectively. In contrast, evolution of hydrogen gas from structure **3** is favorable with a reaction energy of -0.68 eV. The resulting structure **6** is also an interesting cluster because it is the first time formation of a staple motif is observed in this investigation. Structure **6** is lower in energy than isomers **4** and **5**, which underscores the importance of the staple motif in nanoparticle and SAM structure. Thus, although the most favorable adsorption geometries for thiols at low coverage involve low-coordinated gold atoms, these structures are not as likely to lead to the formation of staples and hydrogen gas. We expect that at higher coverages, such as those needed for full passivation of the nanoparticle surface, gold-thiolate staples will form.

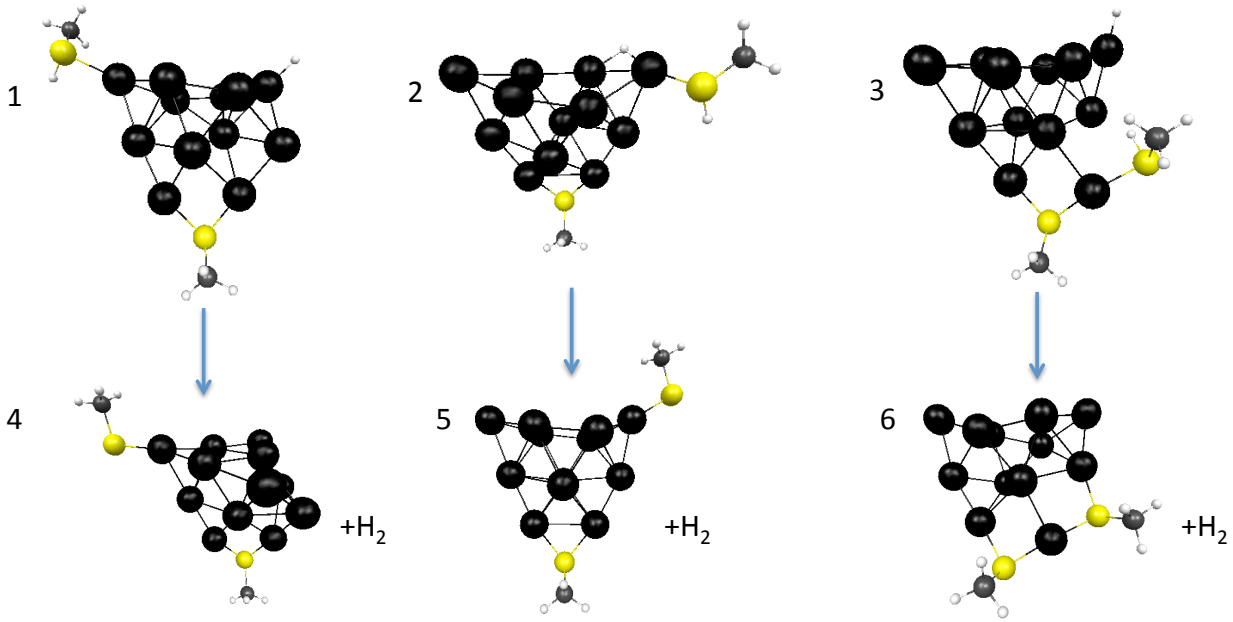

Figure 7.4 The second thiol adsorption to the vertices of Au_{12}.
Structure 1. Second thiol uncoordinated gold site
Structure 2. Second thiol coordinated to hydrogen site
Structure 3. Second thiol coordinated to thiolate site
Structure 4. Evolution of hydrogen gas and thiolate formation from structures 1.
Structure 5. Evolution of hydrogen gas and thiolate formation from structure 2.
Structure 6. Evolution of hydrogen gas and thiolate formation from structure 3.
Gold = black, sulfur = yellow, carbon = grey, and hydrogen = white

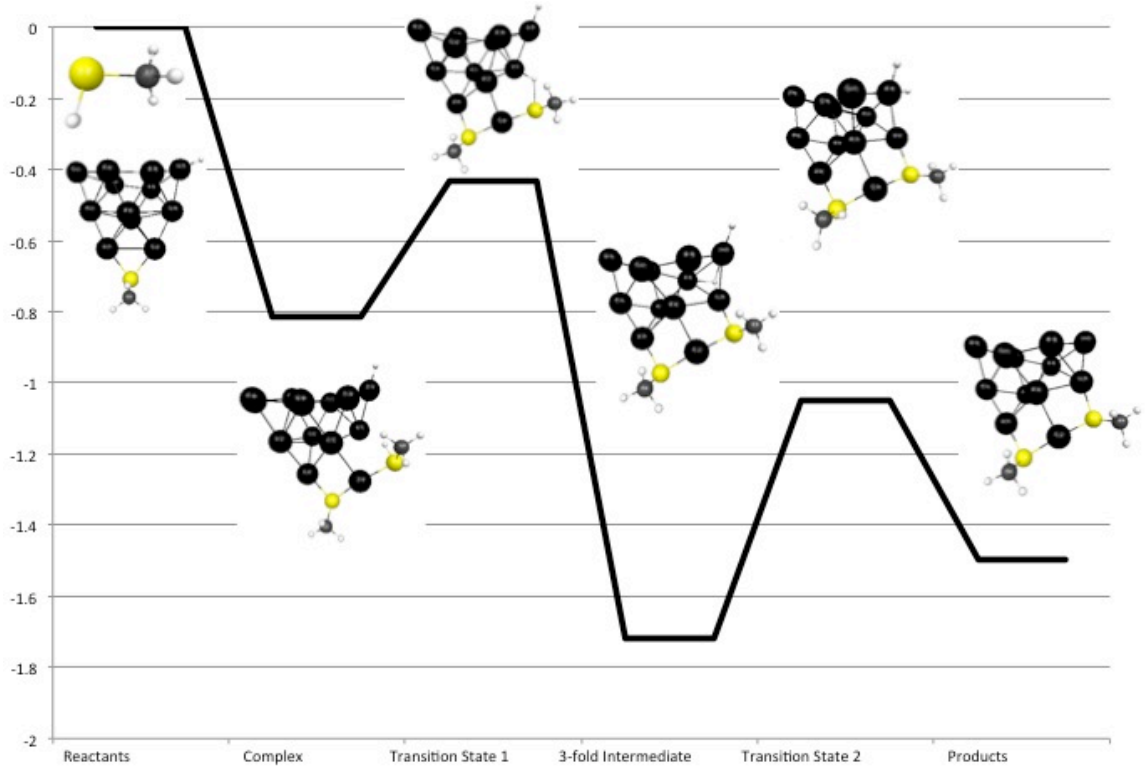

Chart 7.3 Reaction pathway of thiol adsorption on $HAu_{12}SCH_3$ 3D and subsequent hydrogen movement on the gold cluster. Gold = black, sulfur = yellow, carbon = grey, and hydrogen = white

A further investigation into the formation of structure **6** from structure **3** is examined (Chart 7.3). The removal of the thiol proton has a barrier height of 0.38 eV. An intermediate with a three-fold binding site for one of the hydrogens forms; this type of structure has not been seen in any of the previous pathways. The three-fold binding site is particularly stable with an energy of -1.72 eV. The transition state between the three-fold intermediate and the final evolution of hydrogen gas has a barrier height of 0.67 eV. During this potential energy surface investigation, another interesting intermediate was found. This structure has two hydrogens that bridge the gold much like a staple motif (Figure 7.5). It is 0.02 eV more stable than the three-fold binding site with an energy of -1.74 eV relative to starting reactants. Although the barriers to form this intermediate are not known at this point, the staple-like motifs could be an interesting target for future experimental and theoretical investigations.

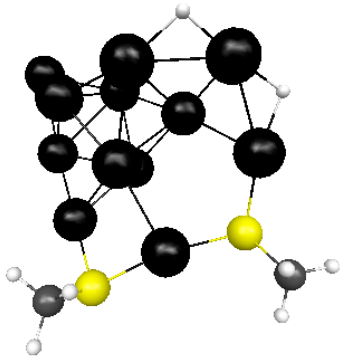

Figure 7.5 Bridging hydrogen motif structure. Gold = black, sulfur = yellow, carbon = grey, and hydrogen = white

7.5 Conclusion

In this work we investigated the adsorption of methylthiol onto various sizes of gold clusters (n = 1-8, 12, 13, 20, 38) with neutral, anionic, and cationic charge states (for Au_{38}, only the 4+ state was considered). We found that all adsorptions are predicted to be exothermic with the exceptions of Au_1^-, which is endothermic, and Au_2^- and Au_3^-, to which the thiol did not adsorb. We also determined that the rate-limiting step for the formation of hydrogen gas and the gold thiolate staple motifs is the removal of the thiol proton. An odd-even effect on the formation of the thiolate and hydrogen is present; we conclude that the odd size clusters have a lower barrier height because they do not have to undergo drastic electronic rearrangement to accommodate the new additions to the cluster, whereas the even clusters would have to rearrange. The movement of the hydrogen atom on two specific gold clusters, Au_3 and Au_{12} 3D, was examined. The hydrogen moves easily around the clusters compared to the energy required to dissociate the hydrogen and form the thiolate on the cluster. One final step investigated was the formation of hydrogen gas. The adsorption of a second thiol to the vertices of Au_3 and Au_{12} 3D was considered. H_2 formation is thermodynamically favored relative to the energy of separated thiol and gold cluster, but is not always exothermic once the second thiol has adsorbed to the gold cluster. Au_3 did not form a staple motif due to its small size, but a staple did form on

Au_{12} 3D when the first and second thiol adsorbed to the same vertex. The most favorable adsorption geometries for thiols at low coverage involve non-adjacent gold atoms, but these structures are not likely to lead to the formation of staples and hydrogen gas. However at higher coverages, such as those present under most experimental conditions, gold-thiolate staples can form.

7.6 Acknowledgment

This material is based upon work supported by the National Science Foundation under Grant No. CHE-1213771.

Chapter 8 - Mechanistic Insights into the Hydrogenation of 2-propenal via Catalysis of $Au_{25}(SH)_{18}^-$

8.1 Abstract

In this body of work, we employ density functional theory (DFT) to investigate the pathway for the hydrogenation of 2-propenal into two products, propylaldehyde or propenol, by the use of $Au_{25}(SH)_{18}^-$ as a catalyst. We also benchmark the dissociation of hydrogen gas on the $Au_{25}(SH)_{18}^-$ cluster at different functional levels and two Grimme dispersion correction levels including BP86-D, BP86-D3, PBE-D, PBE-D3, TPSS-D, TPSS-D3, SSB-D, B3LYP-D, and B3LYP-D3.

8.1 Introduction

Gold nanoparticles have a wide variety of uses such as drug delivery and therapy,[1,2] sensors,[4] electronics,[5] and optics,[6] and now have been found to be good catalysts[3] for selective oxidation and hydrogenation reactions.[150] Gold nanoparticles are used in selective oxidation of CO,[151-153] styrene,[154,155] and cyclohexane.[156] The catalytic oxidation of CO to CO_2 is usually done with a gold catalyst on a metal oxide support such as titania or ceria. Nie *et al*. found that although bare Au on TiO_2 is catalytically active, $Au_{25}(SR)_{18}$ on TiO_2 is not. They also found that if CeO_2 is used instead of TiO_2 as a support for $Au_{25}(SR)_{18}$, the gold nanoparticle is an effective catalyst.[153] The oxidation of styrene makes use of both metal oxide supported gold nanoparticles and unsupported or free gold nanoparticles. The metal oxide support is SiO_2 which leads to the gold nanoparticle being durable and reusable as a catalyst.[154] Either free or supported gold nanoparticles can oxidize styrene to benzaldehyde as the major product (selectivity ~70%) and styrene epoxide (selectivity 25%) and minor byproduct acetophenone (selectivity ~5%). Liu *et*

al. made hydroxyapatite (HAP) supported gold nanoparticles for the oxidation of cyclohexane. Using HAP supported gold nanoparticles, Liu and coworkers were able to get approximately 99% selectivity of cyclohexanone and cyclohexanol.

Less work has been done on selective hydrogenation reactions using unsupported gold nanoparticles as the catalyst. Yamamoto *et al*. compared $Au_{25}(SG)_{18}$ and N,N-dimethylformamide (DMF) stabilized gold nanoparticles for the hydrogenation of 4-nitrophenol (PNP) to 4-aminophenol with sodium borohydride ($NaBH_4$) as the hydrogen source.[157] They found that $Au_{25}(SG)_{18}$ was more catalytically active than the DMF stabilized gold nanoparticles. Zhu *et al.* studied the selective hydrogenation of α,β-unsaturated ketones and aldehydes by utilizing $Au_{25}(SCH_2CH_2Ph)_{18}^-$ and $Au_{25}(SC_{12}H_{25})_{18}^-$ as catalysts and hydrogen gas as the hydrogen source.[158] Zhu and coworkers found that the carbon-oxygen double bond is preferentially hydrogenated over the carbon-carbon double bond with 76% selectivity for the unsaturated alcohol compared to 14% selectivity for the aldehyde and 10% for the saturated alcohol. These findings are surprising since most hydrogenation reactions preferentially hydrogenate carbon-carbon double bonds compared to carbon-oxygen double bonds.

Although catalysis on supported and unsupported thiolate-stabilized nanoparticles have been of interest recently, the mechanisms for these reactions have not yet been studied. In this work, we investigate the mechanism for the hydrogenation of α,β-unsaturated aldehydes catalyzed by unsupported $Au_{25}(SH)_{18}^-$ for comparison with the work of Zhu *et al.* in reference [158]. 2-Propenal is chosen as our model reactant (Figure 8.1) since it is the simplest model compound that contains both a carbon-oxygen double bond and a carbon-carbon double bond.

8.3 Computational Details

Using density functional theory (DFT) as implemented in the Amsterdam Density Functional (ADF)[54] package, we benchmarked the dissociation of hydrogen gas on $Au_{25}(SH)_{18}^-$. All structures were optimized using the Becke-Perdew (BP86)[46,47] exchange correlation functional. As used in this work, the notation B//A implies that a single point energy using functional B was performed at the optimized geometry from functional A. Single point energies were performed with the following functionals: Perdew, Burke, and Ernzerhof (PBE);[48] Tao, Perdew, Staroverov, and Scuseria (TPSS);[49] Swart, Solà, and Bickelhaupt (SSB-D);[159,160] and the Becke 3-parameter functional with Lee, Yang, and Parr correlation (B3LYP)[46,50] in ADF that follows the Gaussian implementation by Stephens, Devlin, Chabalowski, and Frisch.[161] A triple-zeta plus polarization (TZP) basis set was employed for all calculations. Relativistic effects were included by the zero order regular approximation (ZORA).[53] We also examined two different Grimme dispersion corrections to the previously mentioned functionals.[119]

8.4 Results and Discussion

8.4.1 Functional and Grimme dispersion correction benchmarking

We started our investigation by benchmarking the dissociation of hydrogen gas on $Au_{25}(SH)_{18}^-$. The dissociation of hydrogen is found to be the first step necessary for the catalysis to progress. The 2-propenal does not chemisorb or physisorb on the gold nanoparticle even when dispersion corrections are taken into account using various dispersion-corrected functionals; this work finds that hydrogen must already be present for the 2-propenal to react. Table 8.1 summarizes the functionals and dispersion corrections used to examine hydrogen gas dissociation on $Au_{25}(SH)_{18}^-$. All structures were optimized at the BP86-D/TZP level of theory

and single point energies using the other functionals were performed to obtain reaction energies. A full optimization of all structures was also performed at the BP86-D3/TZP level of theory.

Table 8.1. Functionals and Grimme dispersion corrections reaction energies of H_2 dissociation on $Au_{25}(SH)_{18}^-$.

Functionals	Reaction Energy (eV)
BP86-D	-0.34
BP86-D3	-0.16
BP86-D3//BP86-D	0.01
PBE-D//BP86-D	-0.09
PBE-D3//BP86-D	0.28
TPSS-D//BP86-D	-0.22
TPSS-D3// BP86-D	0.25
SSB-D//BP86-D	0.25
B3LYP-D//BP86-D	-0.18
B3LYP-D3//BP86-D	0.21

From Table 8.1, the dissociation of H_2 on $Au_{25}(SH)_{18}^-$ may have a range of reaction energies depending on the level of theory used. For the functionals and dispersion corrections examined in this work, the most favored reaction occurs with BP86-D with a reaction energy of -0.34 eV, and the least favored reaction is PBE-D3 with a reaction energy of 0.28 eV. In all cases the Grimme D correction predicts hydrogen dissociation on the catalyst to be more favored than the Grimme D3 correction. All of the Grimme D corrections with the exception of the SSB functional predict exothermic reactions. The Grimme D3 corrections predict endothermic reactions with the exception of the optimized BP86 functional. We can conclude from the table that there is a dependence on the functional and Grimme dispersion correction chosen for the dissociation of H_2 on $Au_{25}(SH)_{18}^-$.

8.4.2 Hydrogenation pathway

Based on our benchmarking results, we chose the BP86 functional to investigate the hydrogenation pathway because it provides the lowest energy reactions for H_2 dissociation for both Grimme dispersion corrections. In Chart 8.1 we compare the pathway for the formation of propylaldehyde and propenol. Figure 8.1 shows all the species formed during the catalysis reaction. All the steps are more favored with the BP86-D functional than with the BP86-D3 functional. The first transition state for the dissociation of H_2 on the core gold of $Au_{25}(SH)_{18}^-$ has a barrier height of 0.34 eV for BP86-D and 1.52 eV for BP86-D3. The second intermediate, where the hydrogen atoms are dissociated on the gold core, is formed with a reaction energy of 0.02 and 0.42 eV for BP86-D and BP86-D3, respectively. The core of this intermediate is distorted compared to the approximately icosahedral core of the initial $Au_{25}(SH)_{18}^-$ catalyst.

The second transition state involves the introduction of the 2-propenal, and there are two possible isomers for this transition state. For the BP86-D functional, the second transition state that leads to propenol as a product has a barrier height of 0.61 eV and the transition state that leads to propylaldehyde has a barrier height of 0.22 eV. The second transition state for the BP86-D3 functional that leads to propenol has a barrier height of 1.73 eV and the barrier height for the transition state that leads to propylaldehyde is 1.97 eV. The second transition state shows a discrepancy between the relative barrier heights. The Grimme D dispersion correction shows that propylaldehyde has a lower barrier height, while the Grimme D3 dispersion correction predicts that propenol has a lower barrier height. Different orientations of propenal are noted for production of the two possible products. The propenal orientation that leads to propenol has the carbon-carbon double bond parallel to the gold surface whereas the propenal orientation that leads to propylaldehyde has the carbon-oxygen bond perpendicular to the gold surface.

Formation of the third intermediate, which consists of propenol or propylaldehyde physisorbed on $Au_{25}(SH)_{18}^-$, is the most exothermic step in the reaction pathway. The formation of propenol in the third intermediate has a reaction energy of -2.53 eV with the BP86-D functional and the formation of propylaldehyde has a reaction energy of -3.17 eV. For the BP86-D3 functional, the formation of propenol has a reaction energy of -1.76 eV and the formation of propylaldehyde has a reaction energy of -2.45 eV.

Once the physisorbed products are released from the gold catalyst, the overall reaction energy for the BP86-D functional for the formation of propenol is -0.94 eV and for the formation of propylaldehyde is -1.62 eV. The overall reaction energy for the BP86-D3 is very similar to BP86-D with the reaction energy for the formation of propenol being -0.92 eV and for the formation of propylaldehyde being -1.61 eV. Our mechanistic pathway investigation shows that the more favored product would be propylaldehyde, which is counter to what Zhu *et al*. find experimentally[158] but agrees with the usual results for carbon-carbon and carbon-oxygen double bond hydrogenation preferences. The difference between our theoretical results presented here and the experimental observations could arise from our simplification of the thiolate ligand employed on the gold nanoparticle. We hypothesize that steric hindrance could be the reason they see the alcohol preferentially formed over the aldehyde, since the reactant must approach the gold core closely in order for a given double bond to be hydrogenated and since the formation of the two products proceeds through transition states with different reactant orientation in TS2.

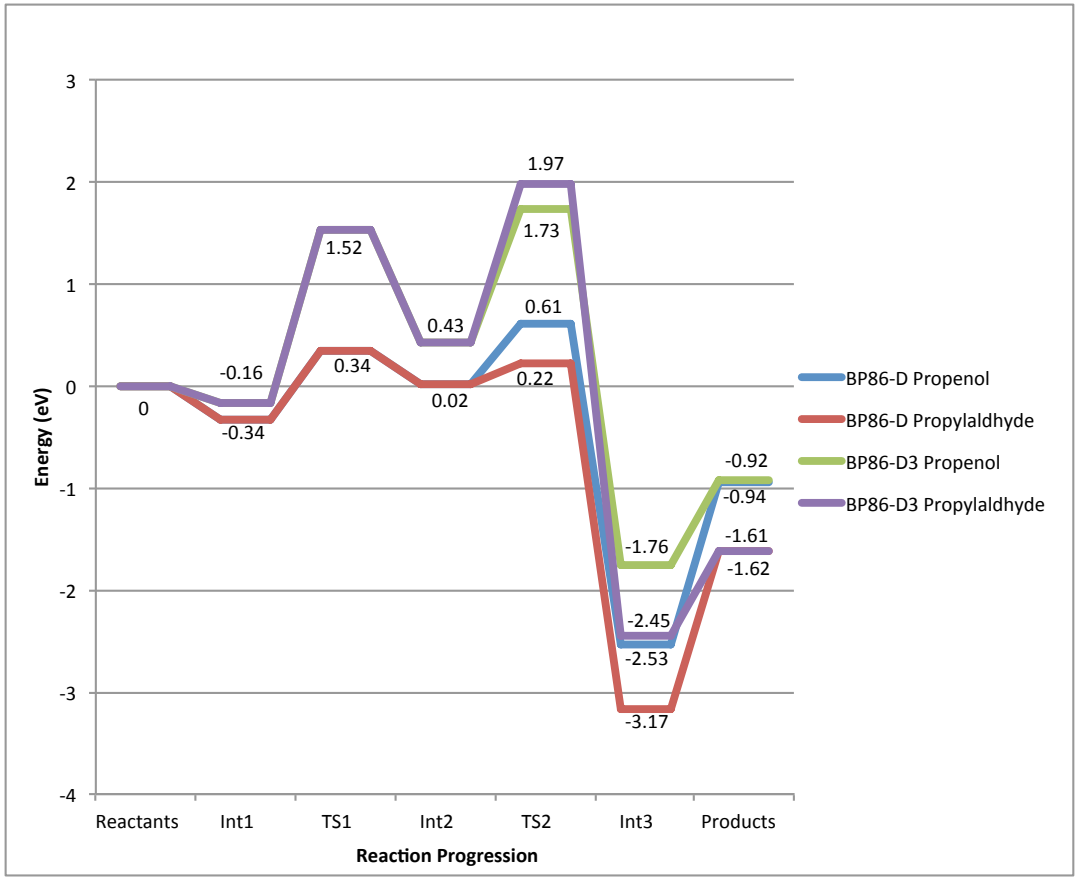

Chart 8.1 The Reaction Pathway of the Selective Hydrogenation of 2-propenal on $Au_{25}(SH)_{18}^-$.

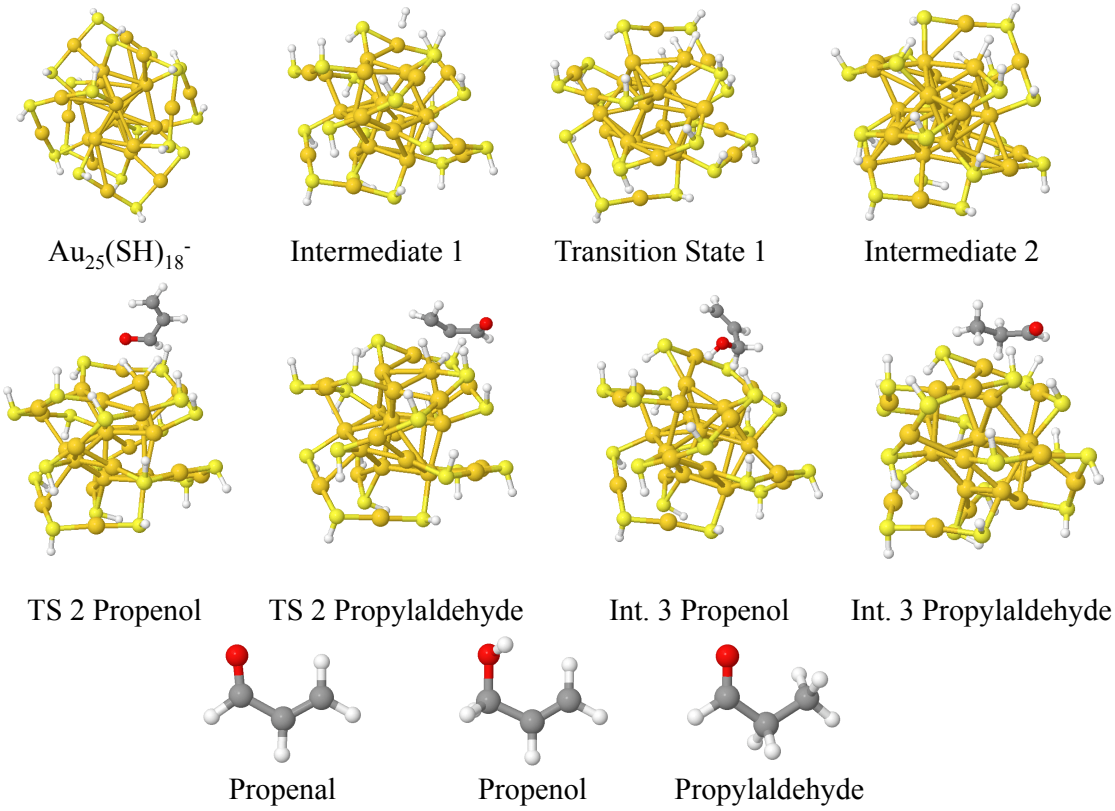

Figure 8.1 Optimized Structures of Species in Selective Hydrogenation of Propenal. Gold = gold, sulfur = yellow, carbon = gray, oxygen = red, and hydrogen = white. TS = Transition State, Int = Intermediate

8.5 Conclusions

In conclusion, this is the first investigation of the pathway for the selective hydrogenation of α,β-unsaturated aldehydes using $Au_{25}(SH)_{18}^-$ as a catalyst. We see from our benchmarking study that there is a dependence on the functional and Grimme dispersion correction chosen for the pathway study. We selected the most favored functional, BP86, and two Grimme dispersion corrections to investigate the mechanistic pathway. Our study shows with both Grimme dispersion corrections that the aldehyde is the preferred product over the alcohol. This is contradictory to what is seen experimentally by Zhu and coworkers, which we hypothesize is due to steric effects due to our use of a smaller R group on the gold nanoparticle.

8.6 Acknowledgements

This material is based on work supported by the National Science Foundation under Grant CHE-1213771. C.M.A. is grateful to the Camille and Henry Dreyfus Foundation for a Camille Dreyfus Teacher-Scholar Award (2011−2016).

Chapter 9 - Conclusions

Gold nanoparticles have been synthesized for years and for a variety of applications. The different syntheses have been created from trial and error in efforts to obtain certain sizes and morphologies. The size and morphology of nanoparticles dictates their properties such as optical, electronic, and catalytic. Most researchers focus their attention on the resulting nanoparticles and their applications.

In the past few years, some researchers have started to look at the underlying growth mechanism of nanoparticles. There have been a limited number of experimental studies and even fewer theoretical studies; this thesis presents a number of the first theoretical studies on gold-thiolate nanoparticle growth mechanisms. I started by looking at the reduction of the initial precursors that are involved in forming gold nanoparticles via the Brust-Schiffrin synthesis. The general precursors in the Brust-Schiffrin synthesis are Au(III), thiol, a reducing agent, and, depending on the number of phases, a phase transfer agent. It has been noted that a two step reduction must occur to form thiolate protected nanoparticles: Au(III) must first be reduced to Au(I) and then further reduced to Au(0). Researchers have examined the first step fairly thoroughly and we can conclude that Au(III) is reduced to Au(I) in high yield. The main unknown is: what Au(I) species are formed? The debate has focused on two specific questions: whether the Au(I) species are polymeric or not, and what ligands are bound to gold? For the first question about whether the Au(I) species is polymeric or not, we conclude that the answer depends on the solvent that is used in the synthesis. In nonpolar solvent, the answer seems to be that they are not polymeric. Based on the findings in my work, I believe this is due to the nonpolar solvent not being able to deal with the charge buildup that occurs and also because the phase transfer agent inhibits their formation. In polar solvent, the answer seems to depend on

additional reaction conditions. Based on both experimental and theoretical results, it appears that if the ratio of thiol to gold is about three to one and the system is in basic solution then polymers can form quite readily. However, if the system is not in a basic solution and the ratio is closer to two to one, polymers are unlikely to form.

In addition, my work has addressed the second question of what ligands are bound to the gold species. This answer again depends on the solvent. In nonpolar solvents, the phase transfer agent typically has a bromide counterion and bromide can easily replace chloride. In polar solvents there is typically not a phase transfer agent, so the halide exchange is less likely. The introduction of the thiol ligand adds another layer of complexity to the ligand question. Thiol can replace halides readily, but the ratio of starting thiol can influence the number of thiols that can react. There are quite a few combinations and the Au(III) species before reduction has occurred can be written in a general form by the equation $AuCl_wBr_xSR_yHSR_z^q$ where $w + x + y + z = 4$ and $q = 3 - (w + x + y)$. A similar equation can be written for the Au(I) species. The general form would be $AuCl_wBr_xSR_yHSR_z^q$ where $w + x + y + z = 2$ and $q = 1 - (w + x + y)$.

The second reduction step to form Au(0) has not been studied experimentally as thoroughly as the first reduction step. Most commonly, the second step is simply written as Au(I) plus a reducing agent goes to Au(0). This is very general and authors often assume that the Au(0) begins as atomic gold, which is a radical species. The other problem is that the reducing agent (hydride) is being treated as a one electron donor instead of a two electron donor and the resulting reaction should be written as Au(I) plus reducing agent goes to Au^-. I have found that the reducing agent can be properly treated as a two electron donor; it will reduce one of the Au(I) species that is in close proximity to another Au(I) species to form $Au_2Cl_wBr_xSR_yHSR_z^q$ where w

$+ x + y + z = 2$ and $q = -(w + x + y)$. This species is a non-radical Au(0) species and in addition I have found that it can further react to form larger clusters.

Nanoparticles can also be synthesized by oxidation rather than by reduction. Oxidation of gold occurs in solvated metal atom dispersion SMAD-produced nanoparticles and in self-assembled monolayers (SAMs). In SMAD, the bare gold atoms bond together to form small seeds or clusters, and then the ligand is introduced. In this work, I found that the outer atoms can be oxidized to form the SR-Au-SR motifs that passivate gold nanoparticles and that the hydrogen atoms from the thiols are reduced to form H_2.

Overall, many new insights into the growth mechanisms of gold nanoparticles have emerged in the past few years; however, there are still unanswered questions. One question is: what are the steps in the growth mechanism between the formation of smaller clusters and the final stable nanoparticle? Another question is: what is the role of the phase transfer agent? Is it a counterion that helps stabilize the charge buildup in the growth process, is it a reverse micelle where the growth of nanoparticles starts, or is it a combination of the two? Hopefully in the future we will be able to answer these and other questions and fully elucidate the growth mechanisms of gold nanoparticles.

References

(1) Shaw, C. F. Gold-Based Therapeutic Agents. *Chem. Rev.* **1999**, *99*, 2589-2600.

(2) Daniel, M.-C.; Astruc, D. Gold Nanoparticles: Assembly, Supramolecular Chemistry, Quantum-Size-Related Properties, and Applications toward Biology, Catalysis, and Nanotechnology. *Chem. Rev.* **2003**, *104*, 293-346.

(3) Crooks, R. M.; Zhao, M.; Sun, L.; Chechik, V.; Yeung, L. K. Dendrimer-Encapsulated Metal Nanoparticles: Synthesis, Characterization, and Applications to Catalysis. *Acc. Chem. Res.* **2000**, *34*, 181-190.

(4) Huang, C.-C.; Yang, Z.; Lee, K.-H.; Chang, H.-T. Synthesis of Highly Fluorescent Gold Nanoparticles for Sensing Mercury(II). *Angew. Chem. Int. Ed.* **2007**, *46*, 6824-6828.

(5) Gittins, D. I.; Bethell, D.; Schiffrin, D. J.; Nichols, R. J. A Nanometre-scale Electronic Switch Consisting of a Metal Cluster and Redox-addressable Groups. *Nature* **2000**, *408*, 67-69.

(6) Kelly, K. L.; Coronado, E.; Zhao, L. L.; Schatz, G. C. The Optical Properties of Metal Nanoparticles: The Influence of Size, Shape, and Dielectric Environment. *J. Phys. Chem. B* **2002**, *107*, 668-677.

(7) Alexandridis, P. Gold Nanoparticle Synthesis, Morphology Control, and Stabilization Facilitated by Functional Polymers. *Chem. Eng. Technol.* **2011**, *34*, 15-28.

(8) Faraday, M. The Bakerian Lecture: Experimental Relations of Gold (and Other Metals) to Light. *Philos. Trans. R. Soc. London* **1857**, *147*, 145-181.

(9) Thompson, D. Michael Faraday's recognition of ruby gold: the birth of modern nanotechnology. *Gold Bull* **2007**, *40*, 267-269.

(10) Turkevich, J.; Stevenson, P. C.; Hillier, J. A study of the nucleation and growth processes in the synthesis of colloidal gold. *Discuss. Faraday. Soc.* **1951**, *11*, 55-75.

(11) Brust, M.; Walker, M.; Bethell, D.; Schiffrin, D. J.; Whyman, R. Synthesis of Thiol-derivatised Gold Nanoparticles in a Two-phase Liquid-Liquid System. *J. Chem. Soc. Chem. Commun.* **1994**, 801-802.

(12) Alvarez, M. M.; Khoury, J. T.; Schaaff, T. G.; Shafigullin, M.; Vezmar, I.; Whetten, R. L. Critical sizes in the growth of Au clusters. *Chem. Phys. Lett.* **1997**, *266*, 91-98.

(13) Goulet, P. J. G.; Lennox, R. B. New Insights into Brust-Schiffrin Metal Nanoparticle Synthesis. *J. Am. Chem. Soc.* **2010**, *132*, 9582-9584.

(14) Barngrover, B. M.; Aikens, C. M. The Golden Pathway to Thiolate-Stabilized Nanoparticles: Following the Formation of Gold(I) Thiolate from Gold(III) Chloride. *J. Am. Chem. Soc.* **2012**, *134*, 12590-12595.

(15) Luo, Z.; Nachammai, V.; Zhang, B.; Yan, N.; Leong, D. T.; Jiang, D.-e.; Xie, J. Toward Understanding the Growth Mechanism: Tracing All Stable Intermediate Species from Reduction of Au(I)-Thiolate Complexes to Evolution of Au_{25} Nanoclusters. *J. Am. Chem. Soc.* **2014**, *136*, 10577-10580.

(16) Jana, N. R.; Peng, X. Single-Phase and Gram-Scale Routes toward Nearly Monodisperse Au and Other Noble Metal Nanocrystals. *J. Am. Chem. Soc.* **2003**, *125*, 14280-14281.

(17) Frenkel, A. I.; Nemzer, S.; Pister, I.; Soussan, L.; Harris, T.; Sun, Y.; Rafailovich, M. H. Size-controlled synthesis and characterization of thiol-stabilized gold nanoparticles. *J. Chem. Phys.* **2005**, *123*, 184701-184706.

(18) Yee, C. K.; Jordan, R.; Ulman, A.; White, H.; King, A.; Rafailovich, M.; Sokolov, J. Novel One-Phase Synthesis of Thiol-Functionalized Gold, Palladium, and Iridium Nanoparticles Using Superhydride. *Langmuir* **1999**, *15*, 3486-3491.

(19) Gentilini, C.; Evangelista, F.; Rudolf, P.; Franchi, P.; Lucarini, M.; Pasquato, L. Water-Soluble Gold Nanoparticles Protected by Fluorinated Amphiphilic Thiolates. *J. Am. Chem. Soc.* **2008**, *130*, 15678-15682.

(20) Bachman, R. E.; Bodolosky-Bettis, S. A.; Pyle, C. J.; Gray, M. A. Reversible Oxidative Addition and Reductive Elimination of Fluorinated Disulfides at Gold(I) Thiolate Complexes: A New Ligand Exchange Mechanism. *J. Am. Chem. Soc.* **2008**, *130*, 14303-14310.

(21) Perala, S. R. K.; Kumar, S. On the Mechanism of Phase Transfer Catalysis in Brust-Schiffrin Synthesis of Metal Nanoparticles. *Langmuir* **2013**, *29*, 14756-14762.

(22) Smoluchowski, M. V. Drei Vortrage uber Diffusion, Brownsche Bewegung und Koagulation von Kolloidteilchen. *Physik. Zeit.* **1916**, *17*, 557-585.

(23) Abécassis, B.; Testard, F.; Kong, Q.; Francois, B.; Spalla, O. Influence of Monomer Feeding on a Fast Gold Nanoparticles Synthesis: Time-Resolved XANES and SAXS Experiments. *Langmuir* **2010**, *26*, 13847-13854.

(24) Perala, S. R. K.; Kumar, S. On the Mechanism of Metal Nanoparticle Synthesis in the Brust-Schiffrin Method. *Langmuir* **2013**, *29*, 9863-9873.

(25) Lin, X. M.; Sorensen, C. M.; Klabunde, K. J. Digestive Ripening, Nanophase Segregation and Superlattice Formation in Gold Nanocrystal Colloids. *J. Nanopart. Res.* **2000**, *2*, 157-164.

(26) Maksymovych, P.; Sorescu, D. C.; Yates Jr., J. T. Gold-Adatom-Mediated Bonding in Self-Assembled Short-Chain Alkanethiolate Species on the Au(111) Surface. *Phys. Rev. Lett.* **2006**, *97*, 146103.

(27) Cossaro, A.; Mazzarello, R.; Rousseau, R.; Casalis, L.; Verdini, A.; Kohlmeyer, A.; Floreano, L.; Scandolo, S.; Morgante, A.; Klein, M. L.et al. X-ray Diffraction and Computation Yield the Structure of Alkanethiols on Gold(111). *Science* **2008**, *321*, 943-946.

(28) Grönbeck, H.; Häkkinen, H.; Whetten, R. L. Gold-Thiolate Complexes Form a Unique c(4x2) Structure on Au(111). *J. Phys. Chem. C* **2008**, *112*, 15490-15492.

(29) Jiang, D.-e.; Dai, S. Cis-trans Conversion of the CH_3S-Au-SCH_3 Complex on Au(111). *Phys. Chem. Chem. Phys.* **2009**, *97*, 146103.

(30) Heaven, M. W.; Dass, A.; White, P. S.; Holt, K. M.; Murray, R. W. Crystal Structure of the Gold Nanoparticle $[N(C_8H_{17})_4][Au_{25}(SCH_2CH_2Ph)_{18}]$. *J. Am. Chem. Soc.* **2008**, *130*, 3754-3755.

(31) Akola, J.; Walter, M.; Whetten, R. L.; Häkkinen, H.; Grönbeck, H. On the Structure of Thiolate-Protected Au_{25}. *J. Am. Chem. Soc.* **2008**, *130*, 3756-3757.

(32) Zhu, M.; Aikens, C. M.; Hollander, F. J.; Schatz, G. C.; Jin, R. Correlating the Crystal Structure of A Thiol-Protected Au_{25} Cluster and Optical Properties. *J. Am. Chem. Soc.* **2008**, *130*, 5883-5885.

(33) Zhu, M.; Eckenhoff, W. T.; Pintauer, T.; Jin, R. Conversion of Anionic $[Au_{25}(SCH_2CH_2Ph)_{18}]^-$ Cluster to Charge Neutral Cluster via Air Oxidation. *J. Phys. Chem. C* **2008**, *112*, 14221-14224.

(34) Zeng, C.; Qian, H.; Li, T.; Li, G.; Rosi, N. L.; Yoon, B.; Barnett, R. N.; Whetten, R. L.; Landman, U.; Jin, R. Total Structure and Electronic Properties of the Gold Nanocrystal $Au_{36}(SR)_{24}$. *Angew. Chem. Int. Ed.* **2012**, *124*, 13291-13295.

(35) Lopez-Acevedo, O.; Tsunoyama, H.; Tsukuda, T.; Häkkinen, H.; Aikens, C. M. Chirality and Electronic Structure of the Thiolate-Protected Au_{38} Nanocluster. *J. Am. Chem. Soc.* **2010**, *132*, 8210-8218.

(36) Qian, H.; Eckenhoff, W. T.; Zhu, Y.; Pintauer, T.; Jin, R. Total Structure Determination of Thiolate-Protected Au_{38} Nanoparticles. *J. Am. Chem. Soc.* **2010**, *132*, 8280-8281.

(37) Jadzinsky, P. D.; Calero, G.; Ackerson, C. J.; Bushnell, D. A.; Kornberg, R. D. Structure of a Thiol Monolayer-Protected Gold Nanoparticle at 1.1 Å Resolution. *Science* **2007**, *318*, 430-433.

(38) Krommenhoek, P. J.; Wang, J.; Hentz, N.; Johnston-Peck, A. C.; Kozek, K. A.; Kalyuzhny, G.; Tracy, J. B. Bulky Adamantanethiolate and Cyclohexanethiolate Ligands Favor Smaller Gold Nanoparticles with Altered Discrete Sizes. *ACS Nano* **2012**, *6*, 4903-4911.

(39) Nishigaki, J.-i.; Tsunoyama, R.; Tsunoyama, H.; Ichikuni, N.; Yamazoe, S.; Negishi, Y.; Ito, M.; Matsuo, T.; Tamao, K.; Tsukuda, T. A New Binding Motif of Sterically Demanding Thiolates on a Gold Cluster. *J. Am. Chem. Soc.* **2012**, *134*, 14295-14297.

(40) Stoeva, S.; Klabunde, K. J.; Sorensen, C. M.; Dragieva, I. Gram-Scale Synthesis of Monodisperse Gold Colloids by the Solvated Metal Atom Dispersion Method and Digestive Ripening and Their Organization into Two- and Three-Dimensional Structures. *J. Am. Chem. Soc.* **2002**, *124*, 2305-2311.

(41) Levine, I. N. *Quantum Chemsitry*; Sixth ed.; Pearson Prentice Hall: Upper Saddle River, 2009.

(42) Hohenberg, P.; Kohn, W. Inhomogeneous Electron Gas. *Phys. Rev.* **1964**, *136*, B864-B871.

(43) Kohn, W.; Sham, L. J. Self-Consistent Equations Including Exchange and Correlation Effects. *Phys. Rev.* **1965**, *140*, A1133-A1138.

(44) Perdew, J. P.; Schmidt, K. Jacob's ladder of density functional approximations for the exchange-correlation energy. *AIP Conference Proceedings* **2001**, *577*, 1-20.

(45) Vosko, S. H.; Wilk, L.; Nusair, M. Accurate spin-dependent electron liquid correlation energies for local spin density calculations: a critical analysis. *Can. J. Phys.* **1980**, *58*, 1200-1211.

(46) Becke, A. D. Density-Functional Exchange-Energy Approximation with Correct Asymptotic Behavior. *Phys. Rev. A* **1988**, *38*, 3098-3100.

(47) Perdew, J. P. Density-functional approximation for the correlation energy of the inhomogeneous electron gas. *Phys. Rev. B* **1986**, *33*, 8822-8824.

(48) Perdew, J. P.; Burke, K.; Ernzerhof, M. Generalized Gradient Approximation Made Simple. *Phys. Rev. Lett.* **1996**, *77*, 3865-3868.

(49) Tao, J.; Perdew, J. P.; Staroverov, V. N.; Scuseria, G. E. Climbing the Density Functional Ladder: Nonempirical Meta-Generalized Gradient Approximation Designed for Molecules and Solids. *Phys. Rev. Lett.* **2003**, *91*, 146401.

(50) Lee, C.; Yang, W.; Parr, R. G. Development of the Colle-Salvetti correlation-energy formula into a functional of the electron density. *Phys. Rev. B* **1988**, *37*, 785-789.

(51) Jensen, F. *Introduction to Computational Chemistry*; Second ed.; John Wiley & Sons Ltd: West Sussex, 2007.

(52) van Lenthe, E.; Baerends, E. J.; Snijders, J. G. Relativistic regular two-component Hamiltonians. *J. Chem. Phys.* **1993**, *99*, 4597-4610.

(53) van Lenthe, E.; Ehlers, A.; Baerends, E.-J. Geometry Optimizations in the Zero Order Regular Approximation for Relativistic Effects. *J. Chem. Phys.* **1999**, *110*, 8943-8953.

(54) te Velde, G.; Bickelhaupt, F. M.; Baerends, E. J.; Fonseca Guerra, C.; van Gisbergen, S. J. A.; Snijders, J. G.; Ziegler, T. Chemistry with ADF. *J. Comput. Chem.* **2001**, *22*, 931-967.

(55) Klamt, A.; Schüürmann, G. COSMO: A New Approach to Dielectric Screening in Solvents with Explicit Expressions for the Screening Energy and its Gradient. *J. Chem. Soc. Perkin Trans. 2* **1993**, 799-805.

(56) Jadzinsky, P. D.; Calero, G.; Ackerson, C. J.; Bushnell, D. A.; Kornberg, R. D. Structure of a Thiol Monolayer-Protected Gold Nanoparticle at 1.1 Å Resolution. *Science* **2007**, *318*, 430-433.

(57) Song, Y.; Harper, A. S.; Murray, R. W. Ligand Heterogeneity on Monolayer-Protected Gold Clusters. *Langmuir* **2005**, *21*, 5492-5500.

(58) Hughes, M. D.; Xu, Y.-J.; Jenkins, P.; McMorn, P.; Landon, P.; Enache, D. I.; Carley, A. F.; Attard, G. A.; Hutchings, G. J.; King, F.et al. Tunable gold catalysts for selective hydrocarbon oxidation under mild conditions. *Nature* **2005**, *437*, 1132-1135.

(59) Link, S.; El-Sayed, M. A. Spectral Properties and Relaxation Dynamics of Surface Plasmon Electronic Oscillations in Gold and Silver Nanodots and Nanorods. *J. Phys. Chem. B* **1999**, *103*, 8410-8426.

(60) Schaaff, T. G.; Shafigullin, M. N.; Khoury, J. T.; Vezmar, I.; Whetten, R. L.; Cullen, W. G.; First, P. N.; Gutiérrez-Wing, C.; Ascensio, J.; Jose-Yacamán, M. J. Isolation of Smaller Nanocrystal Au Molecules: Robust Quantum Effects in Optical Spectra. *J. Phys. Chem. B* **1997**, *101*, 7885-7891.

(61) Lopez-Acevedo, O.; Tsunoyama, H.; Tsukuda, T.; Häkkinen, H.; Aikens, C. M. Chirality and Electronic Structure of the Thiolate-Protected Au_{38} Nanocluster. *J. Am. Chem. Soc.* **2010**, *132*, 8210-8218.

(62) Qian, H.; Eckenhoff, W. T.; Zhu, Y.; Pintauer, T.; Jin, R. Total Structure Determination of Thiolate-Protected Au_{38} Nanoparticles. *J. Am. Chem. Soc.* **2010**, *132*, 8280-8281.

(63) Heaven, M. W.; Dass, A.; White, P. S.; Holt, K. M.; Murray, R. W. Crystal Structure of the Gold Nanoparticle $[N(C_8H_{17})_4][Au_{25}(SCH_2CH_2Ph)_{18}]$. *J. Am. Chem. Soc.* **2008**, *130*, 3754-3755.

(64) Zhu, M.; Aikens, C. M.; Hollander, F. J.; Schatz, G. C.; Jin, R. Correlating the Crystal Structure of A Thiol-Protected Au25 Cluster and Optical Properties. *J. Am. Chem. Soc.* **2008**, *130*, 5883-5885.

(65) Akola, J.; Walter, M.; Whetten, R. L.; Häkkinen, H.; Grönbeck, H. On the Structure of Thiolate-Protected Au_{25}. *J. Am. Chem. Soc.* **2008**, *130*, 3756-3757.

(66) Lopez-Acevedo, O.; Akola, J.; Whetten, R. L.; Grönbeck, H.; Häkkinen, H. Structure and Bonding in the Ubiquitous Icosahedral Metallic Gold Cluster Au144(SR)60. *J. Phys. Chem. C* **2009**, *113*, 5035-5038.

(67) Grönbeck, H.; Häkkinen, H.; Whetten, R. L. Gold-Thiolate Complexes Form a Unique c(4 x 2) Structure on Au(111). *J. Phys. Chem. C* **2008**, *112*, 15940-15942.

(68) Maksymovych, P.; Sorescu, D. C.; Yates, J. T., Jr. Gold-Adatom-Mediated Bonding in Self-Assembled Short-Chain Alkanethiolate Species on the Au(111) Surface. *Phys. Rev. Lett.* **2006**, *97*, 146103.

(69) Cossaro, A.; Mazzarello, R.; Rousseau, R.; Casalis, L.; Verdini, A.; Kohlmeyer, A.; Floreano, L.; Scandolo, S.; Morgante, A.; Klein, M. L.et al. X-ray Diffraction and Computation Yield the Structure of Alkanethiols on Gold(111). *Science* **2008**, *321*, 943-946.

(70) Jiang, D.-e.; Dai, S. Cis-trans conversion of the CH3S-Au-SCH3 complex on Au(111). *Phys. Chem. Chem. Phys.* **2009**, *11*, 8601-8605.

(71) Pei, Y.; Gao, Y.; Shao, N.; Zeng, X. C. Thiolate-Protected Au20(SR)16 Cluster: Prolate Au8 Core with New [Au3(SR)4] Staple Motif. *J. Am. Chem. Soc.* **2009**, *131*, 13619-13621.

(72) Jiang, D.-e.; Chen, W.; Whetten, R. L.; Chen, Z. What Protects the Core When the Thiolated Au Cluster is Extremely Small? *J. Phys. Chem. C* **2009**, *113*, 16983-16987.

(73) Tlahuice, A.; Garzón, I. L. On the structure of the Au18(SR)14cluster. *Phys. Chem. Chem. Phys.* **2012**, *14*, 3737-3740.

(74) Bau, R. Crystal Structure of the Antiarthritic Drug Gold Thiomalate (Myochrysine): A Double-Helical Geometry in the Solid State. *J. Am. Chem. Soc.* **1998**, *120*, 9380-9381.

(75) Barngrover, B. M.; Aikens, C. M. Electron and Hydride Addition to Gold(I) Thiolate Oligomers: Implications for Gold-Thiolate Nanoparticle Growth Mechanisms. *J. Phys. Chem. Lett.* **2011**, *2*, 990-994.

(76) Pei, Y.; Pal, R.; Liu, C.; Gao, Y.; Zhang, Z.; Zeng, X. C. Interlocked Catenane-Like Structure Predicted in $Au_{24}(SR)_{20}$: Implication to Structural Evolution of Thiolated Gold Clusters from Homoleptic Gold(I) Thiolates to Core-Stacked Nanoparticles. *J. Am. Chem. Soc.* **2012**, *134*, 3015-3024.

(77) Pye, C. C.; Ziegler, T. An implementation of the conductor-like screening model of solvation within the Amsterdam density functional package. *Theor. Chem. Acc.* **1999**, *101*, 396-408.

(78) Klamt, A. Conductor-like Screening Model for Real Solvents: A New Approach to the Quantitative Calculation of Solvation Phenomena. *J. Phys. Chem.* **1995**, *99*, 2224-2235.

(79) Klamt, A.; Jonas, V. Treatment of the Outlying Charge in Continuum Solvation Models. *J. Chem. Phys.* **1996**, *105*, 9972-9981.

(80) Gies, A. P.; Hercules, D. M.; Gerdon, A. E.; Cliffel, D. E. Electrospray Mass Spectrometry Study of Tiopronin Monolayer-Protected Gold Nanoclusters. *J. Am. Chem. Soc.* **2007**, *129*, 1095-1104.

(81) Angel, L. A.; Majors, L. T.; Dharmaratne, A. C.; Dass, A. Ion Mobility Mass Spectrometry of $Au_{25}(SCH_2CH_2Ph)_{18}$ Nanoclusters. *ACS Nano* **2010**, *4*, 4691-4700.

(82) Dass, A. Mass Spectrometric Identification of $Au_{68}(SR)_{34}$ Molecular Gold Nanoclusters with 34-Electron Shell Closing. *J. Am. Chem. Soc.* **2009**, *131*, 11666-11667.

(83) Dass, A.; Stevenson, A.; Dubay, G. R.; Tracy, J. B.; Murray, R. W. Nanoparticle MALDI-TOF Mass Spectrometry without Fragmentation: $Au_{25}(SCH_2CH_2Ph)_{18}$ and Mixed Monolayer $Au_{25}(SCH_2CH_2Ph)_{18-x}(L)_x$. *J. Am. Chem. Soc.* **2008**, *130*, 5940-5946.

(84) Dass, A.; Dubay, G. R.; Fields-Zinna, C. A.; Murray, R. W. FAB Mass Spectrometry of $Au_{25}(SR)_{18}$ Nanoparticles. *Anal. Chem.* **2008**, *80*, 6845-6849.

(85) Negishi, Y.; Chaki, N. K.; Shichibu, Y.; Whetten, R. L.; Tsukuda, T. Origin of Magic Stability of Thiolated Gold Clusters: A Case Study on $Au_{25}(SC_6H_{13})_{18}$. *J. Am. Chem. Soc.* **2007**, *129*, 11322-11323.

(86) Kim, K.; Lee, Y. M.; Lee, H. B.; Shin, K. S. Silver salts of aromatic thiols applicable as core materials of molecular sensors operating via SERS and fluorescence. *Biosens. Bioelectron.* **2009**, *24*, 3615-3621.

(87) Howell, J. A. S. Structure and bonding in cyclic thiolate complexes of copper, silver and gold. *Polyhedron* **2006**, *25*, 2993-3005.

(88) Grönbeck, H.; Walter, M.; Häkkinen, H. Theoretical Characterization of Cyclic Thiolated Gold Clusters. *J. Am. Chem. Soc.* **2006**, *128*, 10268-10275.

(89) Shao, N.; Pei, Y.; Gao, Y.; Zeng, X. C. Onset of Double Helical Structure in Small-Sized Homoleptic Gold Thiolate Clusters. *J. Phys. Chem. A* **2009**, *113*, 629-632.

(90) Kacprzak, K. A.; Lopez-Acevedo, O.; Häkkinen, H.; Grönbeck, H. Theoretical Characterization of Cyclic Thiolated Copper, Silver, and Gold Clusters. *J. Phys. Chem. C* **2010**, *114*, 13571-13576.

(91) Simpson, C. A.; Farrow, C. L.; Tian, P.; Billinge, S. J. L.; Huffman, B. J.; Harkness, K. M.; Cliffel, D. E. Tiopronin Gold Nanoparticle Precursor Forms Aurophilic Ring Tetramer. *Inorg. Chem.* **2010**, *49*, 10858-10866.

(92) LeBlanc, D. J.; Lock, C. J. L. cyclo-Hexakis[(2,4,6-triisopropylthiophenolato-S:S)gold(I)] Diethyl Ether Solvate. *Acta Cryst. C* **1997**, *53*, 1765-1768.

(93) Wiseman, M. R.; Marsh, P. A.; Bishop, P. T.; Brisdon, B. J.; Mahon, M. F. Homoleptic Gold Thiolate Catenanes. *J. Am. Chem. Soc.* **2000**, *122*, 12598-12599.

(94) Ahmed, L. S.; Dilworth, J. R.; Miller, J. R.; Wheatley, N. Silver(I)-silver(I) interactions in the tetrameric silver thiolate phosphine complex [Ag4(SPh)4(PPh3)4]. *Inorg. Chim. Acta* **1998**, *278*, 229-231.

(95) Dance, I. G. On the molecularity of crystalline cyclohexanethiolatosilver(I). *Inorg. Chim. Acta* **1977**, *25*, L17-L18.

(96) Dance, I. G.; Fitzpatrick, L. J.; Rae, A. D.; Scudder, M. L. The intertwined double-(-AgSR-).infin.-strand chain structure of crystalline (3-methylpentane-3-thiolato) silver, in relation to $(AgSr)_8$ molecules in solution. *Inorg. Chem.* **1983**, *22*, 3785-3788.

(97) Dance, I. G.; Fitzpatrick, L. J.; Craig, D. C.; Scudder, M. L. Monocyclic copper and silver tertiary alkanethiolates: formation and molecular structures of $(CuSBu\text{-}tert)_4(Ph_3P)_2$, $(AgSCMeEt_2)_8(Ph_3P)_2$ and $(AgSBu\text{-}tert)_{14}(Ph_3P)_4$ and structural principles. *Inorg. Chem.* **1989**, *28*, 1853-1861.

(98) Dance, I. G.; Fisher, K. J.; Banda, R. M. H.; Scudder, M. L. Layered structure of crystalline compounds silver thiolates (AgSR). *Inorg. Chem.* **1991**, *30*, 183-187.

(99) Aikens, C. M. Origin of Discrete Optical Absorption Spectra of $M_{25}(SH)_{18}^-$ Nanoparticles (M = Au, Ag). *J. Phys. Chem. C* **2008**, *112*, 19797-19800.

(100) Parker, J. F.; Weaver, J. E. F.; McCallum, F.; Fields-Zinna, C. A.; Murray, R. W. Synthesis of Monodisperse $[Oct_4N+][Au_{25}(SR)_{18}^-]$ Nanoparticles, with Some Mechanistic Observations. *Langmuir* **2010**, *26*, 13650-13654.

(101) Sardar, R.; Shumaker-Parry, J. S. 9-BBN Induced Synthesis of Nearly Monodisperse ω-Functionalized Alkylthiol Stabilized Gold Nanoparticles. *Chem. Mater.* **2009**, *21*, 1167-1169.

(102) Nagaraju, D. H.; Lakshminarayanan, V. Electrochemical Synthesis of Thiol-Monolayer-Protected Clusters of Gold. *Langmuir* **2008**, *24*, 13855-13857.

(103) Zhu, M.; Eckenhoff, W. T.; Pintauer, T.; Jin, R. Conversion of Anionic $[Au_{25}(SCH_2CH_2Ph)_{18}]^-$ Cluster to Charge Neutral Cluster via Air Oxidation. *J. Phys. Chem. C* **2008**, *112*, 14221-14224.

(104) Walter, M.; Akola, J.; Lopez-Acevedo, O.; Jadzinsky, P. D.; Calero, G.; Ackerson, C. J.; Whetten, R. L.; Grönbeck, H.; Häkkinen, H. A unified view of ligand-protected gold clusters as superatom complexes. *Proc. Natl. Acad. Sci.* **2008**, *105*, 9157-9162.

(105) Guidez, E. B.; Hadley, A.; Aikens, C. M. Initial Growth Mechanisms of Gold-Phosphine Clusters. *J. Phys. Chem. C* **2011**, *115*, 6305-6316.

(106) Barngrover, B. M.; Aikens, C. M. Incremental Binding Energies of Gold(I) and Silver(I) Thiolate Clusters. *J. Phys. Chem. A* **2011**, *115*, 11818-11823.

(107) Brust, M.; Fink, J.; Bethell, D.; Schiffrin, D. J.; Kiely, C. Synthesis and Reactions of Functionalised Gold Nanoparticles. *J. Chem. Soc., Chem. Commun.* **1995**, 1655.

(108) Barngrover, B. M.; Aikens, C. M. Electron and Hydride Addition to Gold(I) Thiolate Oligomers: Implications for Gold-Thiolate Nanoparticle Growth Mechanisms. *J. Phys. Chem. Lett.* **2011**, *2*, 990-994.

(109) Li, Y.; Zaluzhna, O.; Xu, B.; Gao, Y.; Modest, J. M.; Tong, Y. J. Mechanistic Insights into the Brust-Schiffrin Two-Phase Synthesis of Organo-chalcogenate-Protected Metal Nanoparticles. *J. Am. Chem. Soc.* **2011**, *133*, 2092-2095.

(110) Zhu, L.; Zhang, C.; Guo, C.; Wang, X.; Sun, P.; Zhou, D.; Chen, W.; Xue, G. New Insight into Intermediate Precursors of Brust-Schriffrin Gold Nanoparticles Synthesis. *J. Phys. Chem. C* **2013**, *117*, 11399-11404.

(111) Hudgens, J. W.; Pettibone, J. M.; Senftle, T. P.; Bratton, R. N. Reaction Mechanism Governing Formation of 1,3-Bis(diphenylphosphino)propane-Protected Gold Nanoclusters. *Inorg. Chem.* **2011**, *50*, 10178-10189.

(112) Fink, J.; Kiely, C. J.; Bethell, D.; Schiffrin, D. J. Self-Organization of Nanosized Gold Particles. *Chem. Mater.* **1998**, *10*, 922-926.

(113) Petroski, J.; Chou, M.; Creutz, C. The Coordination Chemistry of Gold Surfaces: Formation and Far-infrared Spectra of Alkanethiolate-capped Gold Nanoparticles. *J. Organ. Chem.* **2009**, *694*, 1138-1143.

(114) Li, Y.; Zaluzhna, O.; Tong, Y. J. Critical Role of Water and the Structure of Inverse Micelles in the Brust-Schiffrin Synthesis of Metal Nanoparticles. *Langmuir* **2011**, *27*, 7366-7370.

(115) Joshi, C. P.; Bigioni, T. P. Model for the Phase Transfer of Nanoparticles Using Ionic Surfactants. *Langmuir* **2014**, *30*, 13837-13843.

(116) Sugie, A.; Somete, T.; Kanie, K.; Muramatsu, A.; Mori, A. Triethylsilane as a Mild and Efficient Reducing Agent for the Preparation of Alkanethiol-capped Gold Nanoparticles. *Chem. Commun.* **2008**, 3882-3884.

(117) Schlesinger, H. I.; Brown, H. C.; Hoekstra, H. R.; Rapp, L. R. Reactions of Diborane with Alkali Metal Hydrides and Their Addition Compounds. New Syntheses of Borohydrides. Sodium and Potassium Borohydrides. *J. Am. Chem. Soc.* **1953**, *75*, 199-204.

(118) Perdew, J. P. Erratum: Density-functional approximation for the correlation energy of the inhomogeneous electron gas. *Phys. Rev. B* **1986**, *34*, 7406-7406.

(119) Grimme, S. Semiempirical GGA-type Density Functional Constructed with a Long-range Dispersion Correction. *J. Comput. Chem.* **2006**, *27*, 1787-1799.

(120) Demartin, F.; Manassero, M.; Naldini, L.; Ruggeri, R.; Sansoni, M. Synthesis and X-ray characterization of an Iodine-bridged Tetranuclear Gold Cluster, di-[small micro]-iodo-tetrakis(triphenylphosphine)-tetrahedro-tetragold. *J. Chem. Soc. Chem. Commun.* **1981**, 222-223.

(121) Zeller, E.; Beruda, H.; Schmidbaur, H. Tetrahedral Gold Cluster $[Au_4]^{2+}$: Crystal Structure of $\{[(tert\text{-}Bu)_3PAu]_4\}^{2+}(BF_4^-)_2 \cdot 2CHCl_3$. *Inorg. Chem.* **1993**, *32*, 3203-3204.

(122) Calhorda, M. J.; Crespo, O.; Gimeno, M. C.; Jones, P. G.; Laguna, A.; López-de-Luzuriaga, J. M.; Perez, J. L.; Ramón, M. A.; Veiros, L. F. Synthesis, Structure, Luminescence, and Theoretical Studies of Tetranuclear Gold Clusters with Phosphinocarborane Ligands. *Inorg. Chem.* **2000**, *39*, 4280-4285.

(123) Jiang, D.-e.; Walter, M. Au_{40}: A Large Tetrahedral Magic Cluster. *Phys. Rev. B* **2011**, *84*, 193402.

(124) Zhang, X.-N.; Wang, R.; Xue, G. Theoretical insights into the formation of thiolate-protected nanoparticles from gold (III) chloride. *Chin. Phys. B* **2014**, *23*, 098201.

(125) Shiang, Y.-C.; Hsu, C.-L.; Huang, C.-C.; Chang, H.-T. Gold Nanoparticles Presenting Hybridized Self-Assembled Aptamers That Exhibit Enhanced Inhibition of Thrombin. *Angew. Chem. Int. Ed.* **2011**, *50*, 7660-7665.

(126) Loaiza, O. A.; Lamas-Ardisana, P. J.; Jubete, E.; Ochoteco, E.; Loinaz, I.; Cabañero, G.; García, I.; Penadés, S. Nanostructured Disposable Impedimetric Sensors as Tools for Specific Biomolecular Interactions: Sensitive Recognition of Concanavalin A. *Anal. Chem.* **2011**, *83*, 2987-2995.

(127) Wang, G.; Park, H.-Y.; Lipert, R. J.; Porter, M. D. Mixed Monolayers on Gold Nanoparticle Labels for Multiplexed Surface-Enhanced Raman Scattering Based Immunoassays. *Anal. Chem.* **2009**, *81*, 9643-9650.

(128) Brust, M.; Walker, M.; Bethell, D.; Schiffrin, D. J.; Whyman, R. Synthesis of Thiol-derivatised Gold Nanoparticles in a Two-phase Liquid-Liquid System. *J. Chem. Soc., Chem. Commun.* **1994**, 801.

(129) Stoeva, S.; Klabunde, K. J.; Sorensen, C. M.; Dragieva, I. Gram-Scale Synthesis of Monodisperse Gold Colloids by the Solvated Metal Atom Dispersion Method and Digestive Ripening and Their Organization into Two- and Three-Dimensional Structures. *J. Am. Chem. Soc.* **2002**, *124*, 2305-2311.

(130) Jose, D.; Matthiesen, J.; Parsons, C.; Sorensen, C. M.; Klabunde, K. J. Size Focusing of Nanoparticles by Thermodynamic Control through Ligand Interactions. Molecular Clusters Compared with Nanoparticles of Metals. *J. Phys. Chem. Lett.* **2012**, *3*, 885-890.

(131) Goulet, P. J. G.; Lennox, R. B. New Insights into Brust-Schiffrin Metal Nanoparticle Synthesis. *J. Am. Chem. Soc.* **2010**, *132*, 9582-9584.

(132) Li, Y.; Zaluzhna, O.; Xu, B.; Gao, Y.; Modest, J. M.; Tong, Y. J. Mechanistic Insights into the Brust-Schiffrin Two-Phase Synthesis of Organo-chalcogenate-Protected Metal Nanoparticles. *J. Am. Chem. Soc.* **2011**, *133*, 2092-2095.

(133) Li, Y.; Zaluzhna, O.; Tong, Y. J. Critical Role of Water and the Structure of Inverse Micelles in the Brust-Schiffrin Synthesis of Metal Nanoparticles. *Langmuir* **2011**, *27*, 7366-7370.

(134) Barngrover, B. M.; Aikens, C. M. The Golden Pathway to Thiolate-Stabilized Nanoparticles: Following the Formation of Gold(I) Thiolates from Gold(III) Chloride. *J. Am. Chem. Soc.* **2012**, *134*, 12590-12595.

(135) Petroski, J.; Chou, M.; Creutz, C. The coordination chemistry of gold surfaces: Formation and far-infrared spectra of alkanethiolate-capped gold nanoparticles. *J. Organomet. Chem.* **2009**, *694*, 1138-1143.

(136) Matthiesen, J.; Jose, D.; Sorensen, C. M.; Klabunde, K. J. Loss of Hydrogen upon Exposure of Thiol to Gold Clusters at Low Temperature. *J. Am. Chem. Soc.* **2012**, *134*, 9376-9379.

(137) Rojas-Cervellera, V.; Giralt, E.; Rovira, C. Staple Motifs, Initial Steps in the Formation of Thiolate-Protected Gold Nanoparticles: How Do They Form? *Inorg. Chem.* **2012**, *51*, 11422-11429.

(138) Jiang, D.-e.; Tiago, M. L.; Luo, W.; Dai, S. The "Staple" Motif: A Key to Stability of Thiolate-Protected Gold Nanoclusters. *J. Am. Chem. Soc.* **2008**, *130*, 2777-2779.

(139) Häkkinen, H.; Yoon, B.; Landman, U.; Li, X.; Zhai, H.-J.; Wang, L.-S. On the electronic and atomic structures of small Au_N^- (N=4-14) clusters: A photoelectron spectroscopy and density-functional study. *J. Phys. Chem. A* **2003**, *107*, 6168.

(140) Li, J.; Li, X.; Zhai, H.-J.; Wang, L.-S. Au20: A tetrahedral cluster. *Science* **2003**, *299*, 864.

(141) Walker, A. V. Structure and energetics of small gold nanoclusters and their positive ions. *J. Chem. Phys.* **2005**, *122*, 094310.

(142) Xiao, L.; Tollberg, B.; Hu, X.; Wang, L. Structural study of gold clusters. *J. Chem. Phys.* **2006**, *124*, 114309.

(143) Mantina, M.; Valero, R.; Truhlar, D. G. Validation study of the ability of density functionals to predict the planar-to-three-dimensional structural transition in anionic gold clusters. *J. Chem. Phys.* **2009**, *131*, 064706.

(144) Li, X.-B.; Wang, H.-Y.; Yang, X.-D.; Zhu, Z.-H.; Tang, Y.-J. Size dependence of the structures and energetic and electronic properties of gold clusters. *J. Chem. Phys.* **2007**, *126*, 084505.

(145) Varganov, S. A.; Olson, R. M.; Gordon, M. S.; Mills, G.; Metiu, H. A study of the reactions of molecular hydrogen with small gold clusters. *J. Chem. Phys.* **2004**, *120*, 5169-5175.

(146) Larsson, J. A.; Nolan, M.; Greer, J. C. Interactions between Thiol Molecular Linkers and the Au_{13} Nanoparticle. *J. Phys. Chem. B* **2002**, *106*, 5931-5937.

(147) Genest, A.; Krüger, S.; Gordienko, A. B.; Rösch, N. Gold-Thiolate Clusters: A Relativistic Density Functional Study of the Model Species $Au_{13}(SR)_n$, R = H, CH_3, n = 4, 6, 8. *Z. Naturforsch.* **2004**, *59b*, 1585-1599.

(148) Michaelian, K.; Rendón, N.; Garzón, I. L. Structure and energetics of Ni, Ag, and Au nanoclusters. *Phys. Rev. B* **1999**, *60*, 2000-2010.

(149) Strømsnes, H.; Jusuf, S.; Schimmelpfennig, B.; Wahlgren, U.; Gropen, O. A theoretical study of the chemisorption of molecular hydrogen on a seven atom gold cluster. *J. Mol. Struct.* **2001**, *567-568*, 137-143.

(150) Li, G.; Jin, R. Atomically Precise Gold Nanoclusters as New Model Catalysts. *Acc. Chem. Res.* **2013**, *46*, 1749-1758.

(151) Bond, G. C.; Thompson, D. T. Catalysis by gold. *Catal. Rev. Sci. Eng.* **1999**, *41*, 319-388.

(152) Haruta, M.; Tsubota, S.; Kobayashi, T.; Kageyama, H.; Genet, M. J.; Delmon, B. Low-Temperature Oxidation of CO over Gold Supported on TiO_2, α-Fe_2O_3, and Co_3O_4. *J. Catal.* **1993**, *144*, 175-192.

(153) Nie, X.; Qian, H.; Ge, Q.; Xu, H.; Jin, R. CO Oxidation Catalyzed by Oxide-Supported $Au_{25}(SR)_{18}$ Nanoclusters and Identification of Perimeter Sites as Active Centers. *ACS Nano* **2012**, *6*, 6014-6022.

(154) Zhu, Y.; Qian, H.; Zhu, M.; Jin, R. Thiolate-Protected Aun Nanoclusters as Catalysts for Selective Oxidation and Hydrogenation Processes. *Adv. Mat.* **2010**, *22*, 1915-1920.

(155) Liu, Y.; Tsunoyama, H.; Akita, T.; Tsukuda, T. Efficient and selective epoxidation of styrene with TBHP catalyzed by Au_{25} clusters on hydroxyapatite. *Chem. Commun.* **2010**, *46*, 550-552.

(156) Liu, Y.; Tsunoyama, H.; Akita, T.; Xie, S.; Tsukuda, T. Aerobic Oxidation of Cyclohexane Catalyzed by Size-Controlled Au Clusters on Hydroxyapatite: Size Effect in the Sub-2 nm Regime. *ACS Catalysis* **2010**, *1*, 2-6.

(157) Yamamoto, H.; Yano, H.; Kouchi, H.; Obora, Y.; Arakawa, R.; Kawasaki, H. N,N-Dimethylformamide-stabilized gold nanoclusters as a catalyst for the reduction of 4-nitrophenol. *Nanoscale* **2012**, *4*, 4148-4154.

(158) Zhu, Y.; Qian, H.; Drake, B. A.; Jin, R. Atomically Precise $Au_{25}(SR)_{18}$ Nanoparticles as Catalysts for the Selective Hydrogenation of α,β-Unsaturated Ketones and Aldehydes. *Angew. Chem. Int. Ed.* **2010**, *49*, 1295-1298.

(159) Swart, M.; Solà, M.; Bickelhaupt, F. M. A new all-round density functional based on spin states and S_N2 barriers. *J. Chem. Phys.* **2009**, *131*, 094103.

(160) Swart, M.; Solà, M.; Bickelhaupt, F. M. Switching between OPTX and PBE exchange functionals. *J. Comput. Methods Sci. Eng.* **2009**, *9*, 69-77.

(161) Stephens, P. J.; Devlin, F. J.; Chabalowski, C. F.; Frisch, M. J. Ab Initio Calculation of Vibrational Absorption and Circular Dichroism Spectra Using Density Functional Force Fields. *J. Phys. Chem.* **1994**, *98*, 11623-11627.

(162) Schmidt, M. W.; Baldridge, K. K.; Boatz, J. A.; Elbert, S. T.; Gordon, M. S.; Jensen, J. H.; Koseki, S.; Matsunaga, N.; Nguyen, K. A.; Su, S.et al. General atomic and molecular electronic structure system. *J. Comput. Chem.* **1993**, *14*, 1347.

(163) Stevens, W. J.; Basch, H.; Krauss, M. Compact effective potentials and efficient shared-exponent basis sets for the first- and second-row atoms. *J. Chem. Phys.* **1984**, *81*, 6026.

(164) Stevens, W. J.; Krauss, M.; Basch, H.; Jasien, P. G. Relativistic compact effective potentials and efficient, shared-exponent basis sets for the third-, fourth-, and fifth-row atoms. *Can. J. Chem.* **1992**, *70*, 612.

(165) Cundari, T. R.; Stevens, W. J. Effective core potential methods for the lanthanides. *J. Chem. Phys.* **1993**, *98*, 5555.

Appendix A - Supporting Information for "The Golden Pathway to Thiolate-Stabilized Nanoparticles: Following the Formation of Gold(I) Thiolate from Gold(III) Chloride"

Table A.1 Acid/Base Reactions for the Removal of the First Thiol Proton

Bases	Reaction Energies (eV)
Cl^-	-0.14
SCH_3^-	-1.03
CH_3O^-	-1.78
$HSCH_3$	1.76
CH_3OH	0.72

Cl^- is a better base for removal of the thiol proton than either the free thiol ($HSCH_3$) or the solvent (CH_3OH). However, basic conditions in which the conjugate base of the thiol or solvent (SCH_3^- and CH_3O^-, respectively) is present would favorably lead to proton dissociation. The reaction energies reported in Table A.1 do not contain zero-point energies; however, these corrections are typically on the order of hundredths of an eV for the systems examined here.

Appendix B - Supporting Information for "Electron and Hydride Addition to Gold(I) Thiolate Oligomers: Implications for Gold-Thiolate Nanoparticle Growth Mechanisms

Because density functional theory is not the most accurate for electron affinities due to self-interaction error, electron affinities are also calculated for $Au_5(SCH_3)_5$ at the MP2 level of theory. These calculations employ the General Atomic and Molecular Electronic Structure System (GAMESS) package.[162] The basis set employed is the Stevens-Basch-Krauss-Jasien-Cundari (SBKJC)[163-165] effective core potential basis set; calculations are performed using both MP2 and BP86 for comparison. Single point calculations with these levels of theory are performed at the BP86/TZP geometries from the main text.

With this smaller basis set, EAs are calculated to be between 0.12 and 0.29 eV more positive with BP86. A much larger method dependence is observed. MP2/SBKJC EAs are 0.42-1.18 eV more positive than BP86/SBKJC EAs. This suggests that BP86 underestimates the degree to which electron addition processes are unlikely.

Table B.1 Electron Affinities (EA) in eV for $Au_5(SCH_3)_5$.

	First EA	Second EA	Third EA
BP86/SBKJC	-0.19	2.09	5.18
MP2/SBKJC	0.66	2.51	6.36

Appendix C - Supporting Information for "Prediction of Non-radical Au(0)-containing Precursors in Nanoparticle Growth Processes"

Dispersion-Corrected Calculations

Dispersion-corrected (BP86-D) calculations of $AuCl_4^-$ and its dimer, $AuCl_2^-$ and its dimer, and $Au_2Cl_2^{2-}$ and its dimer are discussed in this section. The reaction energies calculated without dispersion corrections (BP86) show unfavorable dimerization of the species; however, the dispersion corrections make all of the dimerization reactions more favorable in methanol. The $AuCl_2^-$ dimer is not favored to form in benzene. The introduction of tetramethylammonium (TMA) makes the dimerization in benzene more favorable.

Table C.1 Non-dispersion and dispersion calculations of Au(III), Au(I), and Au(0) dimers in methanol.

BP86/TZP Methanol	No dispersion (eV)	Dispersion (eV)
$Au_2Cl_2^{2-}$ dimer	0.417	-0.598
$AuCl_2^-$ dimer	0.073	-0.148
$AuCl_4^-$ dimer	0.104	-0.339

Table C.2 Non-dispersion and dispersion calculations of the dimer, trimer, and tetramer of $AuCl_2^-$.

BP86/TZP	Methanol		Benzene	
	No dispersion (eV)	Dispersion (eV)	No dispersion (eV)	Dispersion (eV)
2 $AuCl_2^-$	0.073	-0.148	*	0.966
3 $AuCl_2^-$	0.237	-0.699		
4 $AuCl_2^-$	0.429	-0.892		

* Non-dispersion-corrected dimer of $AuCl_2^-$ did not optimize in benzene; the two complexes moved apart (> 30Å) during optimization.

Table C.3 Non-dispersion and dispersion calculations of the interaction energies in the dimer, trimer, and tetramer of TMA-$AuCl_2$

BP86/TZP	Benzene	
	No dispersion (eV)	Dispersion (eV)
2 TMA-$AuCl_2$	-0.310	-0.958
3 TMA-$AuCl_2$	*	-2.035
4 TMA-$AuCl_2$	*	-2.810

* Non-dispersion-corrected systems did not optimize

a.

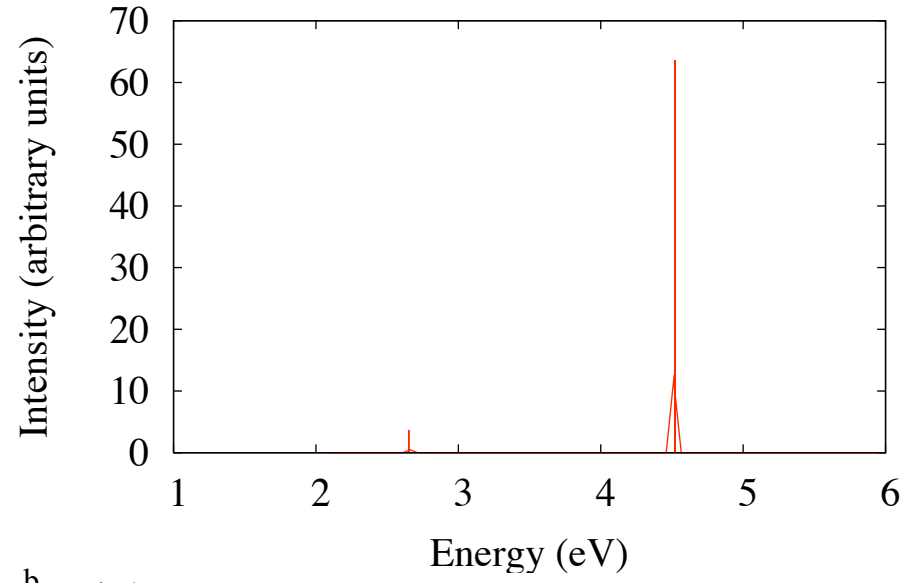

b.

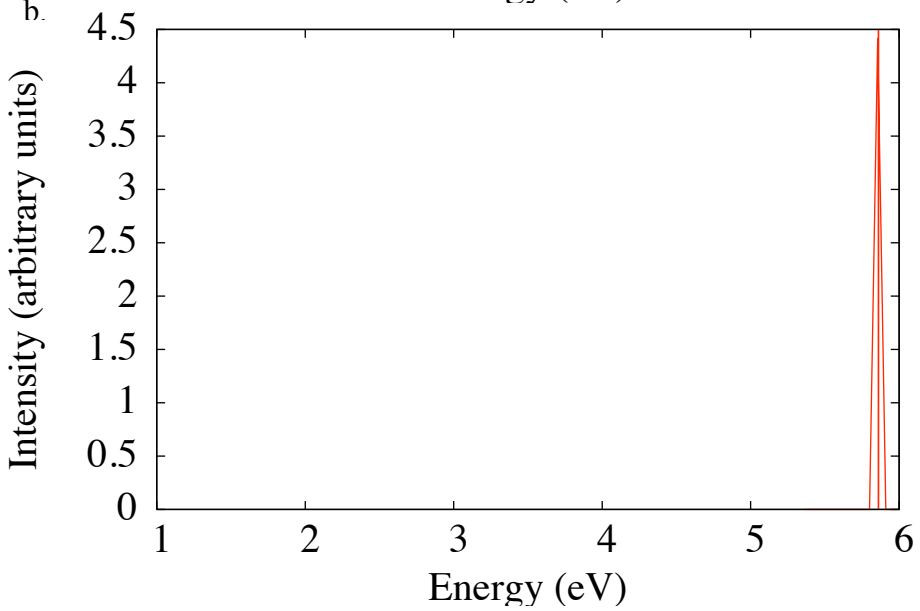

c.

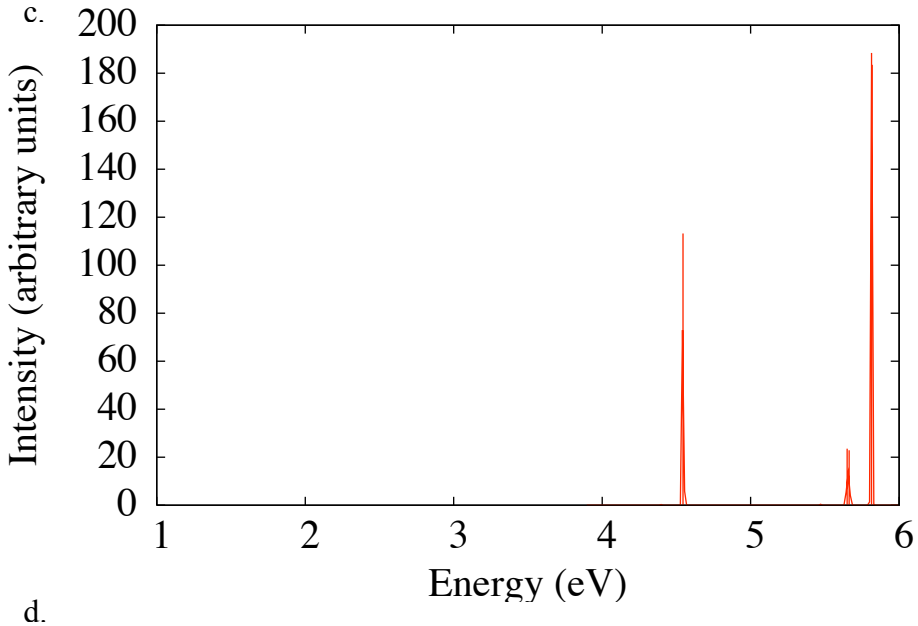
Intensity (arbitrary units)
200
180
160
140
120
100
80
60
40
20
0
1
2
3
4
5
6
Energy (eV)

d.

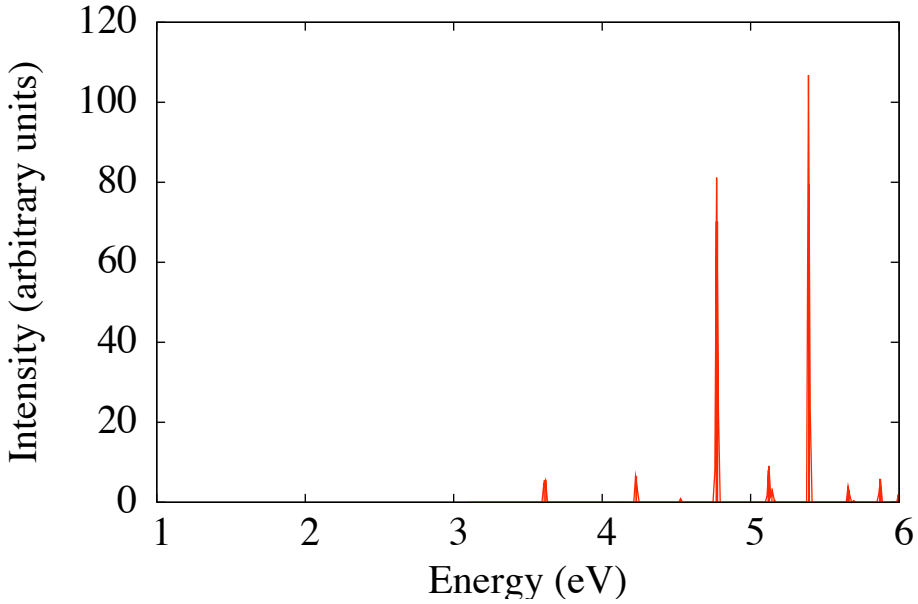
Intensity (arbitrary units)
120
100
80
60
40
20
0
1
2
3
4
5
6
Energy (eV)

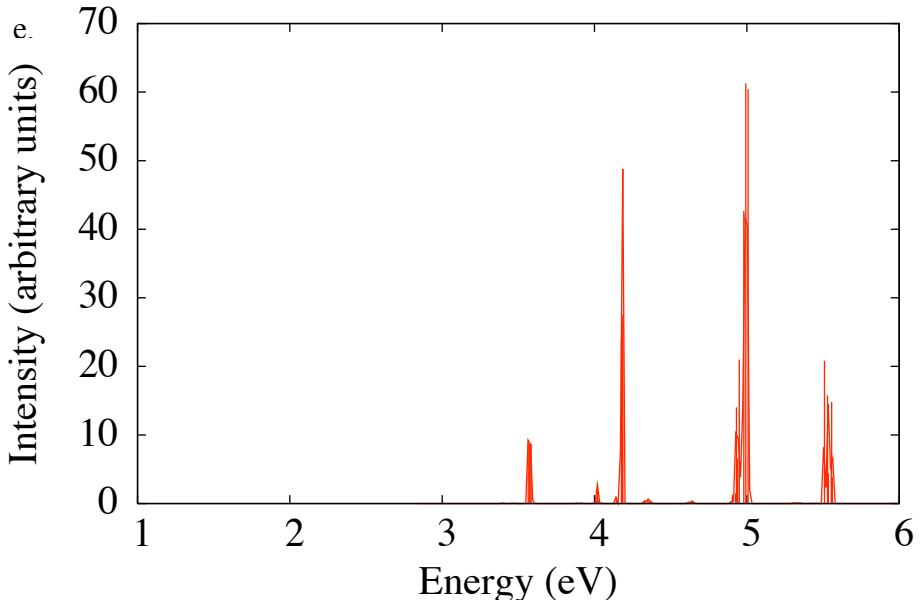

Figure C.1 BP86/TZP time-dependent density functional theory (TDDFT) absorption spectra for a. $AuCl_4^-$ b. $AuCl_2^-$ c. $Au_2Cl_2^{2-}$ d. $Au_3Cl_3^{2-}$ e. $Au_4Cl_4^{2-}$

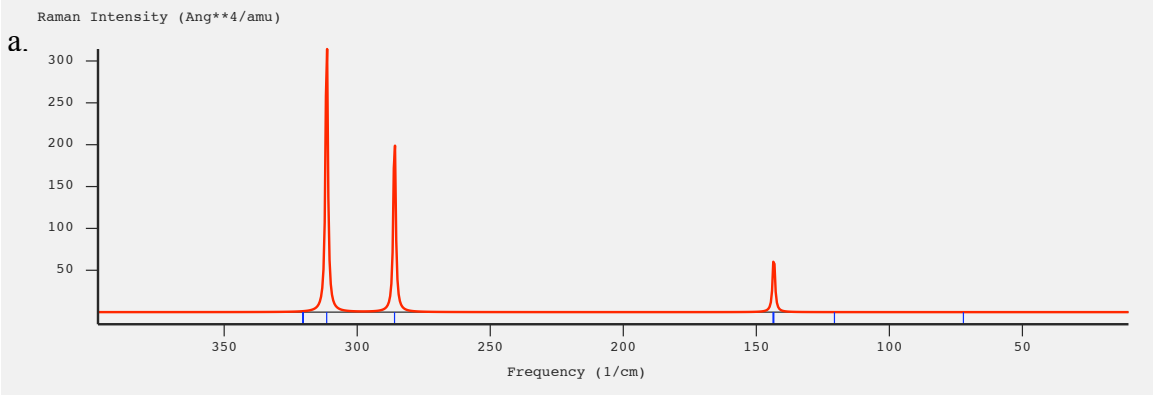

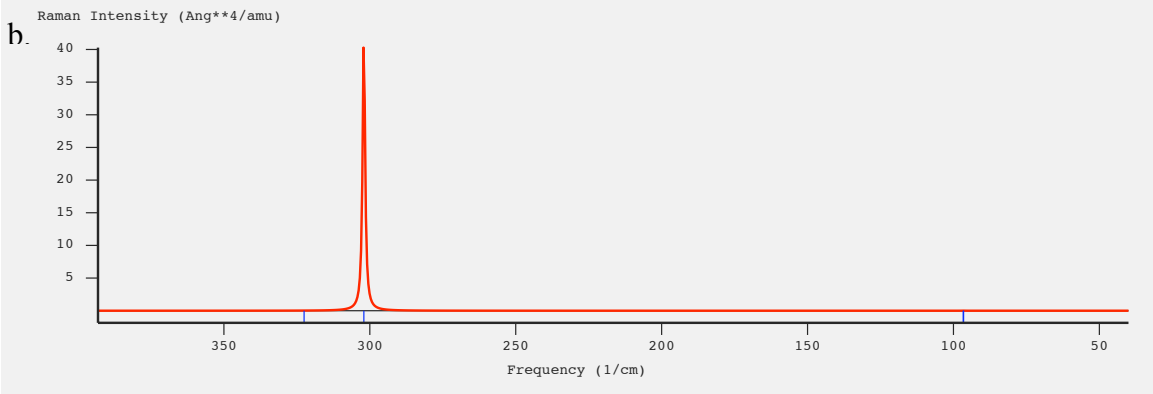

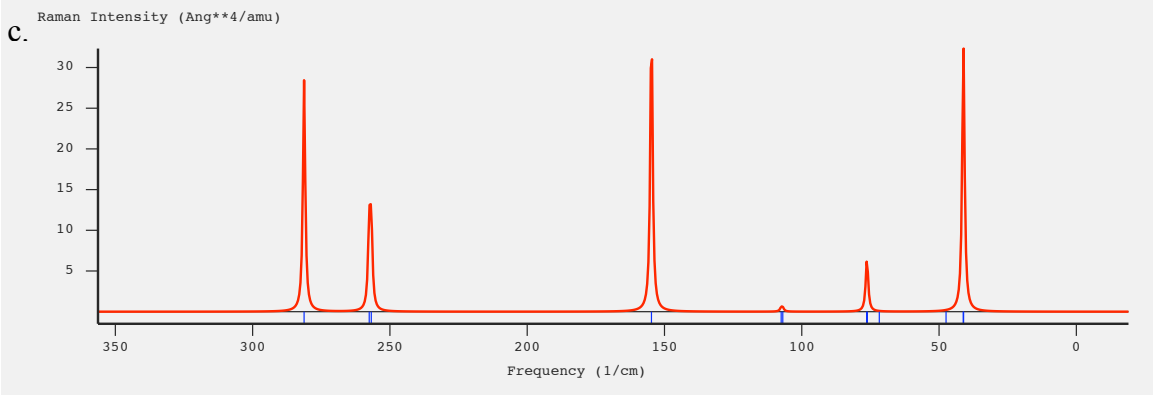

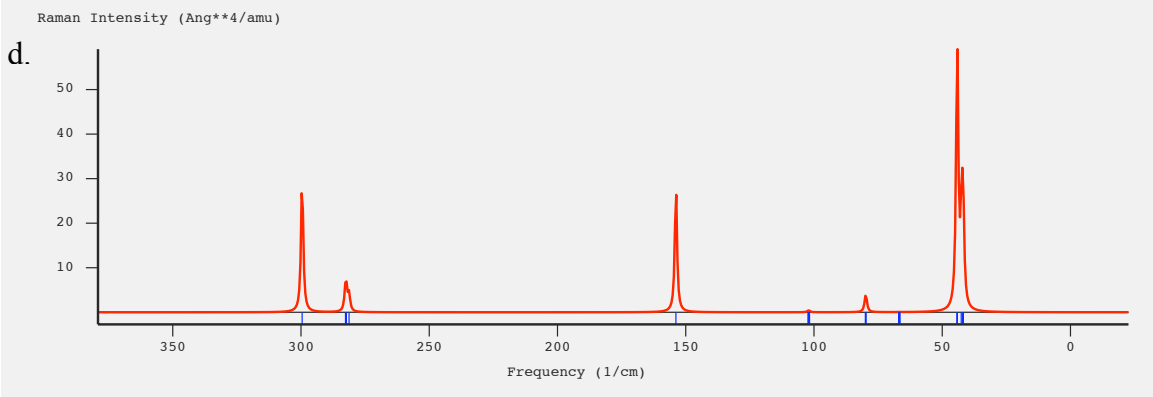

Figure C.2 BP86/TZP TDDFT Raman spectra for a. $AuCl_4^-$ b. $AuCl_2^-$ c. $Au_3Cl_3^{2-}$ d. $Au_4Cl_4^{2-}$

a.

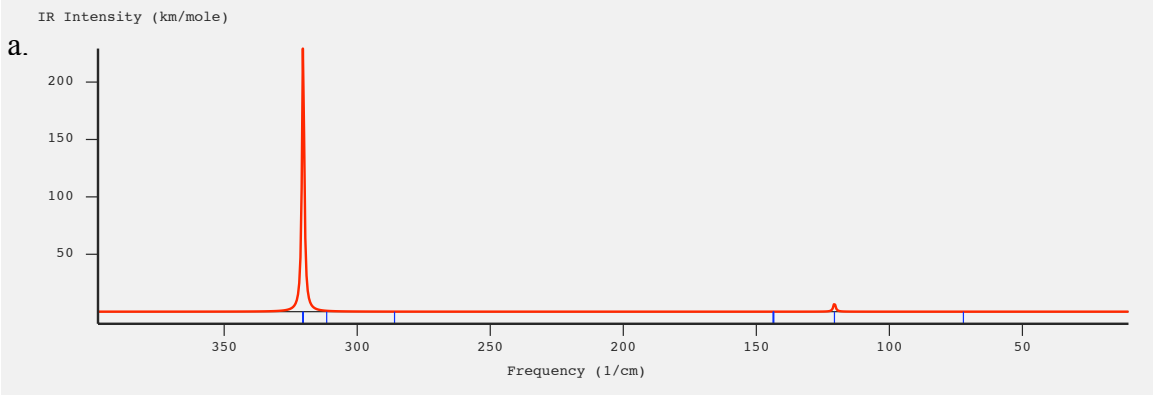
IR Intensity (km/mole)
200
150
100
50
350
300
250
200
150
100
50
Frequency (1/cm)

b.

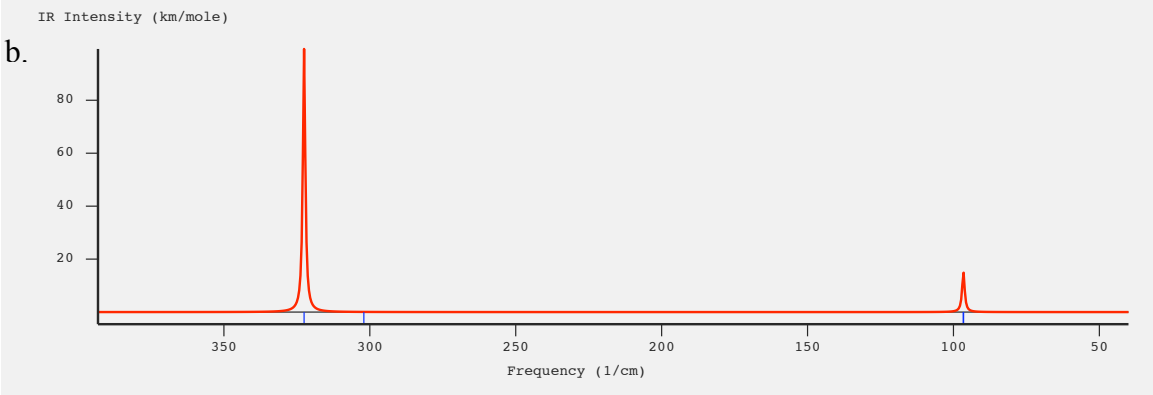
IR Intensity (km/mole)
80
60
40
20
350
300
250
200
150
100
50
Frequency (1/cm)

c.

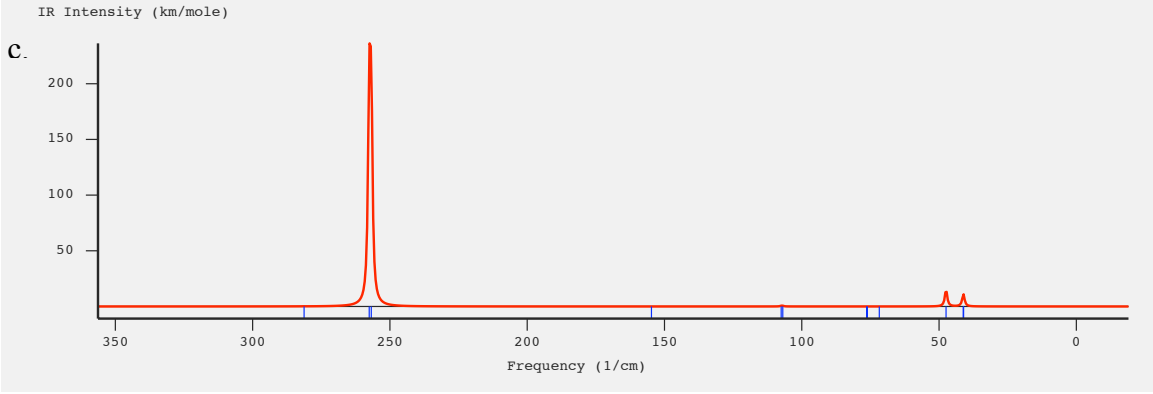
IR Intensity (km/mole)
200
150
100
50
350
300
250
200
150
100
50
0
Frequency (1/cm)

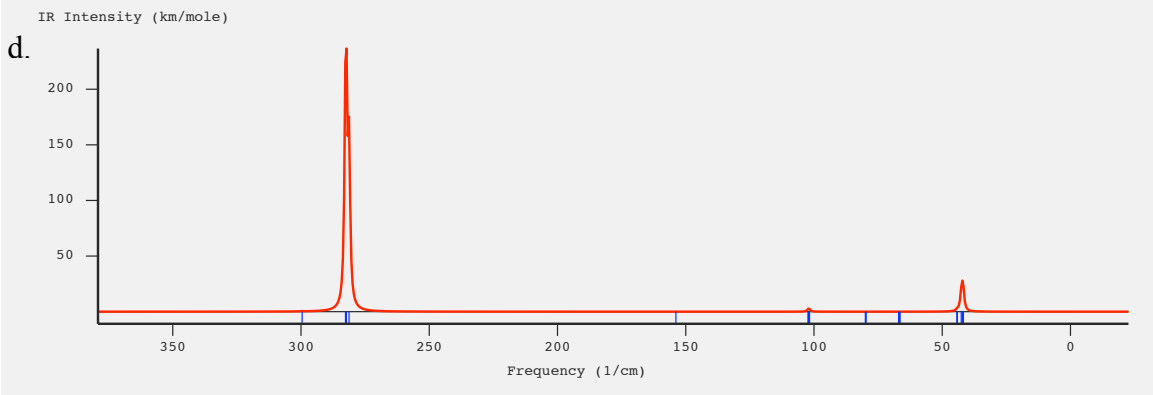

Figure C.3 BP86/TZP TDDFT Infrared spectra for a. $AuCl_4^-$ b. $AuCl_2^-$ c. $Au_3Cl_3^{2-}$ d. $Au_4Cl_4^{2-}$